DOT/FAA/AR-95/10

Office of Aviation Research
Washington, D.C. 20591

Certification Methodology for Stiffener Terminations

April 1996

Final Report

This document is available to the U.S. public through the National Technical Information Service, Springfield, Virginia 22161.

U.S. Department of Transportation
Federal Aviation Administration

NOTICE

This document is disseminated under the sponsorship of the U.S. Department of Transportation in the interest of information exchange. The United States Government assumes no liability for the contents or use thereof. The United States Government does not endorse products or manufacturers. Trade or manufacturer's names appear herein solely because they are considered essential to the objective of this report.

Technical Report Documentation Page

1. Report No.	2. Government Accession No.	3. Recipient's Catalog No.
DOT/FAA/AR-95/10		

4. Title and Subtitle	5. Report Date
CERTIFICATION METHODOLOGY FOR STIFFENER TERMINATIONS	April 1996
	6. Performing Organization Code
	8. Performing Organization Report No.
7. Author(s) C.H. Shah, H.P. Kan and M. Mahler	
9. Performing Organization Name and Address Military Aircraft Division Northrop Grumman Corporation One Northrop Avenue Hawthorne, California 90250-3277	10. Work Unit No. (TRAIS)
	11. Contract or Grant No. Tasks 4 and 9, NAS1-19347
12. Sponsoring Agency Name and Address U.S. Department of Transportation Federal Aviation Administration Office of Aviation Research Washington, D.C. 20591 National Aeronautical and Space Administration Langley Research Center Hampton, Virginia 23681-0001	13. Type of Report and Period Covered Final Report May 1992 – January 1995
	14. Sponsoring Agency Code ACD-210

15. Supplementary Notes

Technical Monitor: P. Shyprykevich, FAA Tech Center
Administrative Support: M. Rouse, NASA LaRC

16. Abstract

An experimental program was conducted to evaluate the failure mode, static strength, and fatigue life of stiffened composite skin with stiffener termination details. Static tension, compression, and constant amplitude compression-compression cyclic loads were applied to three specimen configurations. Analyses were conducted and results were compared with the test data. A statistical method was used to assess the scatter of the static strength and fatigue life data.

The results of the combined experimental and analytical program were used to define a recommended certification approach for commercial aircraft composite structures with stiffener terminations and to other structurally similar cases.

The program was undertaken to quantify the fatigue scatter in element/subcomponent type structure. Previous results based on coupon and bolted joint tests showed that scatter was high with the modal Weibull shape parameter $\approx$ 1.25. The fatigue test results from stiffener terminations element showed that the scatter is not different from the previous coupon data.

17. Key Words	18. Distribution Statement
Composites, Static Tests, Fatigue Tests, Stiffener Termination, Structural Certification	Document is available to the public through the National Technical Information Service, Springfield, Virginia, 22161

19. Security Classif. (of this report)	20. Security Classif. (of this page)	21. No. of Pages	22. Price
UNCLASSIFIED	UNCLASSIFIED	84	

Form DOT F 1700.7 (8-72)

Reproduction of completed page authorized

PREFACE

This report was prepared by the Northrop Grumman Corporation, Military Aircraft Division, Hawthorne, California, covering work performed under Tasks 4 and 9 of NASA Contract NAS1-19347 between May 1992 and January 1995. The specific tasks were conducted under an Interagency Agreement between the Federal Aviation Administration Technical Center, Atlantic City International Airport, New Jersey and the National Aeronautical and Space Administration, Langley Research Center, Hampton, Virginia. Technical direction was provided by P. Shyprykevich, FAA Technical Center with the advice of J. Soderquist, FAA Headquarters. Administrative support was provided by M. Rouse, NASA Langley Research Center.

The work was performed in Northrop Grumman's Structural Integrity and Materials Technology Department under the overall supervision of Dr. R. B. Deo. Mr. C. H. Shah was the Principal Investigator with the support of the following Northrop Grumman personnel:

Stress Analysis	M. Mahler
Statistical Analysis and Certification Approach	Dr. H. P. Kan
Specimen Design	C. Shah, E. Wolf
Fabrication Drawing	M. Cvitanich, T. Candusso
Specimen Fabrication	J. Enriquez
Specimen Testing	P. Corcoran, T. McCollum, D. Enno
Documentation	R. Cordero, H. Casarez, J. Baller

TABLE OF CONTENTS

Section **Page**

EXECUTIVE SUMMARY xi
1. INTRODUCTION 1
2. STIFFENER TERMINATION DESIGN 3
    2.1 Technology Assessment 3
        2.1.1 Survey of Design Practices 3
        2.1.2 Available Test Data 5
        2.1.3 Analysis Methods 5
        2.1.4 Summary of Technology Assessment 7
    2.2 Selection of Stiffener Termination Configuration 7
    2.3 Stiffener Termination Test Specimen Design 9
3. TEST PROGRAM 19
    3.1 Test Matrix 19
    3.2 Fabrication 19
    3.3 Test Setup 25
    3.4 Testing 25
4. TEST RESULTS AND DISCUSSION 29
    4.1 Static Tests 29
        4.1.1 Tension Tests 29
        4.1.2 Compression Tests 33
    4.2 Fatigue Tests 35
5. ANALYSIS AND CORRELATION 39
    5.1 Finite Element Analysis 39
    5.2 Local Failure Analysis 55
    5.3 Statistical Data Analysis 57
6. CERTIFICATION APPROACH 63
    6.1 Static Strength Configuration 63
    6.2 Durability Certification 66
7. CONCLUSIONS AND RECOMMENDATIONS 67
    7.1 Summary 67
    7.2 Concluding Remarks 67
    7.3 Recommendations 68
8. REFERENCES 69
APPENDIX—STIFFENER TERMINATION CADAM DRAWINGS

LIST OF FIGURES

Figure		Page
1	COMMONLY USED STIFFENER CONFIGURATIONS.	4
2	STIFFENER TERMINATION CONFIGURATIONS	4
3	I-STIFFENER TERMINATION	6
4	BOEING B-737 HORIZONTAL STABILIZER STIFFENED SKIN	8
5	INFLUENCE OF STIFFENER LENGTH ON AXIAL STRESS DISTRIBUTION	11
6	INFLUENCE OF STIFFENER LENGTH ON SKIN/STIFFENER LOAD DISTRIBUTION	12
7	PREDICTED AXIAL DEFORMATIONS FOR THE TWO LOADING CONFIGURATIONS	13
8	PREDICTED AXIAL STRESS DISTRIBUTION FOR THE TWO LOADING CONFIGURATIONS	14
9	INFLUENCE OF NUMBER OF 0° PLIES IN CAP ON SKIN/STIFFENER LOAD DISTRIBUTION	15
10	STIFFENER TERMINATION TEST SPECIMEN DESIGN	16
11	SKIN AND STIFFENER LAYUP SEQUENCE DETAIL	17
12	STRAIN GAGE LOCATIONS–16 AXIAL GAGE CONFIGURATION	21
13	STRAIN GAGE LOCATIONS–8 AXIAL GAGE CONFIGURATION	22
14	STRAIN GAGE LOCATIONS–4 AXIAL GAGE CONFIGURATION	23
15	TOOLING SCHEMATIC	24
16	COMPRESSION TEST SETUP	26
17	COMPRESSION TEST FIXTURES	26
18	COMPRESSION SPECIMEN INSIDE TEST FIXTURE	27
19	STATIC TEST RESULTS - TENSION AND COMPRESSION	31
20	TYPICAL FAILURE - STATIC TENSION	32
21	BUCKLING INDUCED FAILURE IN STATIC COMPRESSION	32
22	INTERLAMINAR STRESSES INITIATED FAILURE IN STATIC COMPRESSION	34
23	INTERLAMINAR STRESSES INITIATED FAILURE IN STATIC COMPRESSION - FLANGE FASTENERS EFFECT	34
24	COMPRESSION-COMPRESSION FATIGUE TEST RESULTS AT R=10	37
25	COMPARISON OF MEASURED AND PREDICTED STRAINS FOR STRAIN GAGE GROUP A OF THE TENSION SPECIMENS	40
26	COMPARISON OF MEASURED AND PREDICTED STRAINS FOR STRAIN GAGE GROUP B OF THE TENSION SPECIMENS	41

LIST OF FIGURES (CONTINUED)

Figure		Page
27	COMPARISON OF MEASURED AND PREDICTED STRAINS FOR STRAIN GAGE GROUP C OF THE TENSION SPECIMENS	41
28	COMPARISON OF MEASURED AND PREDICTED STRAINS FOR STRAIN GAGE GROUP D OF THE TENSION SPECIMENS	42
29	COMPARISON OF MEASURED AND PREDICTED STRAINS FOR STRAIN GAGE GROUP E OF THE TENSION SPECIMENS	42
30	COMPARISON OF MEASURED AND PREDICTED STRAINS FOR STRAIN GAGE GROUP F OF THE TENSION SPECIMENS	43
31	COMPARISON OF MEASURED AND PREDICTED STRAINS FOR STRAIN GAGE GROUP G OF THE TENSION SPECIMENS	43
32	COMPARISON OF MEASURED AND PREDICTED STRAINS FOR STRAIN GAGE GROUP H OF THE TENSION SPECIMENS	44
33	COMPARISON OF MEASURED AND PREDICTED STRAINS FOR STRAIN GAGE GROUP I OF THE TENSION SPECIMENS	44
34	COMPARISON OF MEASURED AND PREDICTED STRAINS FOR STRAIN GAGE GROUP A OF THE COMPRESSION SPECIMENS WITH 75° TERMINATION ANGLE	48
35	COMPARISON OF MEASURED AND PREDICTED STRAINS FOR STRAIN GAGE GROUP B OF THE COMPRESSION SPECIMENS WITH 75° TERMINATION ANGLE	48
36	COMPARISON OF MEASURED AND PREDICTED STRAINS FOR STRAIN GAGE GROUP C OF THE COMPRESSION SPECIMENS WITH 75° TERMINATION ANGLE	49
37	COMPARISON OF MEASURED AND PREDICTED STRAINS FOR STRAIN GAGE GROUP D OF THE COMPRESSION SPECIMENS WITH 75° TERMINATION ANGLE	49
38	COMPARISON OF MEASURED AND PREDICTED STRAINS FOR STRAIN GAGE GROUP E OF THE COMPRESSION SPECIMENS WITH 75° TERMINATION ANGLE	50
39	COMPARISON OF MEASURED AND PREDICTED STRAINS FOR STRAIN GAGE GROUP F OF THE COMPRESSION SPECIMENS WITH 75° TERMINATION ANGLE	50
40	COMPARISON OF MEASURED AND PREDICTED STRAINS FOR STRAIN GAGE GROUP G OF THE COMPRESSION SPECIMENS WITH 75° TERMINATION ANGLE	51
41	COMPARISON OF MEASURED AND PREDICTED STRAINS FOR STRAIN GAGE GROUP H OF THE COMPRESSION SPECIMENS WITH 75° TERMINATION ANGLE	51

LIST OF FIGURES (CONTINUED)

Figure		Page
42	COMPARISON OF MEASURED AND PREDICTED STRAINS FOR STRAIN GAGE GROUP I OF THE COMPRESSION SPECIMENS WITH 75° TERMINATION ANGLE	52
43	COMPARISON OF MEASURED AND PREDICTED STRAINS FOR STRAIN GAGE GROUP A OF THE COMPRESSION SPECIMENS WITH 45° TERMINATION ANGLE	54
44	COMPARISON OF MEASURED AND PREDICTED STRAINS FOR STRAIN GAGE GROUP B OF THE COMPRESSION SPECIMENS WITH 45° TERMINATION ANGLE	54
45	COMPARISON OF MEASURED AND PREDICTED STRAINS FOR STRAIN GAGE GROUP C OF THE COMPRESSION SPECIMENS WITH 45° TERMINATION ANGLE	55
46	COMPARISON OF MEASURED AND PREDICTED INITIAL FAILURE LOAD FOR THE THREE SPECIMEN CONFIGURATIONS	58
47	PROBABILITY DISTRIBUTION FOR THE NORMALIZED STATIC STRENGTH DATA	59
48	PROBABILITY DISTRIBUTION FOR THE NORMALIZED FATIGUE LIFE	61
49	KEY ELEMENTS OF THE OVERALL COMPOSITE STRUCTURAL CERTIFICATION METHODOLOGY	64

LIST OF TABLES

Table		Page
1	SUMMARY OF SELECTED COSMOS/M RESULTS FOR STIFFENER TERMINATION CONFIGURATIONS	10
2	STIFFENER TERMINATION TEST MATRIX	20
3	SUMMARY OF STATIC TESTS	30
4	SUMMARY OF FATIGUE TESTS AT R=10	36
5	SUMMARY OF ANALYSIS AND EXPERIMENTAL DATA CORRELATION FOR STATIC TENSION SPECIMENS	40
6	SUMMARY OF STIFFENER/SKIN SEPARATION ANALYSIS	58

EXECUTIVE SUMMARY

Stiffened composite panels with stiffener terminations are a major concern in certification of composite aircraft structures. The geometric discontinuity at the stiffener termination site induces high out-of-plane stresses and initiates stiffener/skin separation failure. This report documents the results of a combined experimental and analytical effort that leads to the formulation of a recommended structural certification approach for stiffener terminations. An experimental program was conducted to determine the static strength and fatigue life of a typical stiffener termination configuration for commercial aircraft composite structure. The test specimen was analyzed to predict both the global structural response and the local failure initiation. Statistical analyses were also conducted to assess the scatter in static strength and fatigue life. Finally, based on the results of the experimental and analytical investigation, a structural certification approach is recommended.

The test specimen design was based on the results of comprehensive technology assessment and a detailed stress analysis. An I-section stiffener cocured to a soft skin was selected based on the design concept of the Boeing's B-737 composite horizontal tail. The dimensions used for the test specimens were determined from the finite element analysis used to simulate the actual structural response.

A total of 21 static and 24 fatigue specimens were tested. Static tests were loaded, either in tension or compression, to failure to determine the initial and overall failure strengths. Fatigue tests were conducted under constant amplitude compression-compression cyclic load with a minimum to maximum load ratio (R-ratio) of 10. Failure in static tension test specimens initiated under the stiffener flange at the base of the stiffener at the stiffener termination ends. The mode of the initial failure was, as expected, stiffener separation from the skin caused by interfacial stresses. Similar initial failures were observed in the static compression test specimens with proper constraints to prevent overall specimen buckling as well as local buckling. The fatigue behavior of the test specimens was observed to be typical of composites, which exhibit relatively high threshold and high life scatter.

Two variations of the baseline specimen configuration were experimentally investigated to reveal the effects of termination angle and flange fasteners. These specimen configurations were tested under static compression and compression-compression fatigue loads. The effect of

stiffener termination angle, when changed from baseline 75° to 45°, on static strength as well as fatigue life was determined to be insignificant. The flange fasteners had no effect on the failure initiation but retarded the growth of the delamination under fatigue load.

An analysis was conducted to predict the overall specimen response as well as the failure initiation. The finite element method was used to determine the relationship between the applied load and the strain response of the specimen. The predicted strains were compared with the measured strains at various strain gage locations. Excellent correlation was found between the measured and predicted strains at key locations. A local elasticity model was used to predict the initiation of stiffener/skin separation at the stiffener termination site. The analytical results were conservative, compared to the test data for all specimen configurations and loading conditions.

A statistical method was employed to assess the scatter in the static strength and fatigue life data. The scatter parameters obtained from the results of this program were comparable to those of composites and bolted joints.

In view of the experimental and analytical results of this program, a certification approach was formulated and recommended to the FAA. In this approach the static strength of composite structures with a properly designed stiffener termination can be certified based on a B-basis design allowable derived from final failure data. This design allowable can be used in an analysis to demonstrate that the initial failure strength exceeds the design limit load. Fatigue life certification of this structural configuration is recommended by the combined use of life factor and load enhancement factor.

In summary, the experimental data generated during the performance of this program provides a useful database that is needed to define a certification procedure for composite structures with stiffener terminations. Further work is suggested to modify or refine the local out-of-plane analysis method for failure initiation prediction.

1. INTRODUCTION.

Stiffened panels are widely used in airframe designs. In stiffened panels, stiffeners are terminated to accommodate cross members or cutouts at numerous locations. These termination locations are sites of geometric discontinuities that induce high interlaminar stresses and stress gradients. These high interlaminar stresses result in stiffener disbonding from the skin. Historically, the matrix dependent nature of interlaminar failures has resulted in large scatter in strength when measured at a coupon level. Thus, statistical measure of scatter for interlaminar failure is required for certification purposes. This has to be accomplished using a higher complexity test element. A stiffener termination element meets these requirements.

FAA Advisory Circular AC20-107A states that the number of cycles to be applied in evaluating the durability and damage tolerance capability of the composite structure should be statistically significant (Sections 7(a) (2)). This type of data is available at the coupon level but needs to be determined at the higher level of structural complexity such as elements, subcomponents, and components. The data generated using the stiffness termination elements should help fill this void.

The objectives of this program were (1) to generate experimental data on a stiffener termination configuration, (2) to verify existing failure analysis methods, and (3) to establish static strength and fatigue life data scatter. The results of this program can be used to establish guidelines for certification of cocured composite built-up structures of which stiffener terminations is an example.

The specific objectives of the present program were accomplished by performing the following activities:

a. Designing and fabricating test specimens to simulate stiffener terminations.

b. Conducting an experimental program to generate static strength and fatigue life data.

c. Conducting static stress analyses to verify the stress distribution and predict the out-of-plane failure.

d. Conducting statistical data analysis to assess the static strength and fatigue life data scatter.

e. Recommending static strength and fatigue life certification procedures for stiffener termination details based on analysis and test results.

The results of the present program are described in detail in the remaining sections. Section 2 summarizes the test specimen design. A comprehensive technology assessment was conducted to select a stiffener and stiffener termination configuration and a design concept that would represent current design practice. In addition, available test data and analysis methods were reviewed. Highlights of this technology assessment are presented in Section 2, along with results of the detailed design analysis which was conducted to optimize the specimen configuration.

Section 3 outlines the experimental program. Test specimen fabrication, the test matrix, and the test setup are discussed in the section. The results of the test program are summarized and discussed in Section 4. A total of 21 static and 24 fatigue specimens were tested. The baseline specimen configuration had a 75° termination angle. The effects of varying the termination angle were investigated by testing specimens with a 45° termination angle. Design features to prevent stiffener/skin separation and disbond propagation were also investigated by installing stiffener flange fasteners near the termination. The specimen configuration and design features are documented in Section 4.

Test specimens were analyzed to determine the global load distribution and to predict the local out-of-plane failure. The finite element method was used for global stress analysis and a linear elasticity model (Reference 1) was used to compute the interlaminar stresses at the termination site. Analytical results were compared with experimental data. The analysis and data correlation are discussed in Section 5. Section 5 also presents a statistical analysis to assess the scatter in static strength and fatigue life data. The statistics obtained from the analysis were compared to those for composite laminates, bolted joints, and bonded joints.

Based on the results of this investigation, procedures for static strength and fatigue life certification of composite built-up structures are presented and discussed in Section 6. The proposed certification approach can be easily integrated into the overall verification methodology for composite aircraft structures. Finally, conclusions and recommendations based on the results of this research are summarized in Section 7.

2. STIFFENER TERMINATION DESIGN.

The test specimen configuration was selected based on the results of a comprehensive technology assessment. After the selection of the baseline specimen configuration, a finite element analysis was conducted to determine the dimensions of the specimen. The dimensions of the specimen were selected so that the actual structural response could be simulated under the test environment. Details of the technology assessment, design analysis, and specimen design procedures are discussed in the following paragraphs.

2.1 TECHNOLOGY ASSESSMENT.

A comprehensive technology assessment was conducted to select a stiffener, stiffener termination geometries, and overall design that would represent current practice. The results of this assessment are summarized below.

2.1.1 Survey of Design Practices.

A survey of research programs sponsored by NASA and DoD on composite stiffeners and stiffener termination design practice (References 2 through 11) was conducted. Results of this survey indicated that three types of stiffener designs are commonly used in industry, as shown in Figure 1. The three designs were I-, hat-, and blade-section stiffeners. Figure 1 also shows applications of various stiffener designs to specific aircraft. These stiffeners are mechanically fastened, cobonded, or cocured to the skins. Stiffeners are terminated throughout the aircraft where cross members and cutouts prevent their continuation. Stiffener ends are either mechanically attached to the cross members or left unattached. Typical applications include:

- Stiffener ends clipped to ribs, frames, windows, or doors jambs.
- Stiffener ends terminated in vicinity of ribs, access panels, and front spars without end clips.

This latter category, which features terminated stiffeners, is of interest in the present task. A summary of the various stiffener termination configurations and their application to specific aircraft is shown in Figure 2.

STIFFENER	APPLICATION
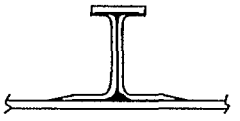	• NASA Postbuckling Study • 737 Horizontal Tail • 777 Empennage • Boeing Damage Tolerance Report
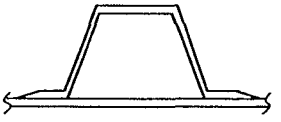	• C-130 Wing Box • L-1011 Vertical Tail • YF-23 ATF • C-141 Cargo Door Skins • AV-8B Harrier Fuselage
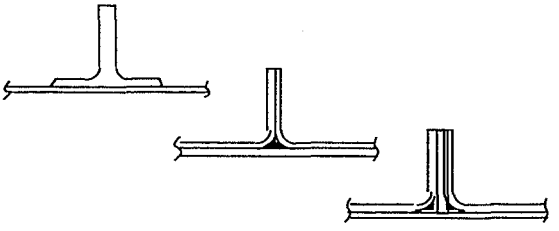	• Douglas Composite Transport Wing Technology Development • B-1B Wing Section • C-130 Wing Box

F93-CS/02

FIGURE 1. COMMONLY USED STIFFENER CONFIGURATIONS.

STIFFENER	TERMINATION CONCEPT/APPLICATIONS	
 I - SECTION	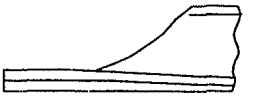 MACHINED RUNOUT • 737 Horizontal Tail	
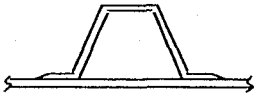 HAT	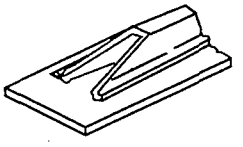 SCARFED • YF-23 • C-130	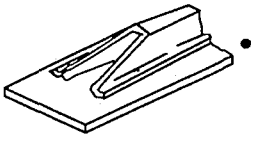 SCARFED WITH FASTENERS • YF-23
	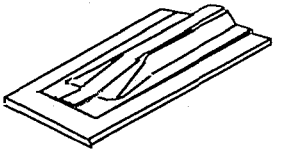 TAPERED • L-1011	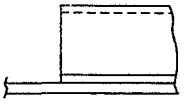 NO SCARF • YF-23
 BLADE	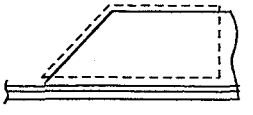 SCARFED WITH FIBERGLASS OVERWRAP • C-130	

F93-CS/03

FIGURE 2. STIFFENER TERMINATION CONFIGURATIONS.

2.1.2 Available Test Data.

A survey of available stiffener termination test data was also conducted. The test data confirm that under axial loading, high interlaminar stresses occur at the termination end, which can cause the stiffener to separate from the skin by delamination. The specific problem of practical stiffener termination design, analysis, and testing under compression load has been addressed in References 1, 7, and 21. The more complex problem of stiffener-skin delamination in stiffened panels has been addressed in References 12 through 20.

Although configuration specific data are available for some stiffener termination designs, a comprehensive certification methodology has not been developed. The analysis methods developed in previous studies and the characterization of the scatter in stiffener termination static and fatigue strengths developed in this program are the essential ingredients of a certification methodology.

2.1.3 Analysis Methods.

Analysis methods to predict failure mode and initial failure strength in composite structures with stiffener termination details are discussed in References 1, 7, and 21 through 28. In Reference 1, a joint effort between McAir and Northrop, two analytical codes were developed. The first code, called SSAM, was based on the finite element approach. The second code, called WEBSTER, was based on the linear theory of elasticity using a complex stress function approach. The WEBSTER code computes the local out-of-plane stresses at the stiffener termination locations and predicts separation of the stiffeners from the skin by employing a quadratic failure criteria with an average stress scheme. This code is a suitable failure prediction tool for the structural configurations considered under the present program. The procedure to apply WEBSTER code to a practical structural problem can be summarized as follows:

- Obtain local applied load (N_X) near the stiffener termination locations as shown in Figure 3a.
- Idealize the stiffener termination configurations as a two dimensional model as, α, shown in Figure 3b.
- Conduct analysis using the WEBSTER code for two transverse configurations to obtain interlaminar stresses as shown in Figure 3c.

This procedure will be applied in Section 5 for local failure prediction.

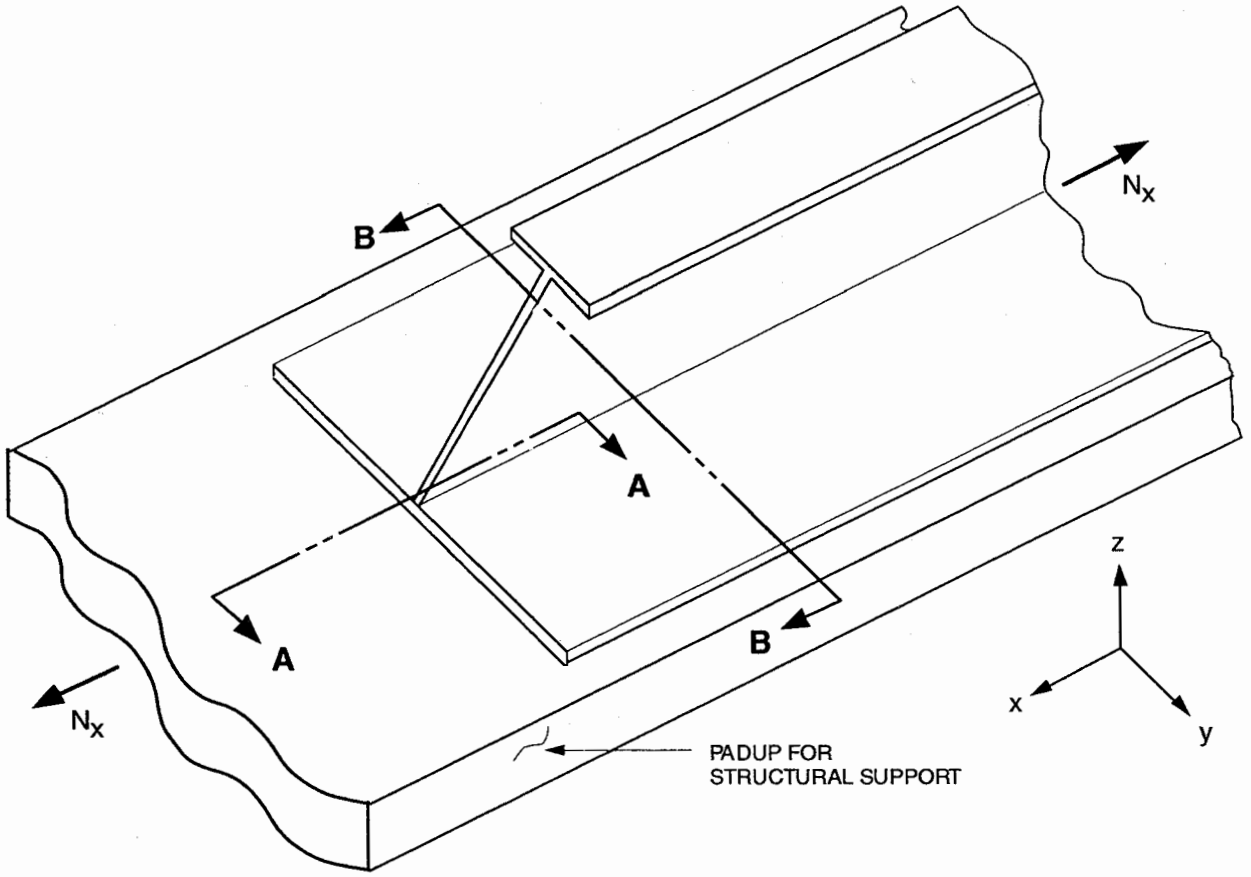

(a) Stiffener Termination Geometry

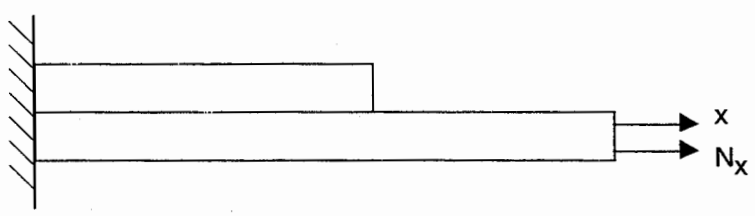

(b) Idealized Model for WEBSTER Code

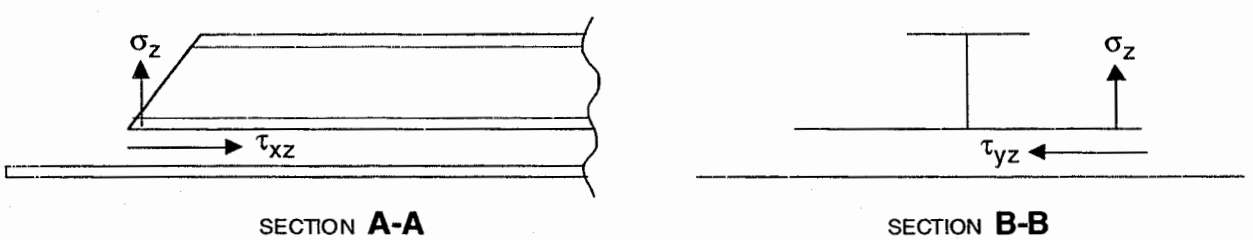

(c) WEBSTER Analysis Conducted for Two Transverse Sections

F93-CS/01/a

FIGURE 3. I-STIFFENER TERMINATION.

2.1.4 Summary of Technology Assessment.

After surveying design practices, it was apparent that many military aircraft manufacturers use hat and blade stiffeners in their design. The blade and hat stiffener are cost effective to manufacture due to fabrication simplicity and low tooling cost. Therefore, military aircraft manufacturers have compiled a relatively large experience base for integrating hat and blade stiffeners in their designs. On the other hand, Boeing (Commercial and Military) prefer the I-section. The I-section stiffener is more complex to fabricate and has higher tooling costs, since it is an open section with flange separated from the skin and tight geometry in the corners. However, I-section stiffeners are finding increased usage in the next generation of commercial aircraft due to their axial load carrying capability, their utility in "soft-skin" damage tolerant designs, and ease of inspection.

The technology assessment showed that a methodology is available for systematic design of the stiffener termination details. However, this methodology relies upon limited test data for stiffener termination configurations. More extensive test data are needed to establish variability and a certification methodology.

2.2 Selection of Stiffener Termination Configuration.

On the basis of forgoing discussion and subsequent discussions with FAA and NASA about the technical merits of various stiffener termination test specimens, the final configuration selected was an I-section stiffener with termination regions along the mid-length of the specimen. The I-section stiffener termination concept from Boeing's B-737 horizontal tail, Figure 4, was suitable for the test program since its I-section stiffener was cocured to a "soft-skin" design (Reference 3).

The B-737 horizontal tail skin has 9 plies of T300/5208 graphite epoxy fabric with (17/66/17) ply content, i.e., 17% 0° plies, 66% ±45° plies, and 17% 90° plies. The I-section stiffener consists of two back-to-back C-sections with 2 plies of T300/5208 graphite epoxy fabric and 2 plies of 0° T300/5208 graphite epoxy tape in the cap. The I-section stiffeners were spaced every 3.85 inches parallel to the rear spar. They were terminated at ribs located every 27 inches and also terminated at length end near the front spar.

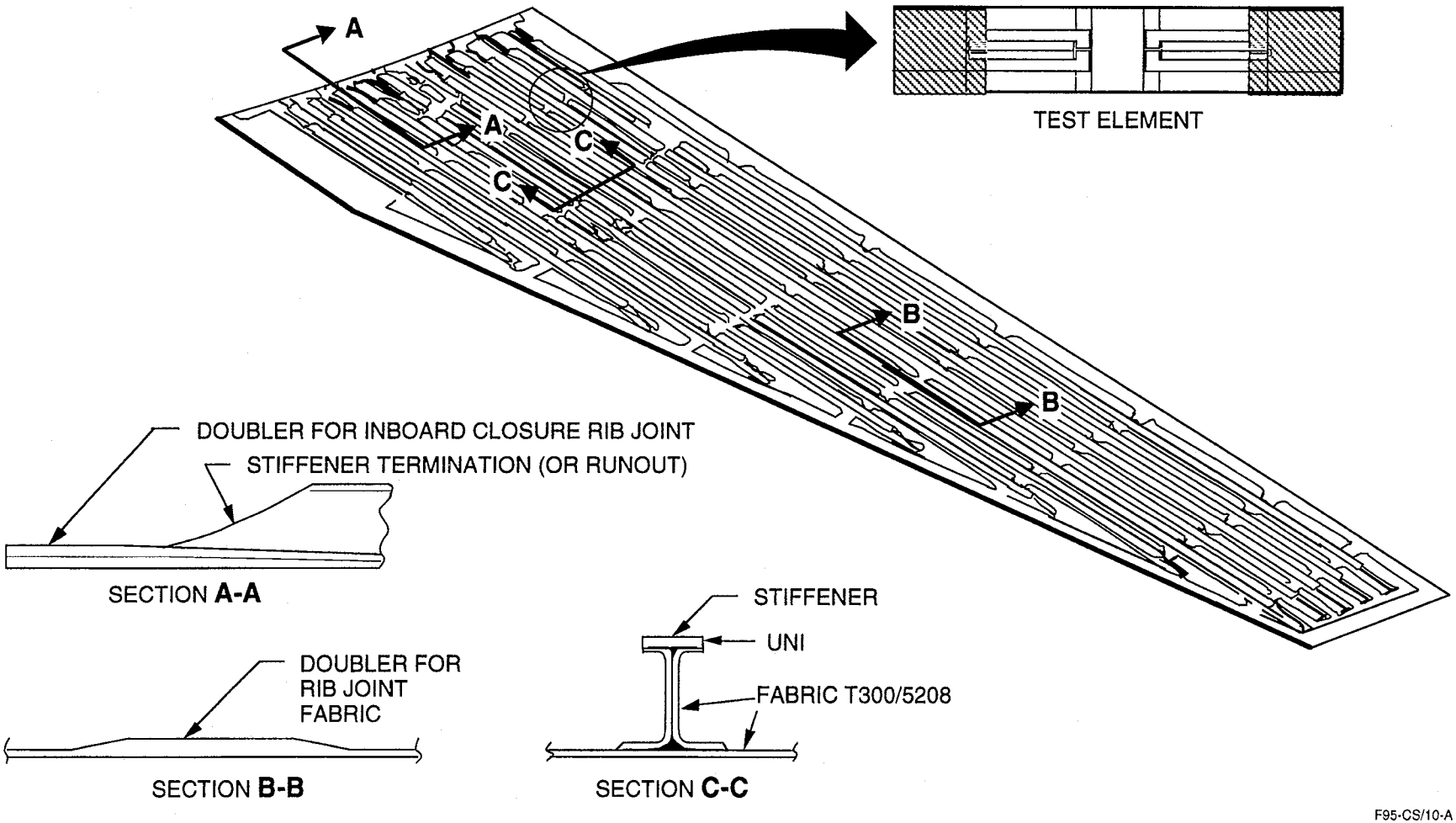

FIGURE 4. BOEING B-737 HORIZONTAL STABILIZER STIFFENED SKIN.

2.3 Stiffener Termination Test Specimen Design.

The overall cross-sectional dimensions for the skin and stiffener were kept the same as the Boeing B-737 horizontal tail configuration. Actual thicknesses of the skin and stiffener were sized to prevent buckling in the test specimen during static compression and repeated compression-compression fatigue loading. The length of the specimen was dictated by requiring a constant stress state extending at least 1 inch along the length before the termination end. AS4/3501-6 graphite epoxy tape was selected for skin and AS4/3501-6 graphite epoxy woven fabric was selected for stiffener fabrication. The material selection was made after consultation with FAA and NASA.

To determine the stress distributions, a two-dimensional finite element model, using COSMOS/M, was developed. Detail finite element models (FEM) were developed and analyzed for two types of specimen end loading configurations: partially and fully loaded stiffeners. For each loading configuration, four geometric variations were analyzed as shown in Table 1.

The fully end loaded stiffener geometry is more desirable than the partially loaded stiffener geometry since it provides uniform strain condition at the load introduction point. However, the fully loaded geometry introduces difficulties in specimen gripping and load eccentricity. Subsequent analytical results, which are discussed below, showed that both load configurations provided similar stress distributions in the stiffener termination area of interest.

Selected FEM stress results for partially loaded stiffener configuration cases are shown in Figure 5. These results show a partially loaded stiffener length of 5.5 inches or greater provides the required constant stress distribution area mentioned above. For the partially loaded stiffener geometries, the influence of stiffener length on skin/stiffener load distribution is shown in Figure 6. Skin/stiffener load distribution for the 5.5-inch stiffener length is comparable to that of 27-inch-long stiffener.

Displacement and stress distributions from FEM analysis for partially and fully loaded stiffener configurations are shown in Figures 7 and 8. It is evident from Figures 7 and 8 that the displacement and stress distributions near the stiffener termination region are similar for the two loading configuration.

FEM analysis was also used to evaluate the influence of the number of 0° plies in the stiffener cap on skin/stiffener distribution. Four cases of stiffener sizing were compared and the results are summarized in Figure 9.

TABLE 1. SUMMARY OF SELECTED COSMOS/M RESULTS FOR STIFFENER TERMINATION CONFIGURATIONS.

SPECIMENS FOR TWO LOADING CONFIGURATIONS	LENGTH OF STIFFENER L, in.	0° PLIES IN STIFFENER CAP	LENGTH OF CONSTANT STRESS in.	PERCENT OF TOTAL LOAD		REMARK
				STIFFENER	SKIN	
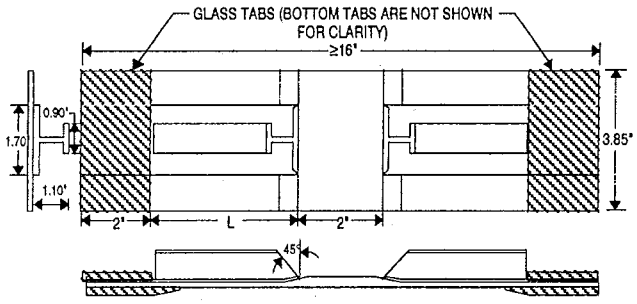 PARTIALLY LOADED STIFFENER	4.5	4	0.8	12.0	88.0	ACCEPTABLE CONSTANT STRESS DISTRUBUTION OVER 1 inch OF LENGTH ACHIEVED BY STIFFENER LENGTH OF 5.5 inch OR GREATER
	5.5	4	1.3	18.0	82.0	
	8	4	3.6	19.5	80.5	
	27	4	20	22.0	78.0	
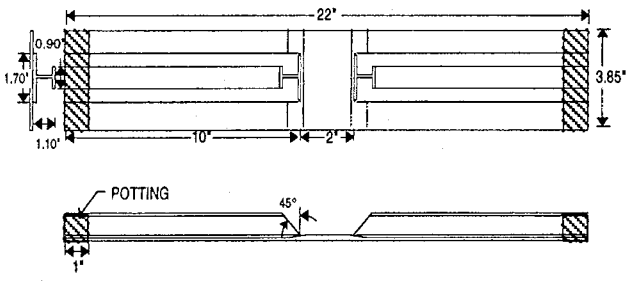 FULLY LOADED STIFFENER	10	4	N.A.	20.0	80.0	ACCEPTABLE SKIN/ STIFFENER LOAD DISTRIBUTION ACHIEVED BY SIX 0° PLIES IN STIFFENER CAP
	10	6	N.A.	22.5	77.5	
	10	8	N.A.	23.0	77.0	
	10	12	N.A.	23.2	76.2	

F95-CS/09

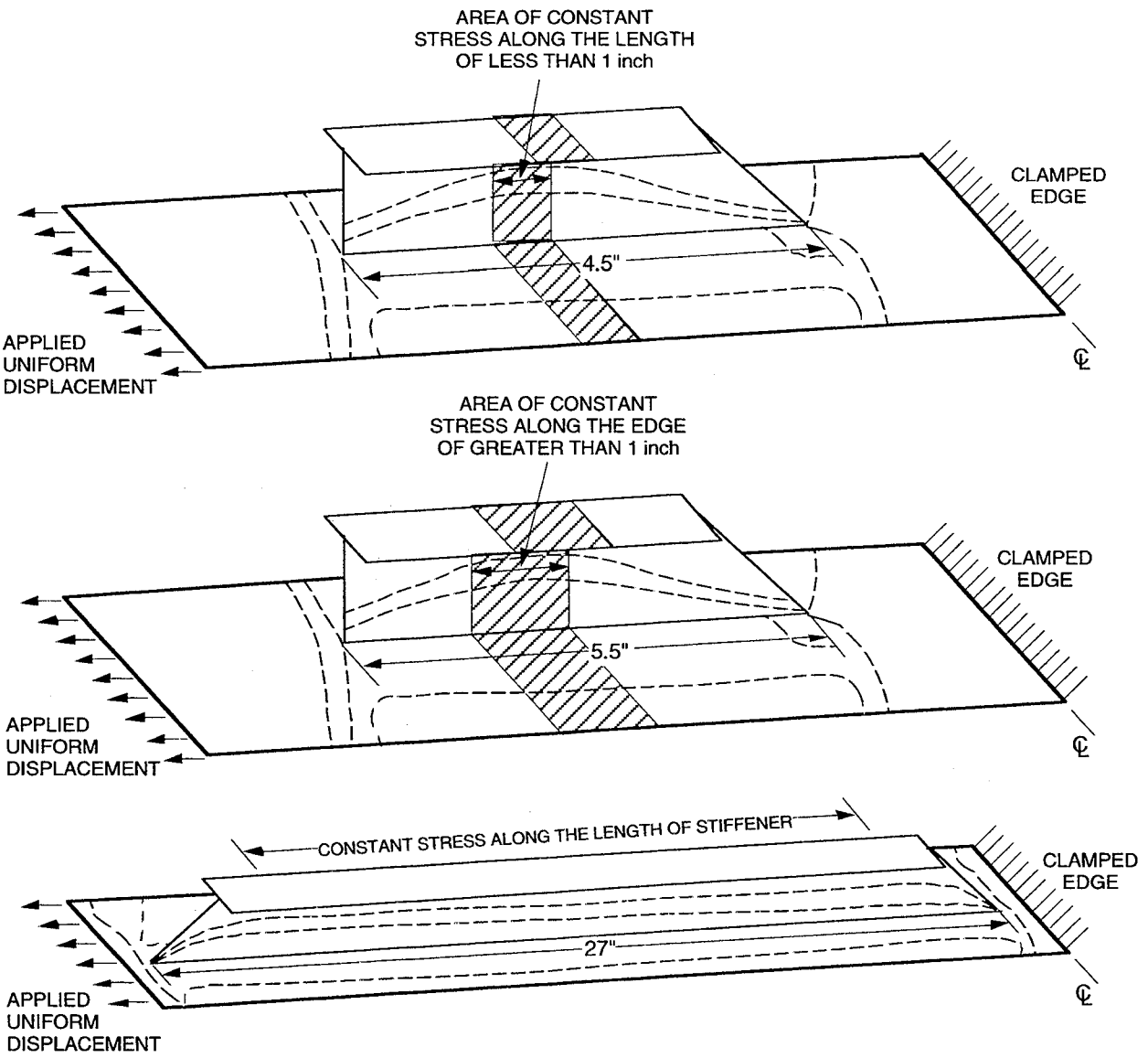

- FOR THE PARTIALLY LOADED STIFFENER GEOMETRY, THE 5.5 inch OR GREATER STIFFENER LENGTH PROVIDES SATISFACTORY STRESS DISTRIBUTION

F93-CS/06

FIGURE 5. INFLUENCE OF STIFFENER LENGTH ON AXIAL STRESS DISTRIBUTION.

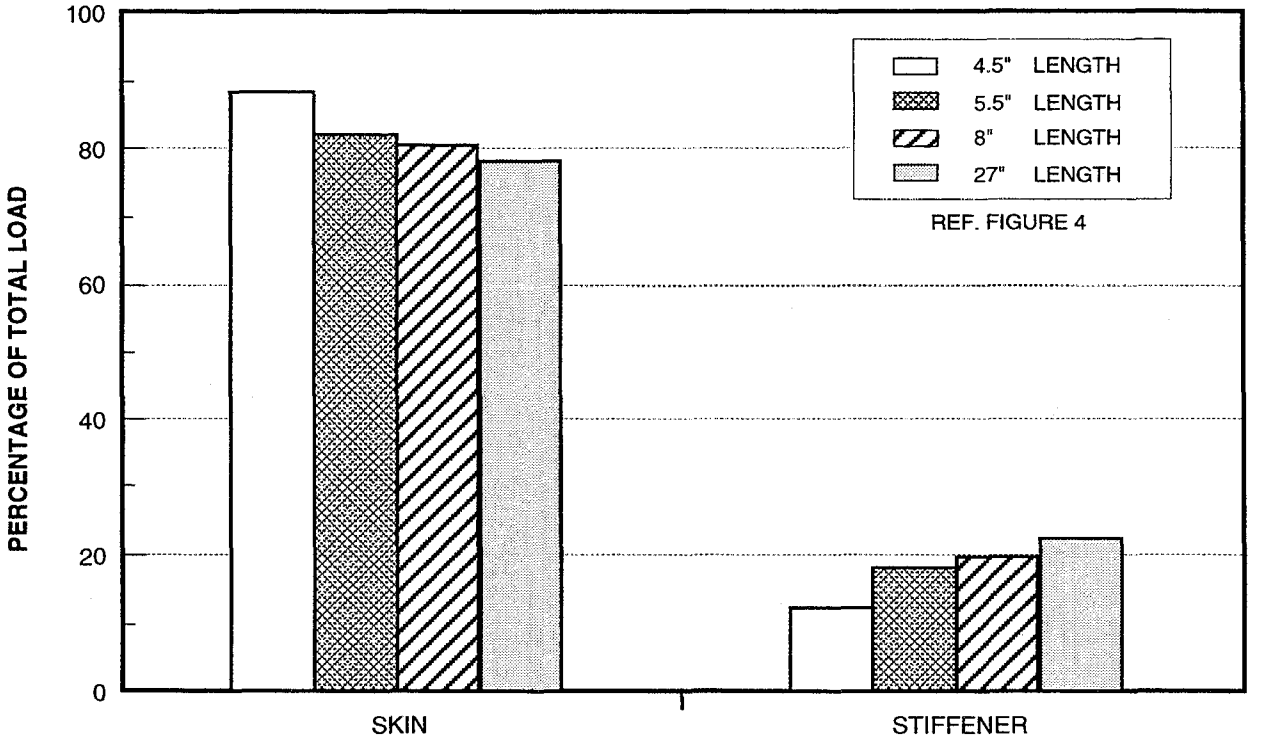

- FOR THE PARTIALLY LOADED STIFFENER GEOMETRY, THE 5.5 inch OR GREATER STIFFENER LENGTH PROVIDES SKIN/STIFFENER LOAD DISTRIBUTION COMPARABLE TO 27-INCH STIFFENER LENGTH

F93-CS/07

FIGURE 6. INFLUENCE OF STIFFENER LENGTH ON SKIN/STIFFENER LOAD DISTRIBUTION.

FINITE ELEMENT RESULTS FOR 5.5-inch LENGTH STIFFENER

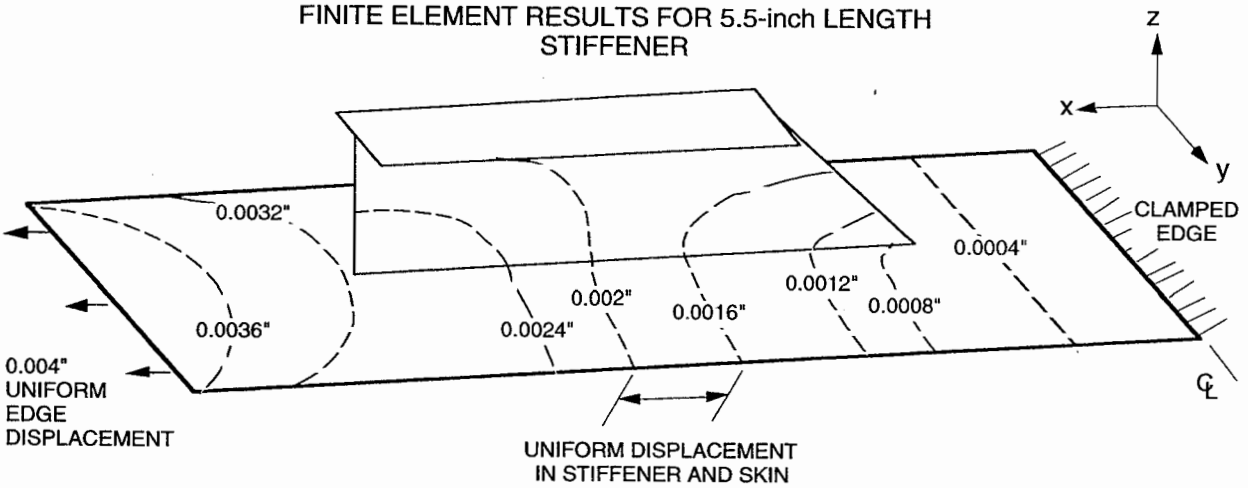

1. PARTIALLY LOADED STIFFENER

FINITE ELEMENT RESULTS FOR 10-inch LENGTH STIFFENER

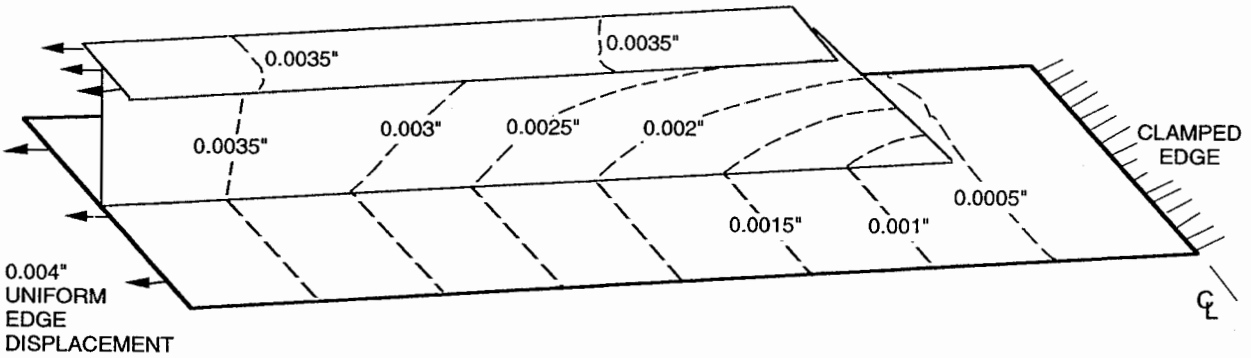

2. FULLY LOADED STIFFENER

- DISPLACEMENTS NEAR THE STIFFENER TERMINATION REGION ARE SIMILAR FOR THE TWO LOADING CONFIGURATIONS

F93-CS/20

FIGURE 7. PREDICTED AXIAL DEFORMATIONS FOR THE TWO LOADING CONFIGURATIONS.

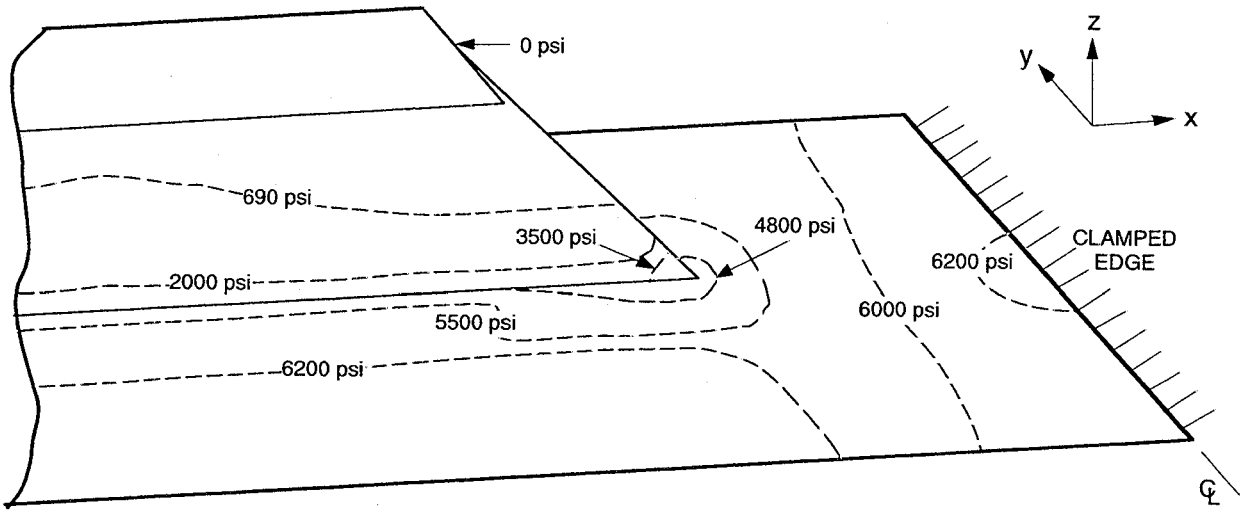

1. PARTIALLY LOADED STIFFENER

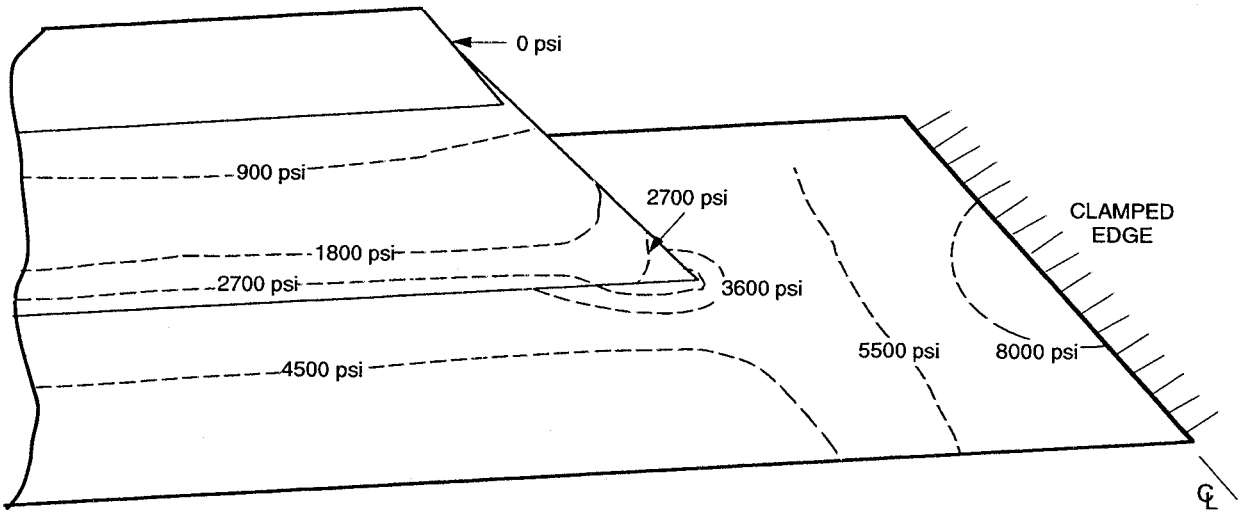

2. FULLY LOADED STIFFENER

•• AXIAL STRESSES NEAR STIFFENER TERMINATION REGION ARE SIMILAR FOR THE TWO LOADING CONFIGURATIONS

F93-CS/21

FIGURE 8. PREDICTED AXIAL STRESS DISTRIBUTION FOR THE TWO LOADING CONFIGURATIONS.

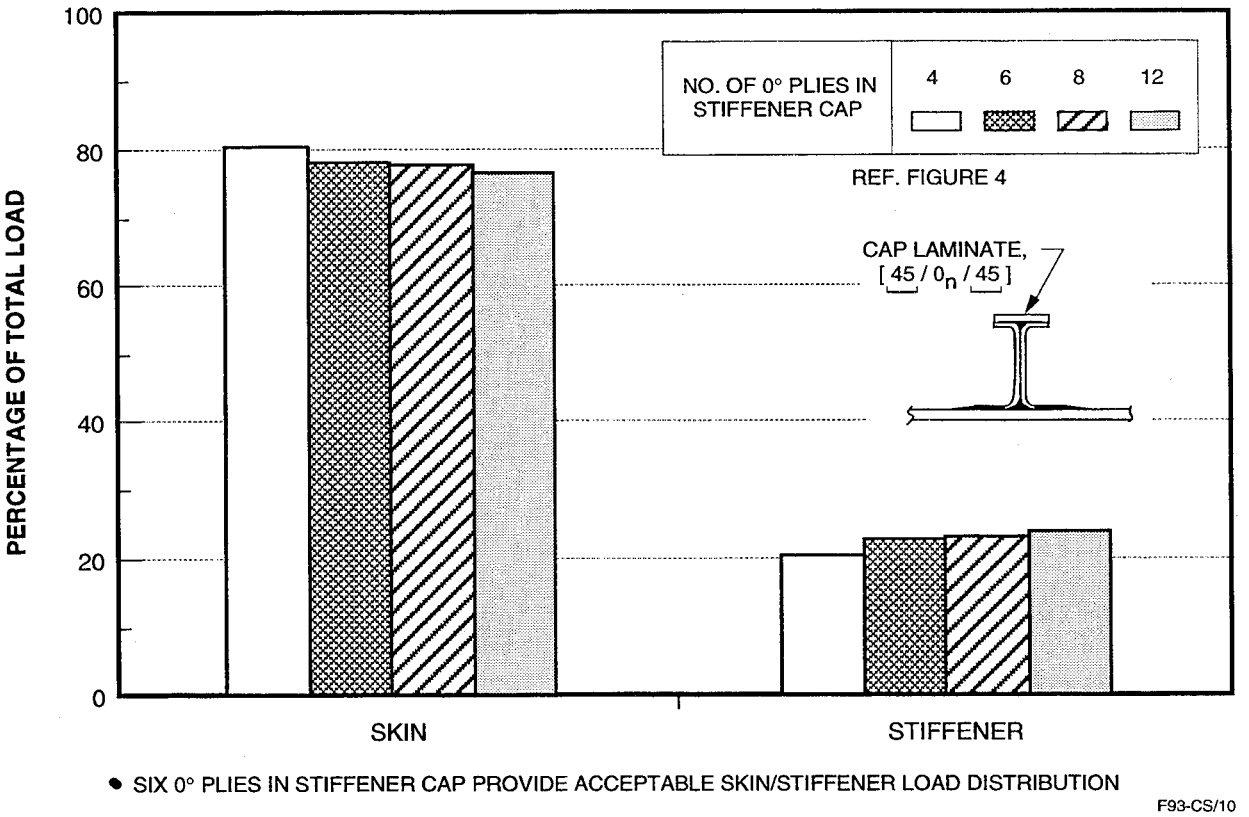

FIGURE 9. INFLUENCE OF NUMBER OF 0° PLIES IN CAP ON SKIN/STIFFENER LOAD DISTRIBUTION.

The final design configuration chosen was the partially-loaded stiffener configuration. The length of the stiffener for the test specimen chosen was 6 inches, which satisfies the 1-inch constant stress criterion. The stiffener cap included six plies of 0° tape, which insures that the stiffener will attract sufficient axial load to simulate a realistic stiffened skin design. The final test specimen design is shown in Figures 10 and 11. The engineering drawing for specimen fabrication can be found in the Appendix.

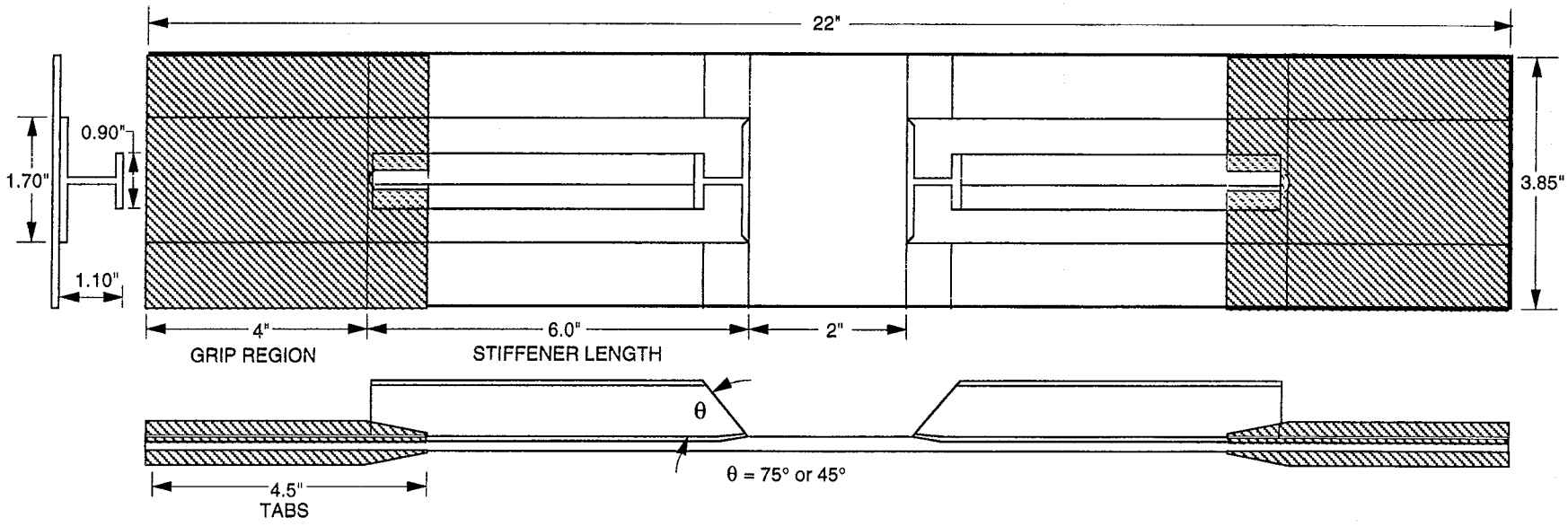

F95-CS/11

FIGURE 10. STIFFENER TERMINATION TEST SPECIMEN DESIGN.

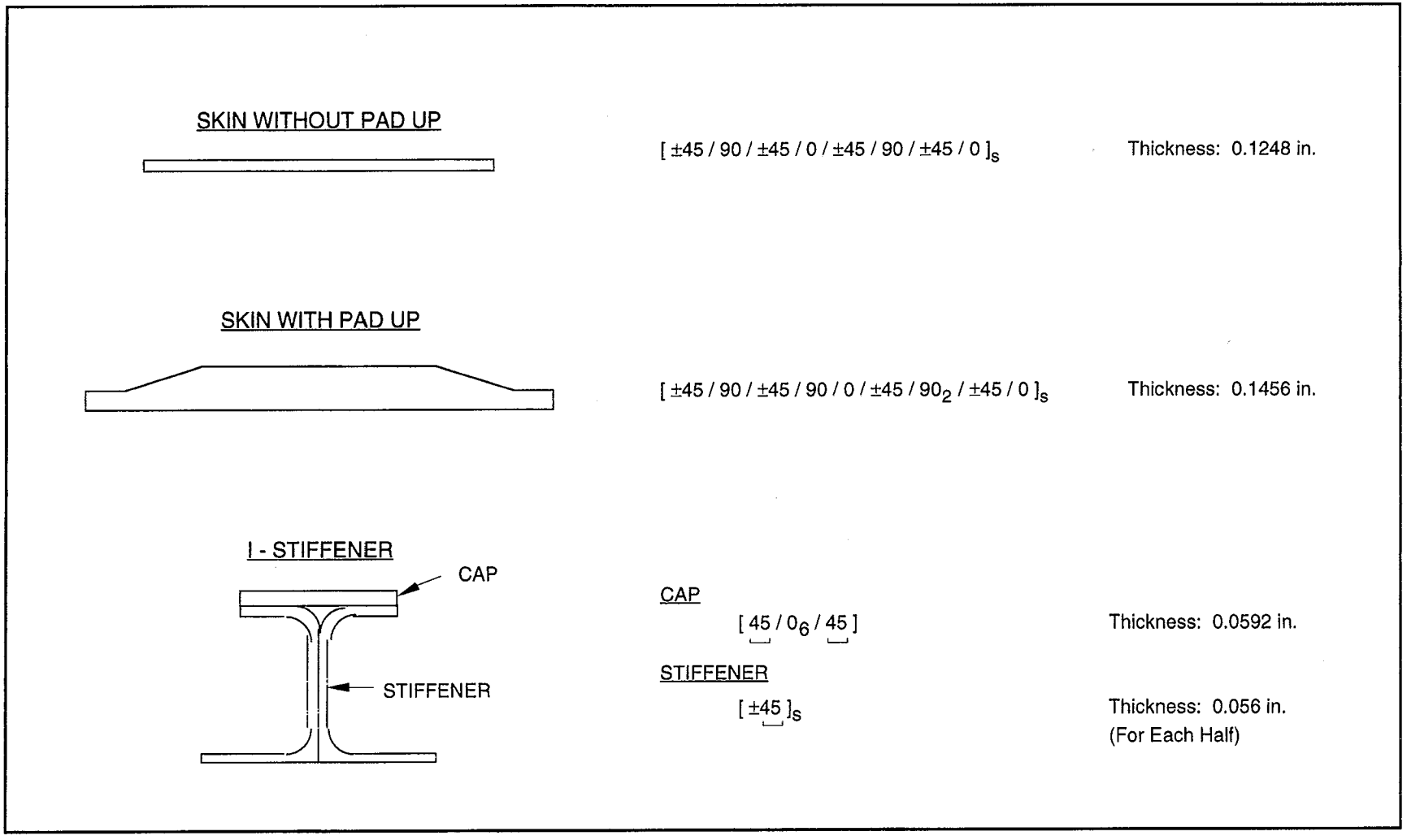

NOTE: PLY WITH ' ⌣ ' INDICATES BI-WOVEN AS4/3501-6. OTHERS ARE UNIDIRECTIONAL AS4/3501-6 PLIES.

F93-CS/16

FIGURE 11. SKIN AND STIFFENER LAYUP SEQUENCE DETAIL.

3. TEST PROGRAM.

In this section the development of the test matrix, fabrication of test specimens, test setup, and testing are discussed.

3.1 TEST MATRIX.

The test matrix for this program was developed based on certification considerations. The number of specimens required for baseline configuration tests had to be statistically viable. Both static and fatigue tests were considered. It was determined that an average of 5 specimens were needed for each test in the baseline category. Baseline category specimens had a 75° termination angle. Tests in this category included static tension and compression and compression-compression fatigue at R=10 for three different load levels. For verification tests other than the baseline category, 3 specimens were allocated. In this category, test specimens included 75° termination angles with fasteners in the stiffener flanges near termination angles and 45° termination angle specimens. The verification category tests were done for static compression and compression-compression fatigue at R=10 for one load level only.

The final test matrix is shown in Table 2, where specimens from different panels were scrambled in random fashion. Specimens were instrumented with axial strain gages in three different configurations as shown in Figures 12 through 14.

3.2 FABRICATION.

A computer aided design and manufacturing drawing was developed to aid in fabrication. Four test specimens were fabricated from one stiffened panel. A copy of this drawing is given in the Appendix. Hard and soft tools were designed and fabricated to manufacture the stiffened panel per the drawing. A schematic diagram of tooling is shown in Figure 15. A standard vendor (Hercules) supplied bagging techniques, and cure cycles were used in the fabrication. A total of 12 panels were fabricated. Each panel was nondestructively examined by C-scan and was found to be acceptable. The panels were machined into test specimens. A total of 48 test specimens were produced. Six- and 12-ply glass tabs were applied to each specimen using FM300M adhesive.

TABLE 2. STIFFENER TERMINATION TEST MATRIX.

GROUP	TERMINATION ANGLE	NUMBER OF TEST ELEMENTS(1)							SPARE	REMARKS
		STATIC				FATIGUE STRESS/ (2 & 5) NUMBER OF CYCLES				
						MAX. COMPRESSION LOAD, lbs				
		TENSION	COMPRES-SION	TENSION	COMPRES-SION	18500 $\sigma_1/(10^4)$	17000 $\sigma_2/(10^5)$	15000 $\sigma_3/(10^6)$		
		FIGURE 1 16 AXIAL STRAIN GAGES		FIGURE 2 8 AXIAL STRAIN GAGES		FIGURE 3 4 AXIAL STRAIN GAGES				
1	75°	7NB3 6NA1	9NB3 5NA2	10NA2 7NB4 2NA2 11NB3	8NB4 6NA2 4NB3 12NA1 10NB4(5) 11NA1(5) 1NA1(5)	9NB4(4) 8NA2(4) 2NB4 12NA2 11NA2 3NB4	10NA1 8NB3 6NB3 4NA2 1NA2 3NA1	9NA2 7NA1 5NB3 4NB4 12NB3 3NA2	3NB3	BASELINE
2	45°	—	—	—	5NA1(5) 1NB4 10NB3(5)	8NA1 6NB4 12NB4	—	—	2NA1	EFFECTS OF TERMINATION ANGLE
3	75°(3)	—	—	—	4NA1(5) 7NA2(5) 5NB4(5)	9NA1 2NB3 1NB3	—	—	11NB4	EFFECTS OF FASTENERS

NOTES:
(1) ALL TESTS AT RTA CONDITION
(2) FATIGUE TESTS AT CONSTANT AMPLITUDE WITH R= 10.0 (COMPRESSION/COMPRESSION) AT 3-5Hz
(3) INSTALL "CHICKEN RIVETS" THROUGH I-STIFFENER FLANGES AT BOTH ENDS OF STIFFENER
(4) MAXIMUM COMPRESSION LOAD OF 19000 lbs WAS APPLIED TO THESE FATIGUE SPECIMENS
(5) MODIFIED BUCKLING CONSTRAINTS WERE USED

F95-CS/12

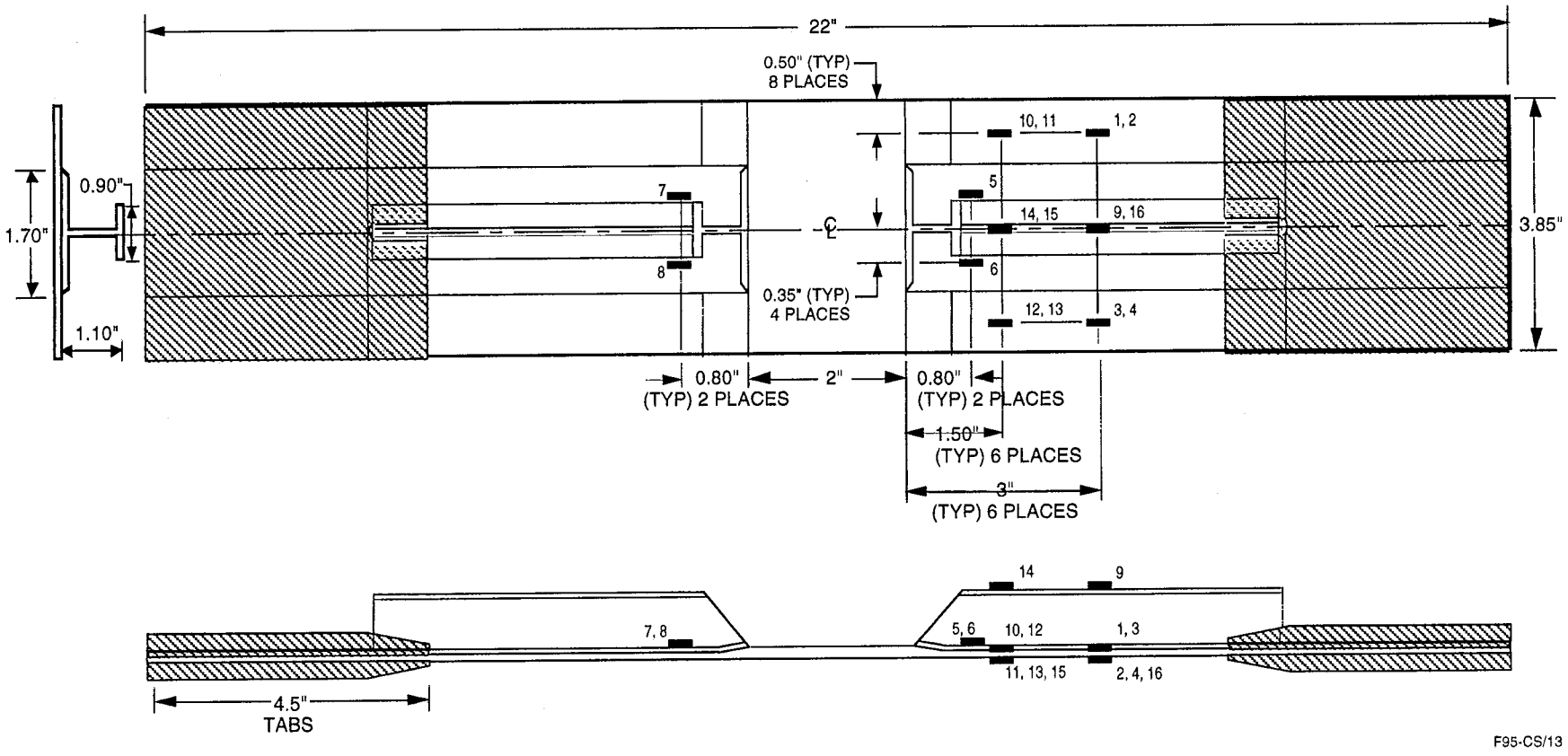

FIGURE 12. STRAIN GAGE LOCATIONS – 16 AXIAL GAGE CONFIGURATION.

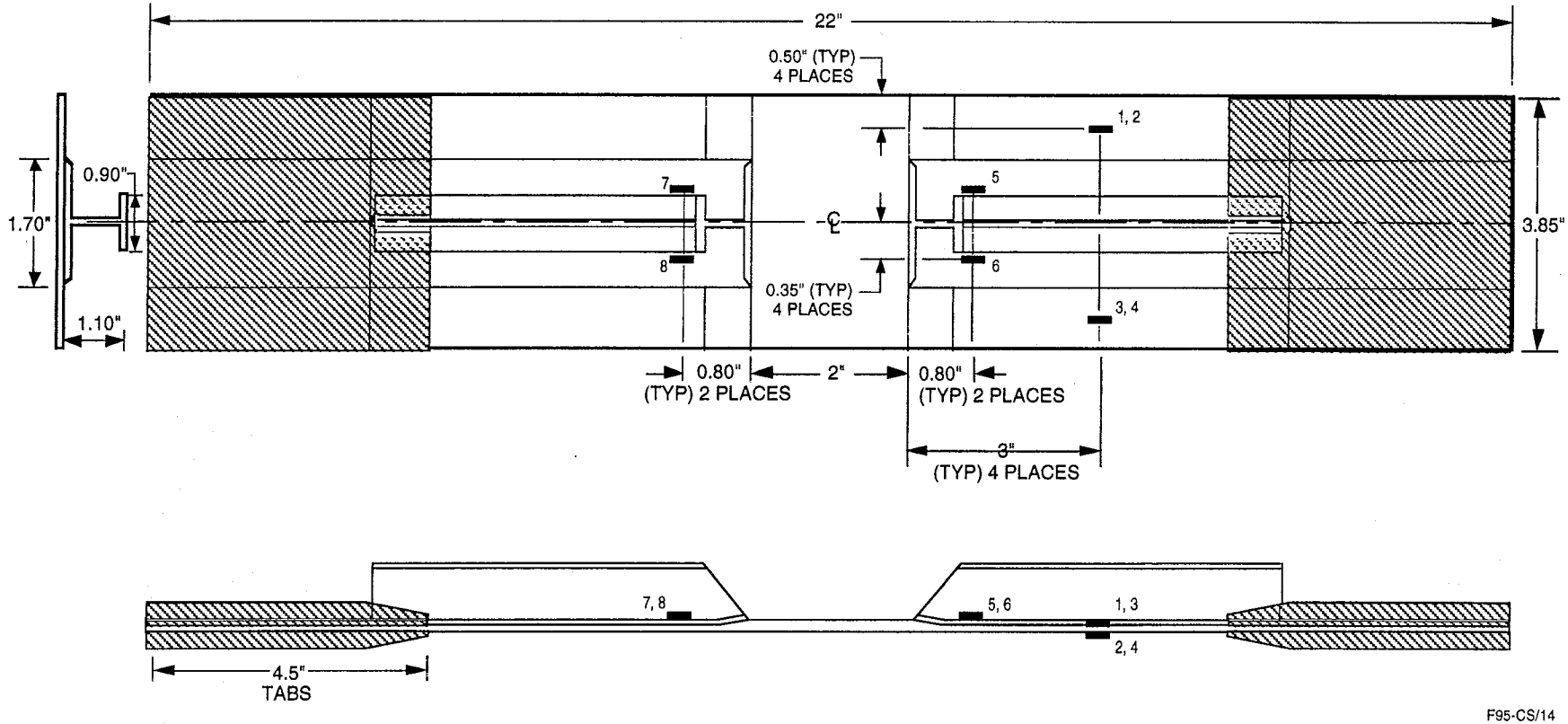

F95-CS/14

FIGURE 13. STRAIN GAGE LOCATIONS – 8 AXIAL GAGE CONFIGURATION.

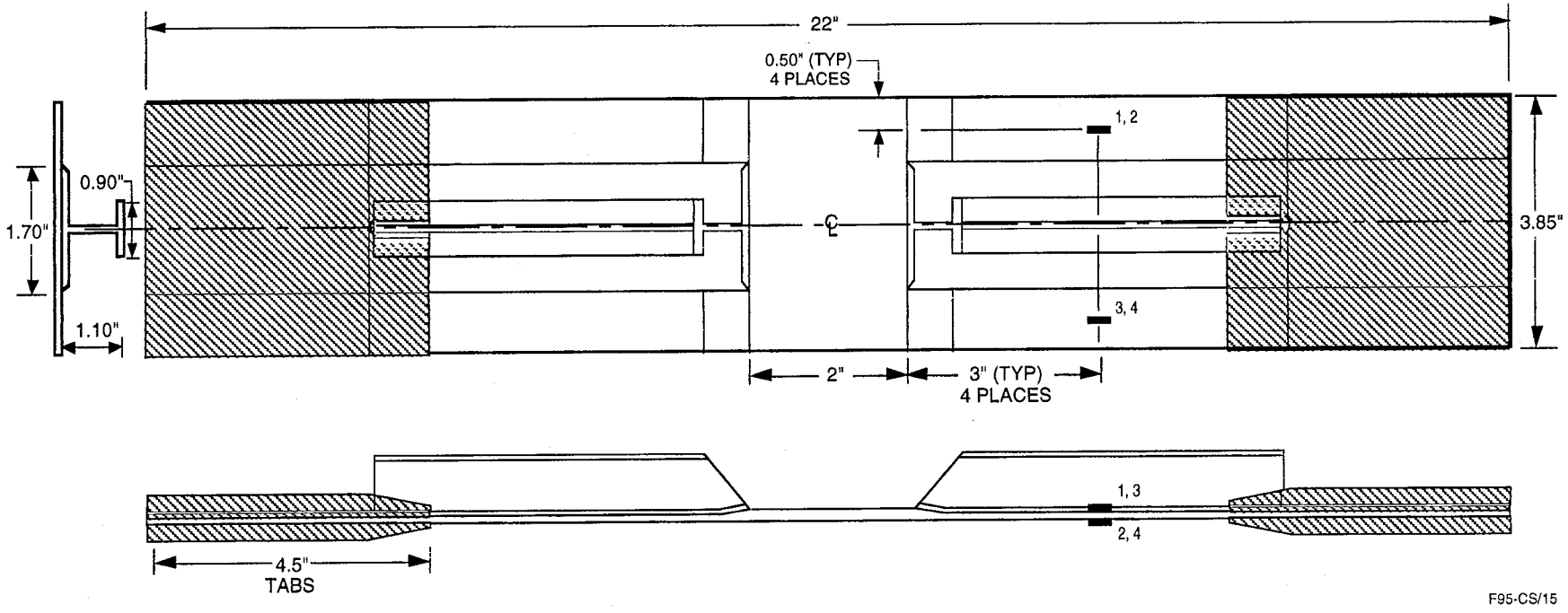

FIGURE 14. STRAIN GAGE LOCATIONS – 4 AXIAL GAGE CONFIGURATION.

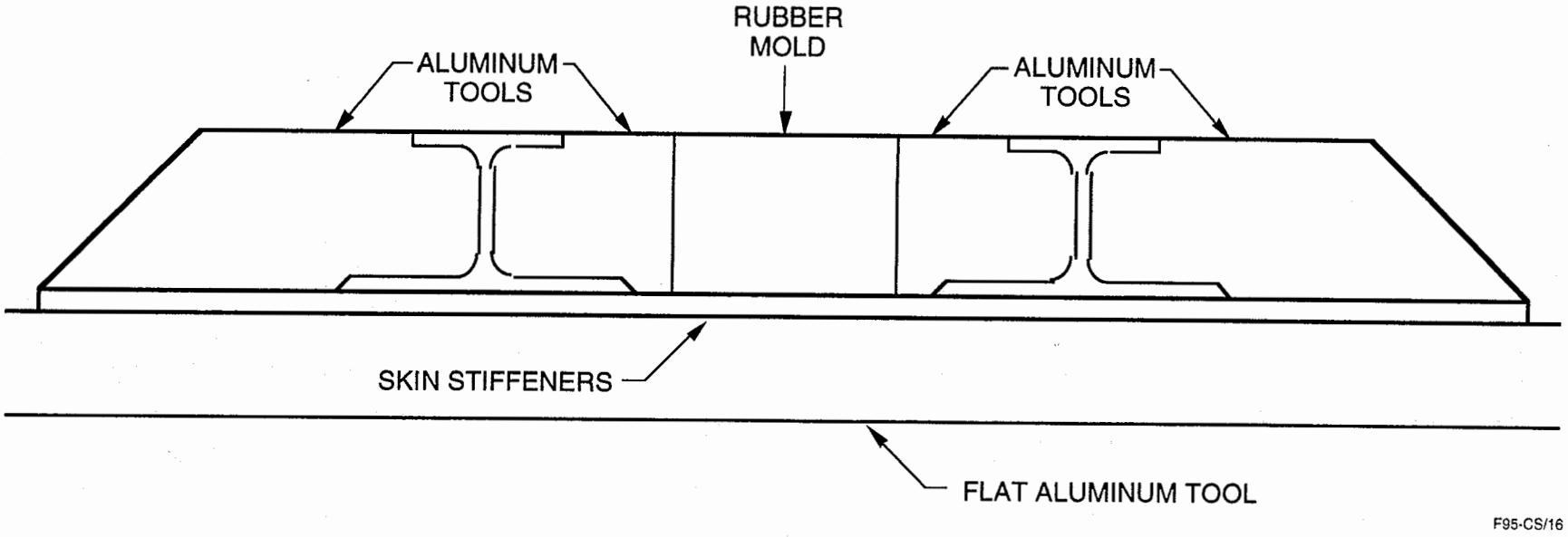

FIGURE 15. TOOLING SCHEMATIC.

3.3 TEST SETUP.

All static tests were performed in a 100-kip MTS test machine with 5000-psi hydraulic grips. Buckling constraint test fixtures were used for compression tests to prevent overall specimen buckling. A photograph of the compression test setup is shown in Figure 16, which depicts a 100-kip MTS machine with the buckling constraint test fixtures. The buckling constraint test fixtures were modified by inserting four machine screws (pins) to prevent buckling after the first seven specimens experienced local buckling failure rather than the intended compression failure. Photographs of modified buckling constraint test fixtures and compression specimens inside the fixtures are shown in Figures 17 and 18, respectively. In the tension test setup, buckling constraints were not used. Fatigue tests were performed in either 50-kip or 100-kip MTS machine with 5000-psi hydraulic grips. The fatigue tests were run in the compression-compression loading mode at R = 10. The fatigue test setup had the modified buckling constraint test fixtures which included four pins. The Cyber Data Acquisition System and Fluke Data Logger were used to acquire data.

3.4 TESTING.

The testing followed the order of the test matrix shown in Table 2. The static tension tests were performed first since they did not require any test fixturing except hydraulic grips. The static compression tests followed. The initial seven compression tests used the buckling constraint test fixtures without pins. The remaining compression tests and compression-compression fatigue tests at R = 10 were performed using the buckling constraint test fixtures with pins. The test results are discussed in detail in the following section.

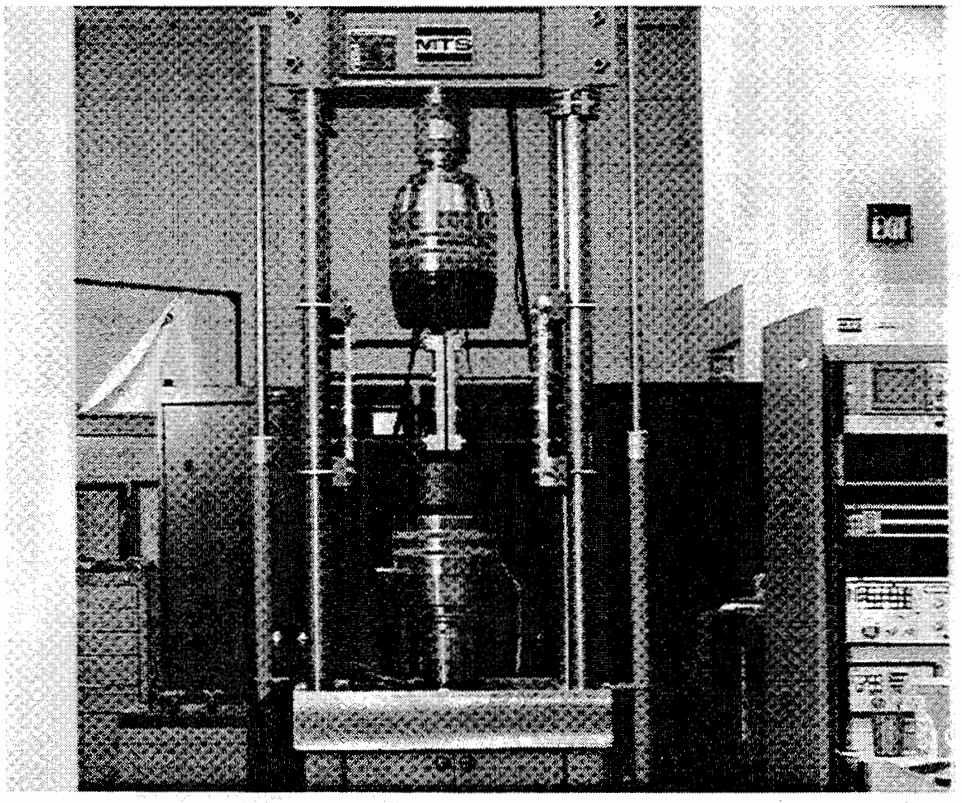

FIGURE 16. COMPRESSION TEST SETUP.

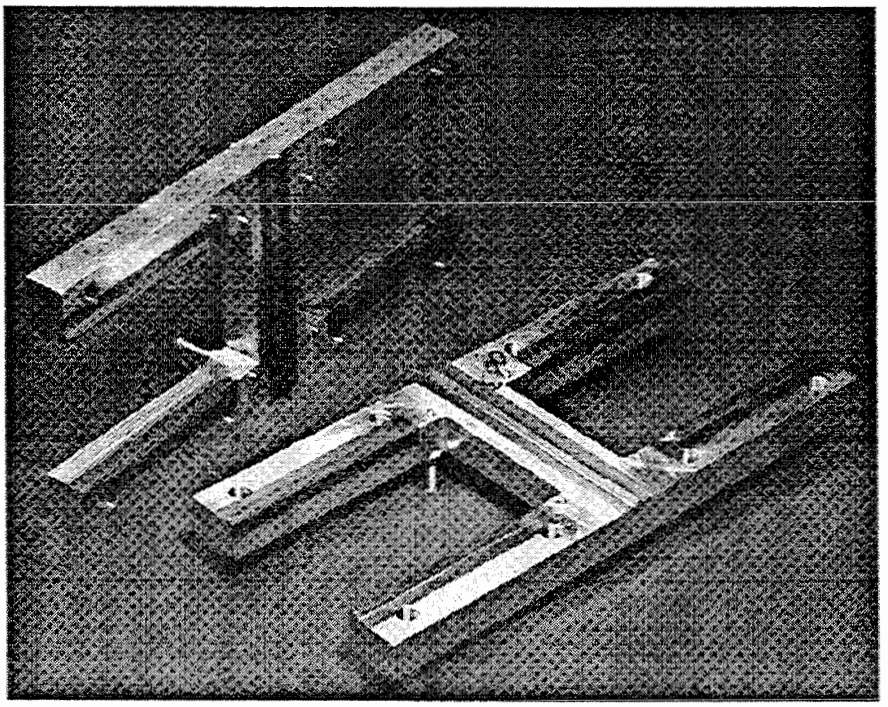

FIGURE 17. COMPRESSION TEST FIXTURES.

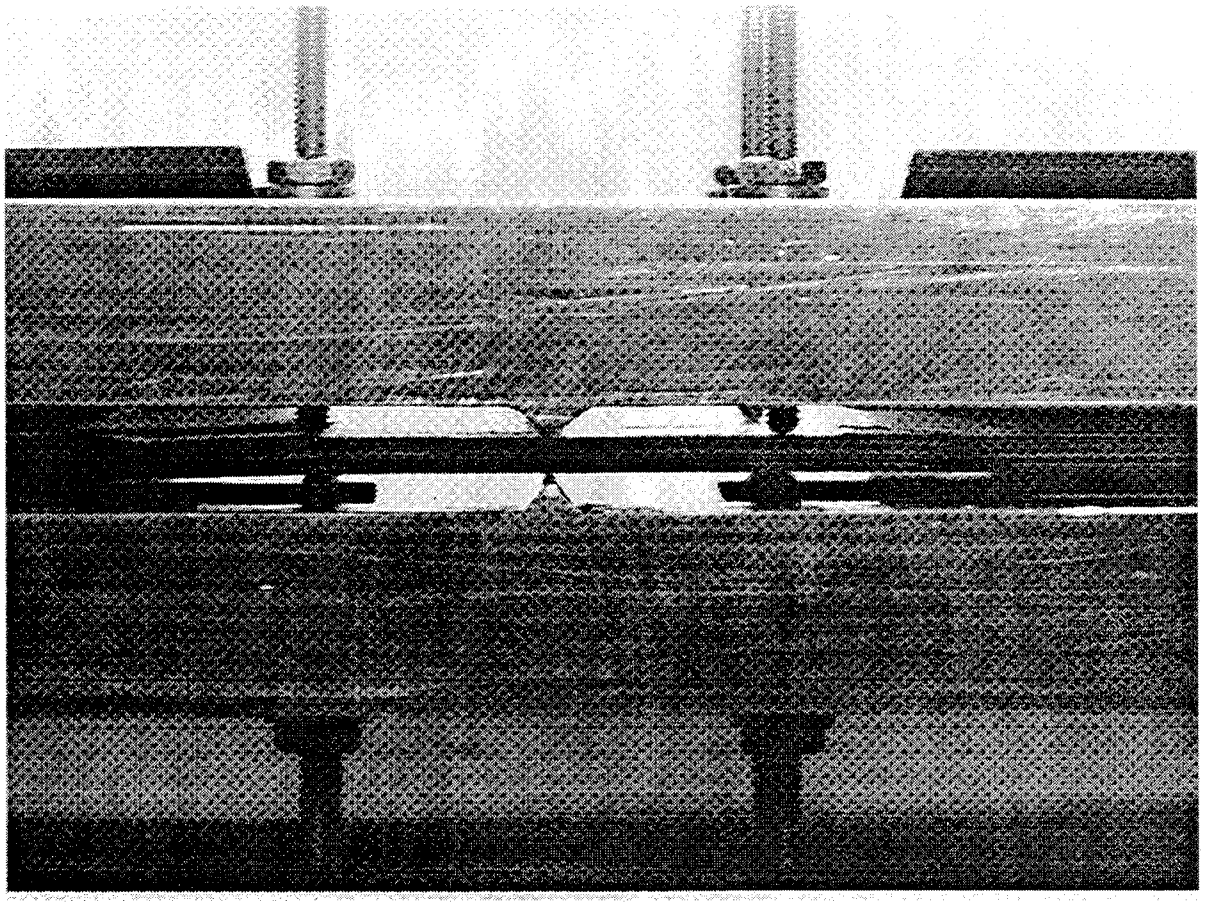

FIGURE 18. COMPRESSION SPECIMEN INSIDE TEST FIXTURE.

4. TEST RESULTS AND DISCUSSION.

A total of 21 static strength and 24 fatigue life tests were conducted under the experimental program. Static tensile and compressive strengths were obtained. Initial failure in the form of skin/stiffener separation was determined based on (1) load-deflection records (2) strain-load records and (3) test event records of noticeable noise during the tests. Fatigue specimens were tested to failure to measure the fatigue lives. However, the fatigue tests were suspended after 10^6 cycles or if it was determined that the growth of skin/stiffener separation had ceased. The latter specimens were tested statically in compression to determine residual strength. The results of the static strength and fatigue life tests are discussed in this section.

4.1 STATIC TESTS.

All static tests were performed in a 100-kip MTS machine. The tension tests were performed without test fixtures. The compression tests were performed by enclosing the test specimen inside buckling constraint test fixture. Test engineers and supporting personnel kept detailed records in an engineering log book during all the tests to assist in preparation of this report. The static tests are discussed in following two subsections.

4.1.1 Tension Tests.

Loads were applied and strains were recorded in two stages, first at 2,000-lb increments up to 10,000 lbs and then at 1,000-lb increments until catastrophic failure load. All tension tests were performed for baseline specimen with a 75° stiffener termination angle. Failure in tension test specimens initiated in the stiffener flanges (upper and/or lower stiffener flange) at the base of stiffener web at the stiffener termination ends. The tension test results are summarized in Table 3 and Figure 19. A photograph of a typical tension failure at a termination caused by interlaminar stresses is shown in Figure 20.

TABLE 3. SUMMARY OF STATIC TESTS.

TERMINATION ANGLE	SPECIMEN ID	INITIAL FAILURE LBS.	ULTIMATE FAILURE LBS
75° BASELINE	**TENSION TESTS(1)**		
	7NB3	21,500	25,000
	6NA1	22,500	27,090
	10NA2	22,500	28,000
	7NB4	21,500	24,070
	2NA2	20,500	26,900
	11NB3	19,500	23,720
	COMPRESSION TESTS: BUCKLING CONSTRAINTS WITHOUT PINS(2)		
	9NB3	-13,000	-16,690
	5NA2	-15,000	-18,040
	8NB4	(3)	-17,910
	6NA2	-15,000	-16,170
	4NB3	-14,000	-15,270
	12NA1	(3)	-16,450
	COMPRESSION TESTS: BUCKLING CONSTRAINTS WITH PINS(1)		
	10NB4	-24,000	-24,690
	11NA1	-22,000	-22,550
	1NA1	-21,400	-23,150
75° EFFECT OF FLANGE FASTENERS	**COMPRESSION TESTS: BUCKLING CONSTRAINTS WITH PINS(1)**		
	4NA1	-22,850	-23,970
	7NA2	-24,400	-26,520
	5NB4	(3)	-25,550
45° EFFECT OF TERMINATION ANGLE	**COMPRESSION TEST: BUCKLING CONSTRAINTS WITHOUT PINS(2)**		
	1NB4	(3)	-17,860
	COMPRESSION TESTS: BUCKLING CONSTRAINTS WITH PINS(1)		
	5NA1	(3)	-27,000
	10NB3	-26,000	-28,000

NOTES: (1) FAILURE WAS INITIATED BY INTERLAMINAR STRESSES.
(2) FAILURE WAS INDUCED BY BUCKLING.
(3) STRAIN GAGE RESPONSE DID NOT REVEAL INITIATION OF FAILURE PRIOR TO ULTIMATE FAILURE IN THESE SPECIMENS.

F95-CS/20

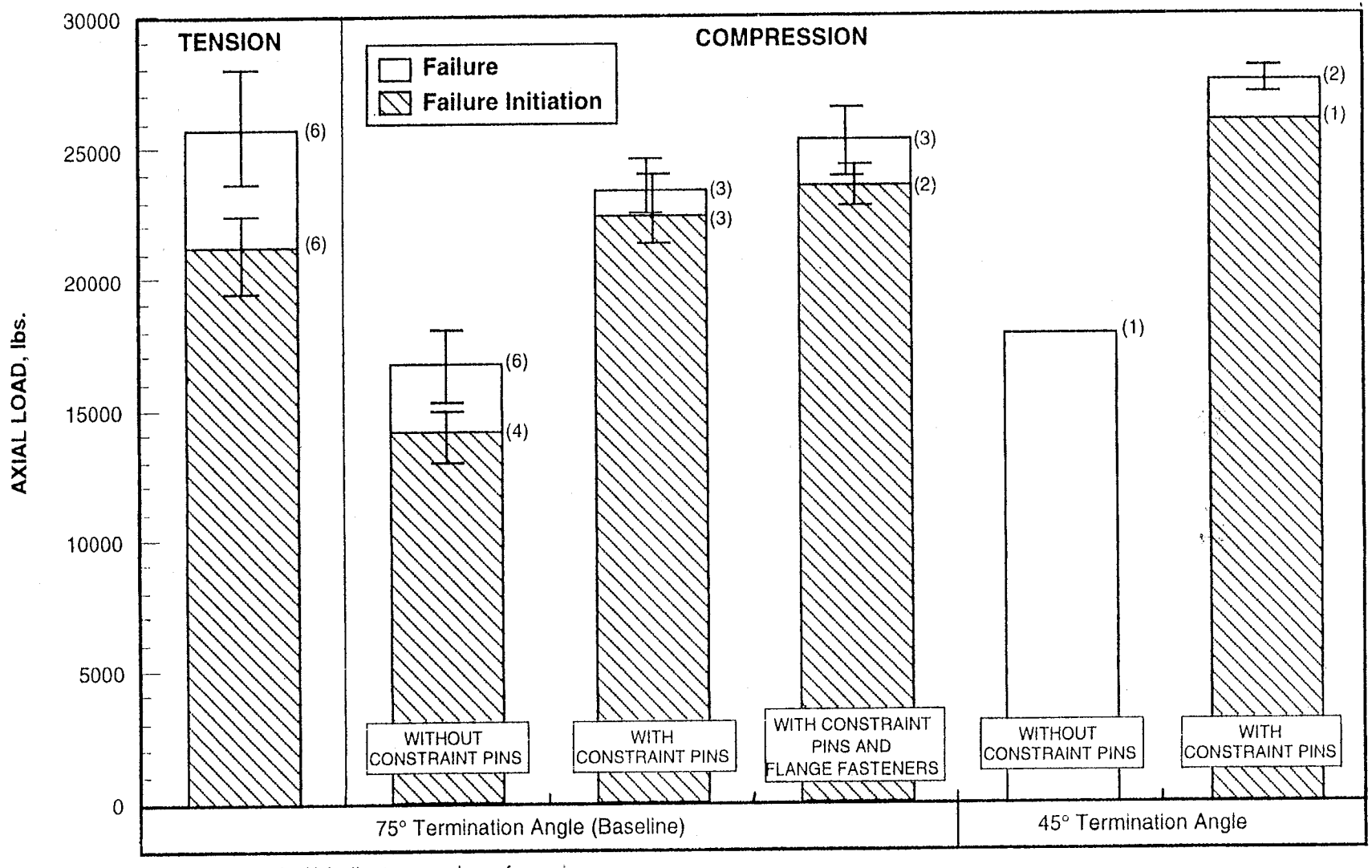

Note: Number in ( ) indicates number of specimens.

F95-CS/22

FIGURE 19. STATIC TEST RESULTS – TENSION AND COMPRESSION.

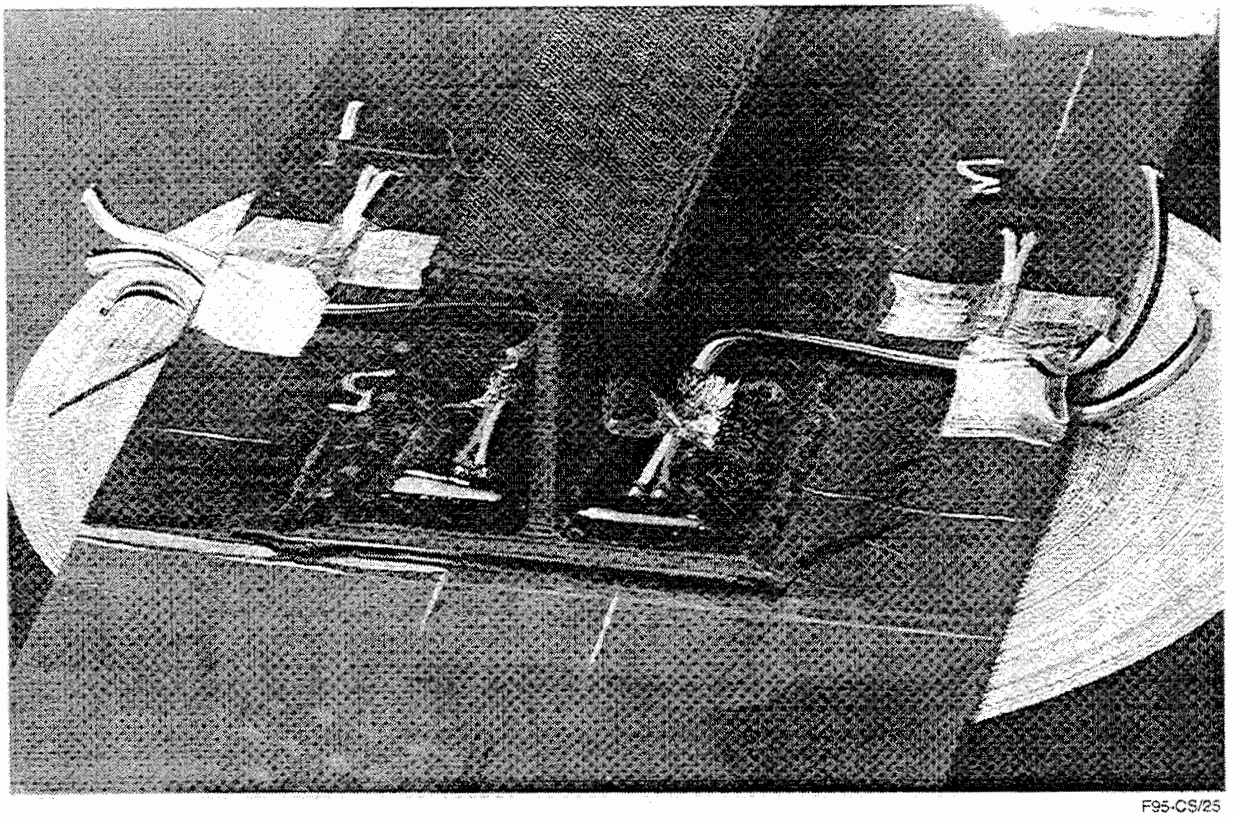

F95-CS/25

FIGURE 20. TYPICAL FAILURE - STATIC TENSION.

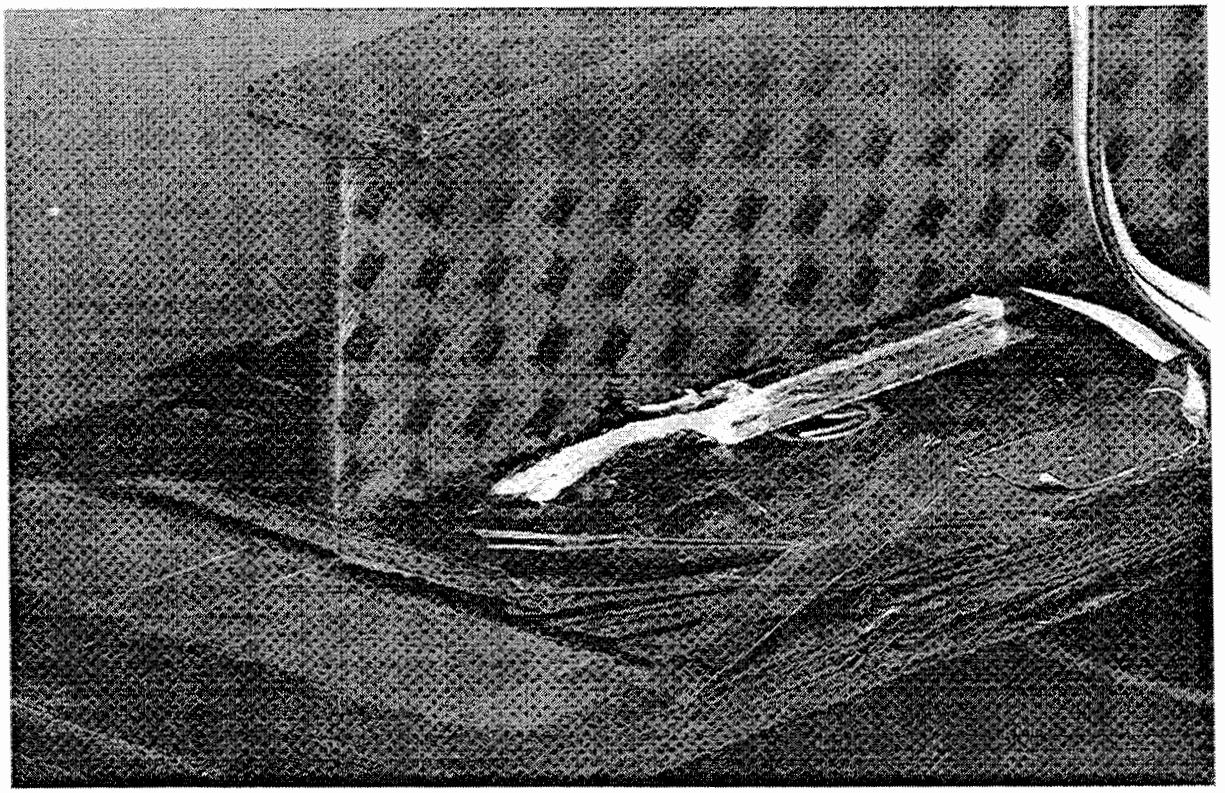

F95-CS/26

FIGURE 21. BUCKLING INDUCED FAILURE IN STATIC COMPRESSION.

4.1.2 Compression Tests.

Each compression test was performed in two phases. In Phase I, the loads were applied and strains were recorded at 2,000-lb increments up to 10,000 lbs. The compression tests were stopped at 10,000 lb to validate proper installation of the test specimen in the 100-kip MTS machine. This was done by keeping the through-thickness and the through-width strains within five percent of the mean strain value. In Phase II, loads were applied in three stages. In the first stage, loads were once again applied at 2,000-lb increments up to 10,000 lb. In the second and third stages, the loads were applied at 1,000-lb increments up to 15,000 lb, and at 500-lb increments until catastrophic failure load, respectively. Compression tests were performed for three groups of specimens. The first group of baseline specimens had the 75° stiffener termination angle. The second group of specimens had a 45° stiffener termination angle to evaluate the effect of varying the termination angle. The third group of specimens featured a 75° stiffener termination angle, with 3/16" diameter HiLok bolts installed in the stiffener flanges near the stiffener termination. The compression test results are also summarized in Table 3 and Figure 19.

As stated in Section 3, the compression tests were performed using two different buckling constraint test fixtures. The first seven tests (six specimens from Group 1 and one from Group 2) were performed using the original buckling test fixture. These seven test specimens failed by local buckling induced skin/stiffener separation at the stiffener termination ends. A photograph of typical local buckling induced failure for a baseline Group 1 specimen is shown in Figure 21. The failure was induced by out-of-plane displacement following local buckling of the 2-inch unsupported region in the midsection of the specimens. The buckling failure phenomenon was not very easy to recognize. The close monitoring of the compression tests six and seven elicited the buckling induced failure. For the subsequent tests, the buckling constraint test fixture was modified by inserting custom designed, machined screws at four locations such that the length of the unsupported region in the midsection of the specimen was reduced to 1 inch. These modifications effectively prevented local buckling in the subsequent compression tests. Photographs of the modified buckling constraint test fixture with pins and with a specimen inside the test fixture are shown in Figures 17 and 18, respectively. The failures in the remainder of the specimens from all three groups were initiated by interlaminar stresses. Photographs of typical failures are shown in Figures 22 and 23.

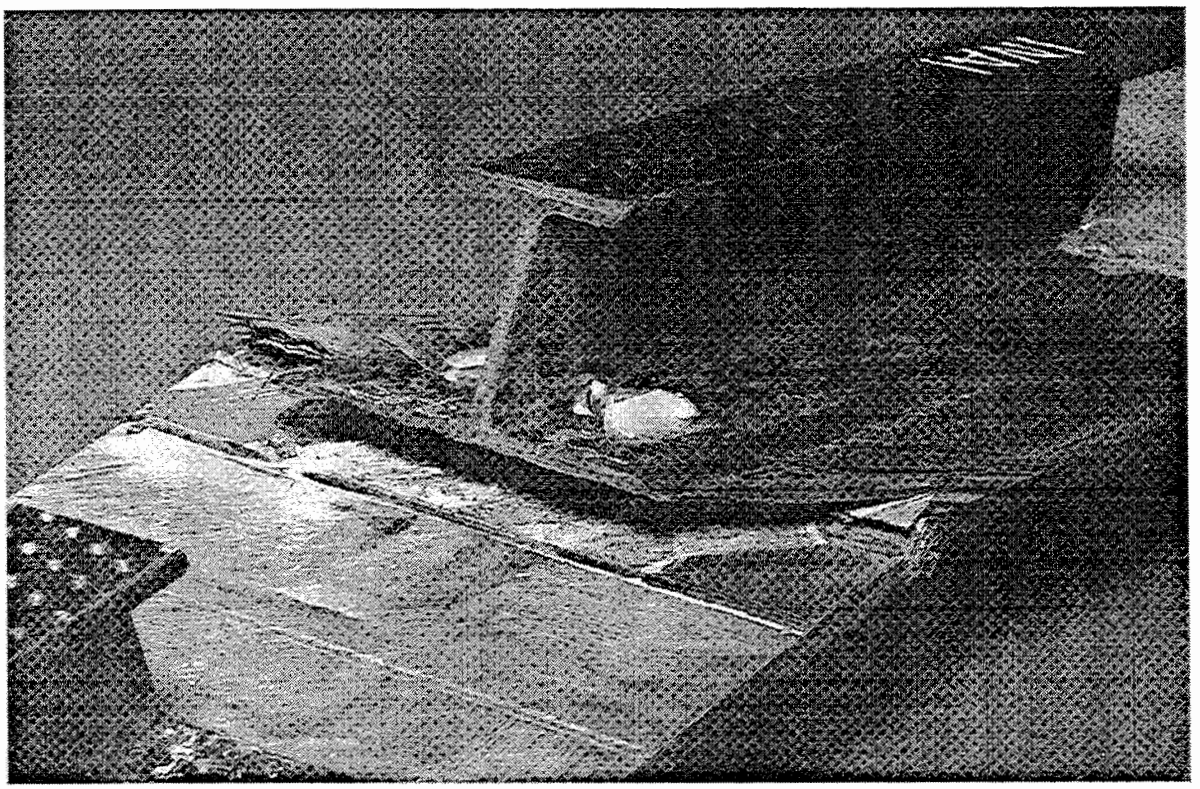

F95-CS/27

FIGURE 22. INTERLAMINAR STRESSES INITIATED FAILURE IN STATIC COMPRESSION.

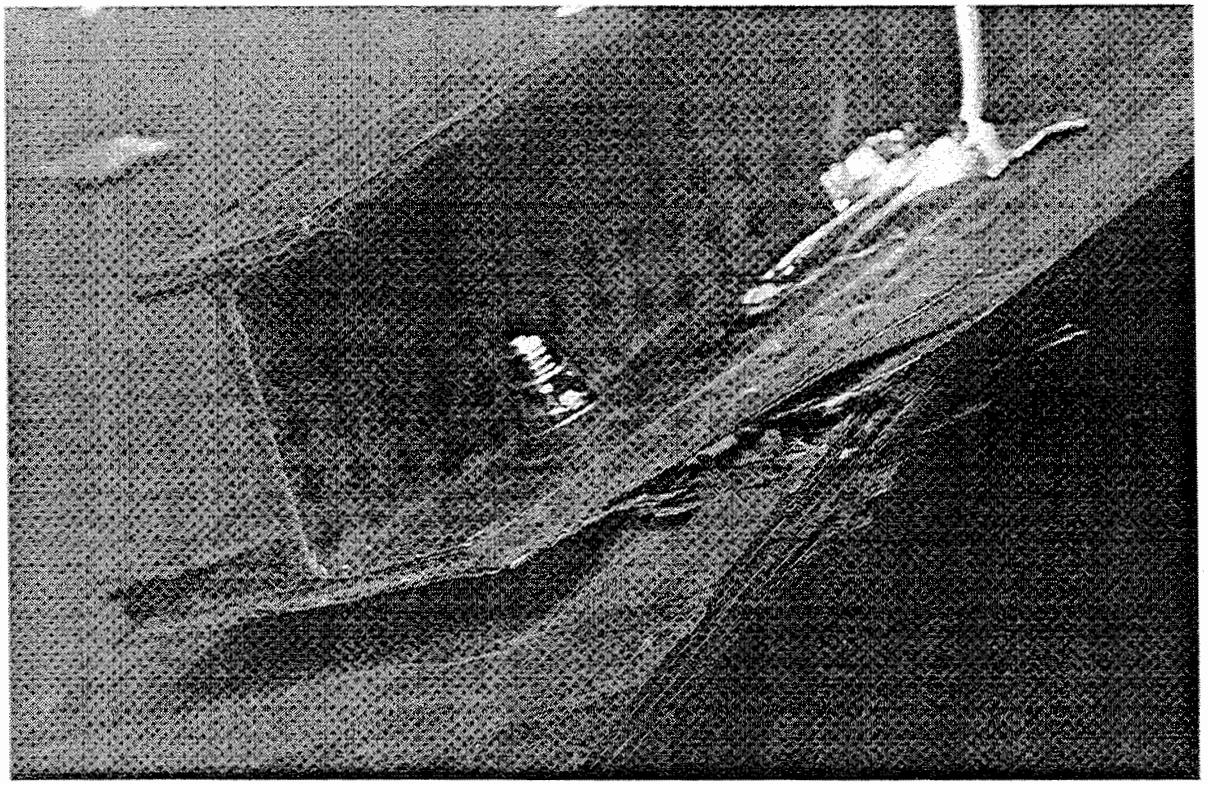

F95-CS/28

FIGURE 23. INTERLAMINAR STRESSES INITIATED FAILURE IN STATIC COMPRESSION - FLANGE FASTENERS EFFECT.

4.2 FATIGUE TESTS.

Compression-compression fatigue tests were conducted at R = 10 using modified buckling constraint test fixtures with pins. The Group 1 baseline test specimens were tested at four different maximum load levels and were cycled to catastrophic failure or to 10^6 cycles (runout), whichever came first. The specimens which were fatigue tested to runout were also tested statically in compression to determine residual strength. The Group 2 and 3 specimens were tested at only one load level. The Group 3 specimens which had fasteners through the stiffener flanges near the stiffener termination ends were tested to $3x10^5$ cycles. In this case, it was determined that failure had already initiated and that the fasteners were preventing the failure from propagating. This group of specimens was also tested statically in compression to determine residual strength. In the fatigue specimens, the interlaminar stresses (see σ_z and σ_{xz} in Figure 3c) were responsible for initiating failure. The fatigue tests were also performed on all three groups of specimens as were the compression tests. The test results are summarized in Table 4 and Figure 24.

TABLE 4. SUMMARY OF FATIGUE TESTS AT R=10 (1)

TERMINATION ANGLE	SPECIMEN ID	MAXIMUM FATIGUE LOAD LBS.	CYCLES TO INITIAL FAILURE	CYCLES TO FAILURE OR RUNOUT	RUNOUT RESIDUAL STRENGTH LBS.
75° BASELINE	9NB4	-19,000	880	1,040	—
	8NA1	-19,000	500	500	—
	2NB4	-18,500	30,000	80,230	—
	12NA2	-18,500	6,950	6,950	—
	11NA2	-18,500	5,630	5,630	—
	3NB4	-18,500	13,630	24,220	—
	10NA1	-17,000	20,730	27,450	—
	8NB3	-17,000	3,000	23,120	—
	6NB3	-17,000	24,150	24,150	—
	4NA2	-17,000	60,670	60,670	—
	1NA2	-17,000	5,000	184,040	—
	3NA1	-17,000	50,000	285,210	—
	9NA2	-15,000	438,000	438,000	—
	7NA1	-15,000	70,760	$>10^6$	-21,550
	5NB3	-15,000	70,000	$>10^6$	-19,870
	4NB4	-15,000	150,000	813,530	—
	12NB3	-15,000	880,000	$>10^6$	-22,410
	3NA2	-15,000	220,000	$>10^6$	-22,550
75° EFFECT OF FLANGE FASTENERS	9NA1	-18,500	3030	$>3 \times 10^5$	-24,550
	2NB3	-18,500	20,000	$>3 \times 10^5$	-28,567
	1NB3	-18,500	30,000	$>3 \times 10^5$	-26,120
45° EFFECT OF TERMINATION ANGLE	8NA1	-18,500	4600	37,880	—
	6NB4	-18,500	10,120	10,120	—
	12NB4	-18,500	10,000	35,740	—

NOTE: (1) ALL TESTS WERE CONDUCTED WITH BUCKLING CONSTRAINT TEST FIXTURES WITH PINS.

F95-CS/21

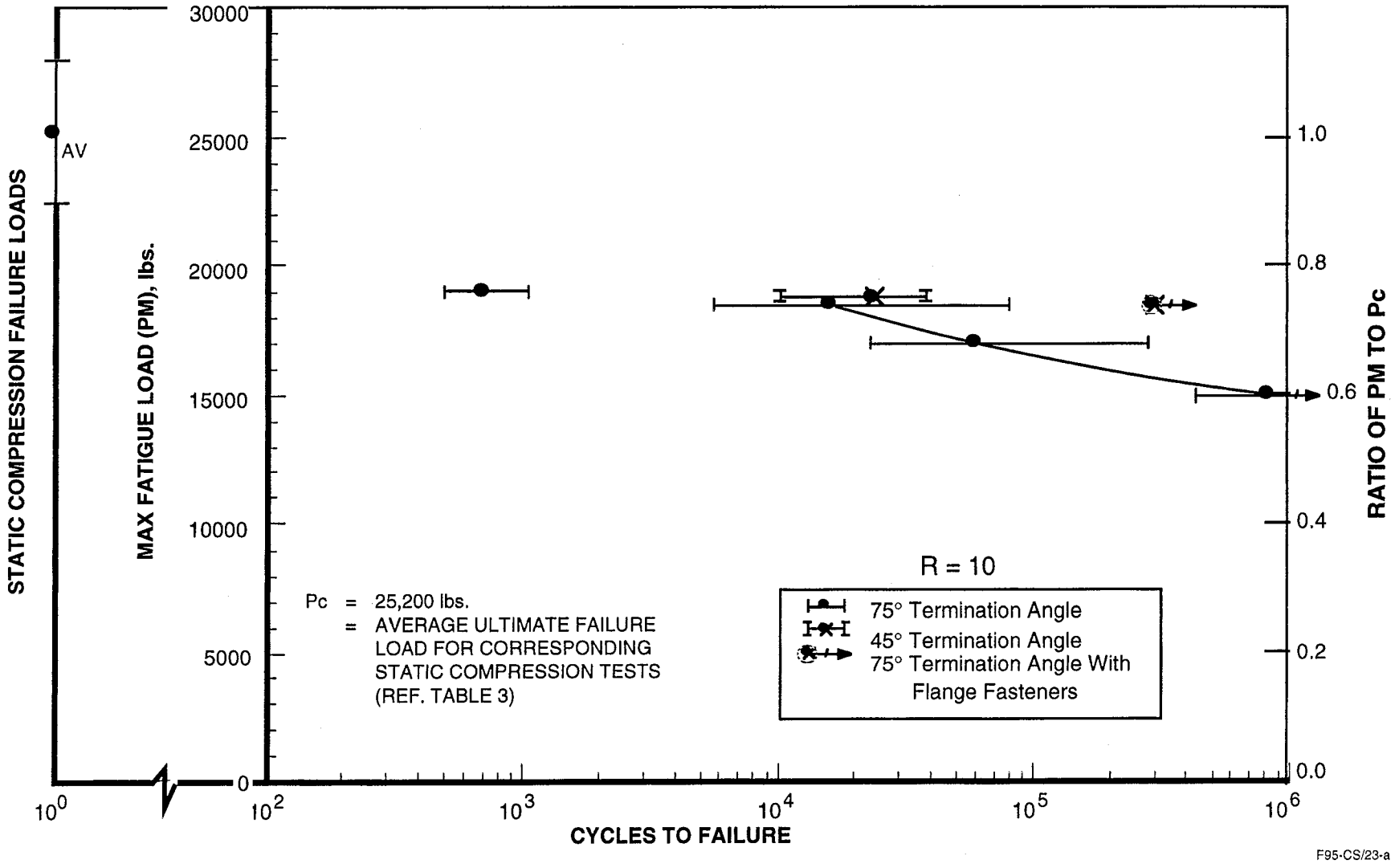

FIGURE 24. COMPRESSION-COMPRESSION FATIGUE TEST RESULTS AT R = 10.

5. ANALYSIS AND CORRELATION.

Two levels of analysis were conducted to evaluate the stress/strain distribution and to predict the strength of composite structures with stiffener terminations. The finite element method (FEM) was used to analyze the global specimen configuration. This method was used to assist specimen design and to verify the stress/strain distribution within the specimen. A two-dimensional finite element code, COSMOS/M, was employed for this purpose. Local analysis, using the elasticity method, was used to simulate the failure at the stiffener termination site. The out-of-plane stress analysis code, WEBSTER, developed in Reference 1, was used for stiffener separation prediction. Details of these analyses are discussed in Sections 5.1 and 5.2.

In addition to the stress analyses, a statistical analysis was also conducted to determine the scatter in the static strength and fatigue life data in order to formulate a certification procedure. The scatter analysis is discussed in Section 5.3.

5.1 FINITE ELEMENT ANALYSIS.

Finite element analysis was used to simulate the global response of the specimen to the applied load. This analysis method was also used in the test specimen design as discussed in Section 2. A two-dimensional finite element model using 3-D space was used for the test specimen analysis. Analyses were conducted for both tension and compression applied loads. For the compression specimens with antibuckling pins, additional constraints were imposed to prevent out-of-plane displacement. The computed strains at the strain gage locations were compared to experimental data. The analytical results and test data correlations are discussed in the following paragraphs.

For the specimens loaded in tension, strain gage data were grouped based on gage location to correlate with analysis results. A summary of the analytical results and test data comparison is given in Table 5 (see Figures 12 and 13 for strain gage locations), and details of the comparisons are shown in Figures 25 through 33. Results from specimens 7NB3, 6NA1, 10NA2, 7NB4, 2NA2 and 11NB3 are included in these comparisons.

TABLE 5. SUMMARY OF ANALYSIS AND EXPERIMENTAL DATA CORRELATION FOR STATIC TENSION SPECIMENS.

STRAIN GAGE LOCATIONS	STRAIN GAGE GROUP/NUMBER	DESCRIPTION	OVERALL PREDICTED STRAIN / AVE. MEASURED STRAIN
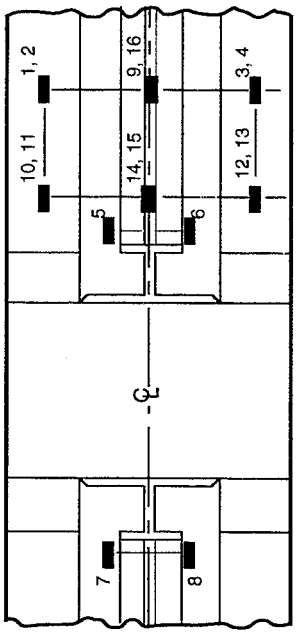	A 1, 3	SKIN STRAIN, STIFFENER FACE, FAR FIELD	0.957
	B 2, 4	SKIN STRAIN, FLAT FACE, FAR FIELD	1.019
	C 5, 6, 7, 8	STIFFENER FLANGE STRAIN	1.077
	D 9	STIFFENER CAP STRAIN, FAR FIELD	1.864
	E 10, 12	SKIN STRAIN, STIFFENER FACE, NEAR TERMINATION	0.935
	F 11, 13	SKIN STRAIN, FLAT FACE, NEAR TERMINATION	1.016
	G 14	STIFFENER CAP STRAIN, NEAR TERMINATION	0.968
	H 15	℄ SKIN STRAIN NEAR TERMINATION	1.020
	I 16	℄ SKIN STRAIN FAR FIELD	0.987

F95-CS/55

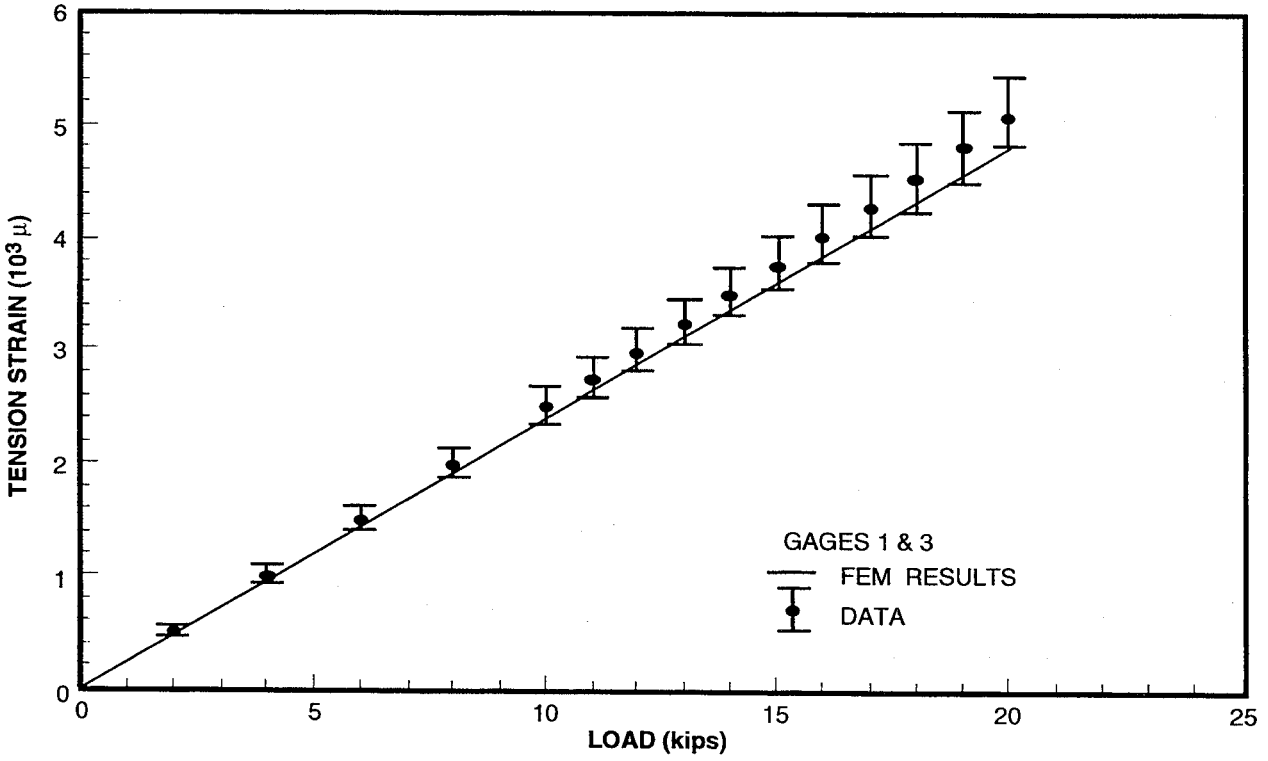

F95-2/1(HC)

FIGURE 25. COMPARISON OF MEASURED AND PREDICTED STRAINS FOR STRAIN GAGE GROUP A OF THE TENSION SPECIMENS.

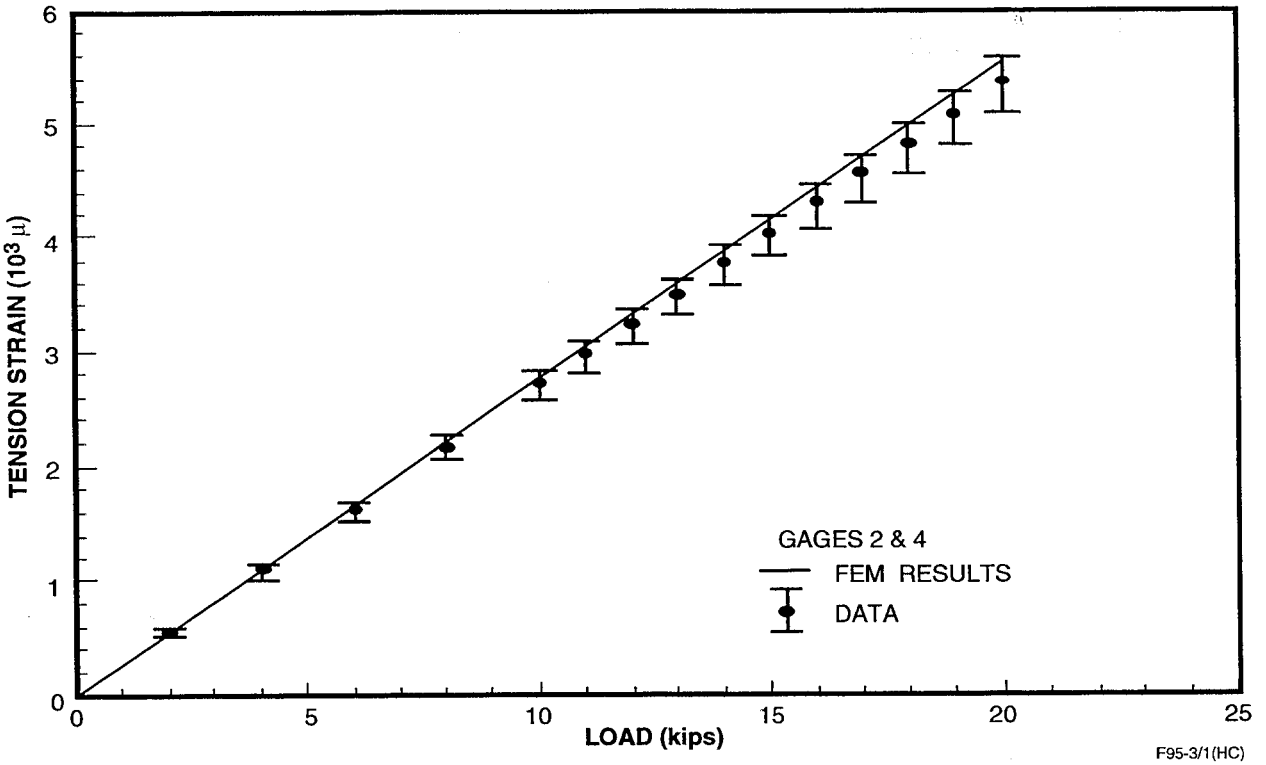

FIGURE 26. COMPARISON OF MEASURED AND PREDICTED STRAINS FOR STRAIN GAGE GROUP B OF THE TENSION SPECIMENS.

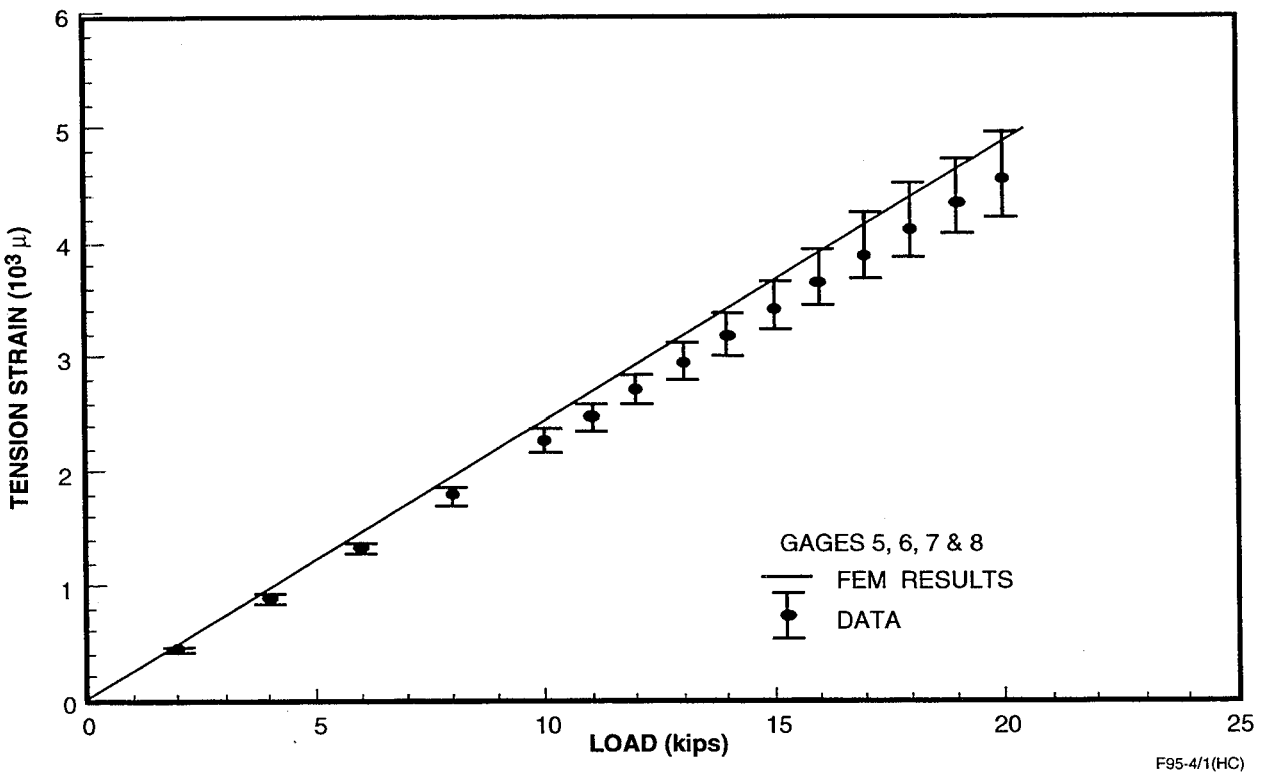

FIGURE 27. COMPARISON OF MEASURED AND PREDICTED STRAINS FOR STRAIN GAGE GROUP C OF THE TENSION SPECIMENS.

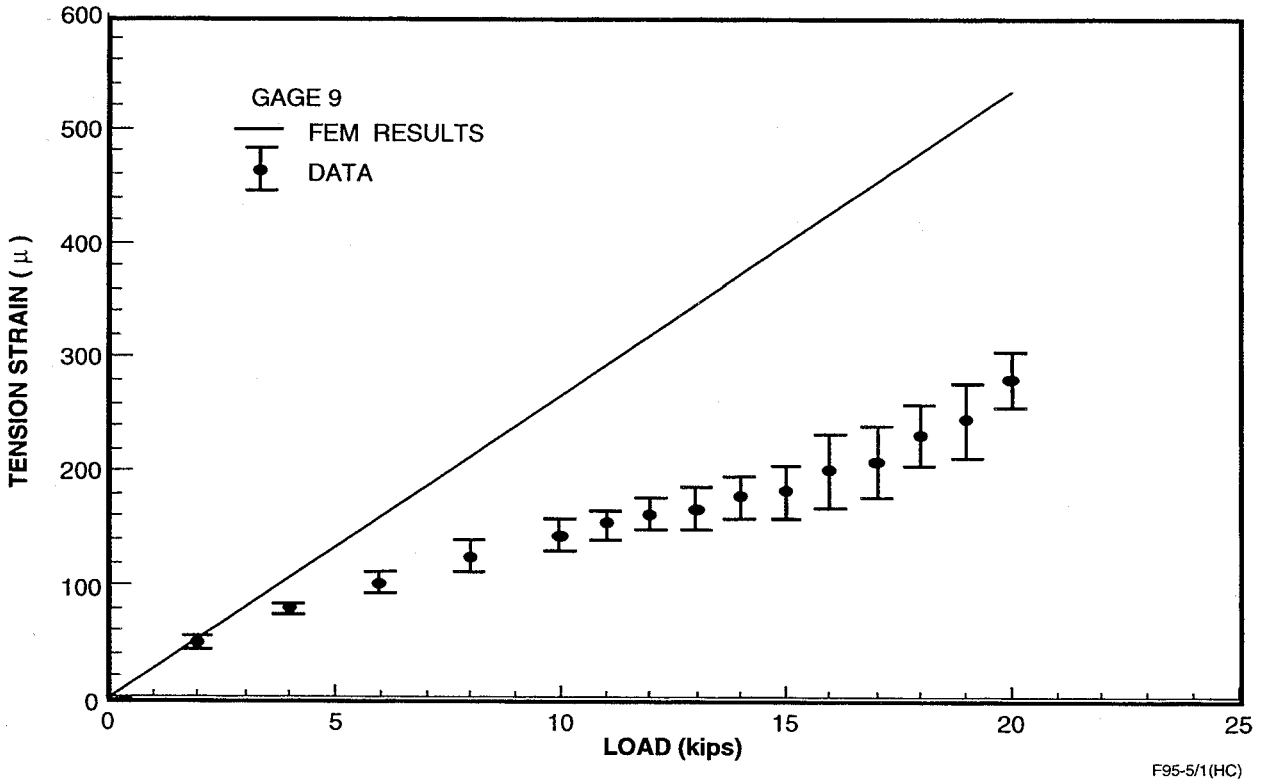

FIGURE 28. COMPARISON OF MEASURED AND PREDICTED STRAINS FOR STRAIN GAGE GROUP D OF THE TENSION SPECIMENS.

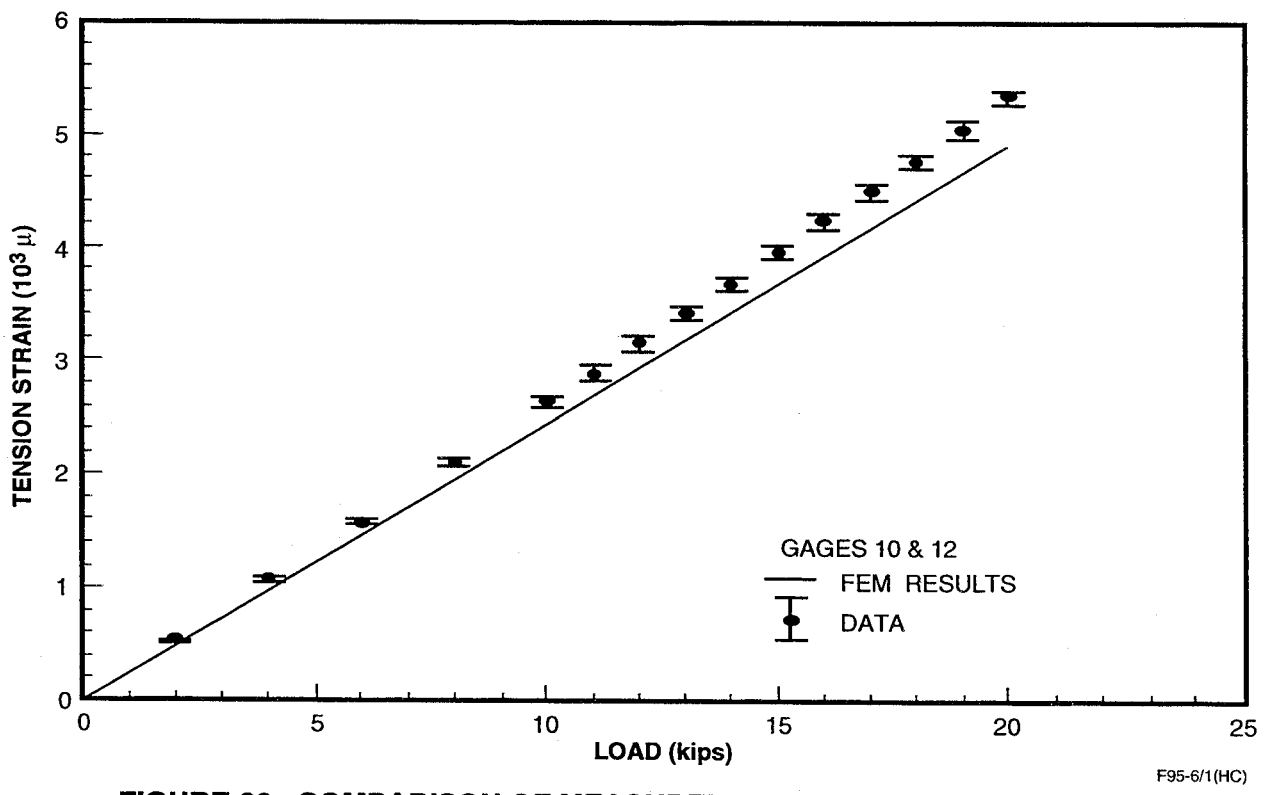

FIGURE 29. COMPARISON OF MEASURED AND PREDICTED STRAINS FOR STRAIN GAGE GROUP E OF THE TENSION SPECIMENS.

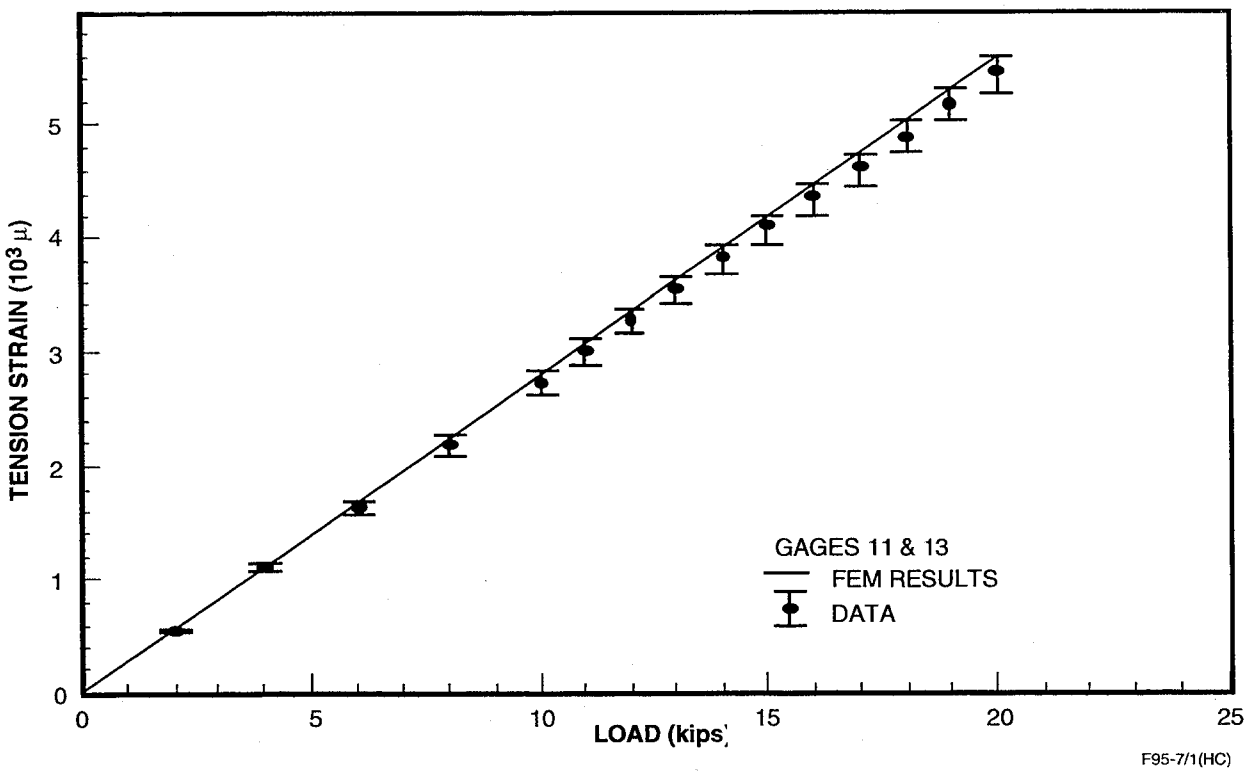

FIGURE 30. COMPARISON OF MEASURED AND PREDICTED STRAINS FOR STRAIN GAGE GROUP F OF THE TENSION SPECIMENS.

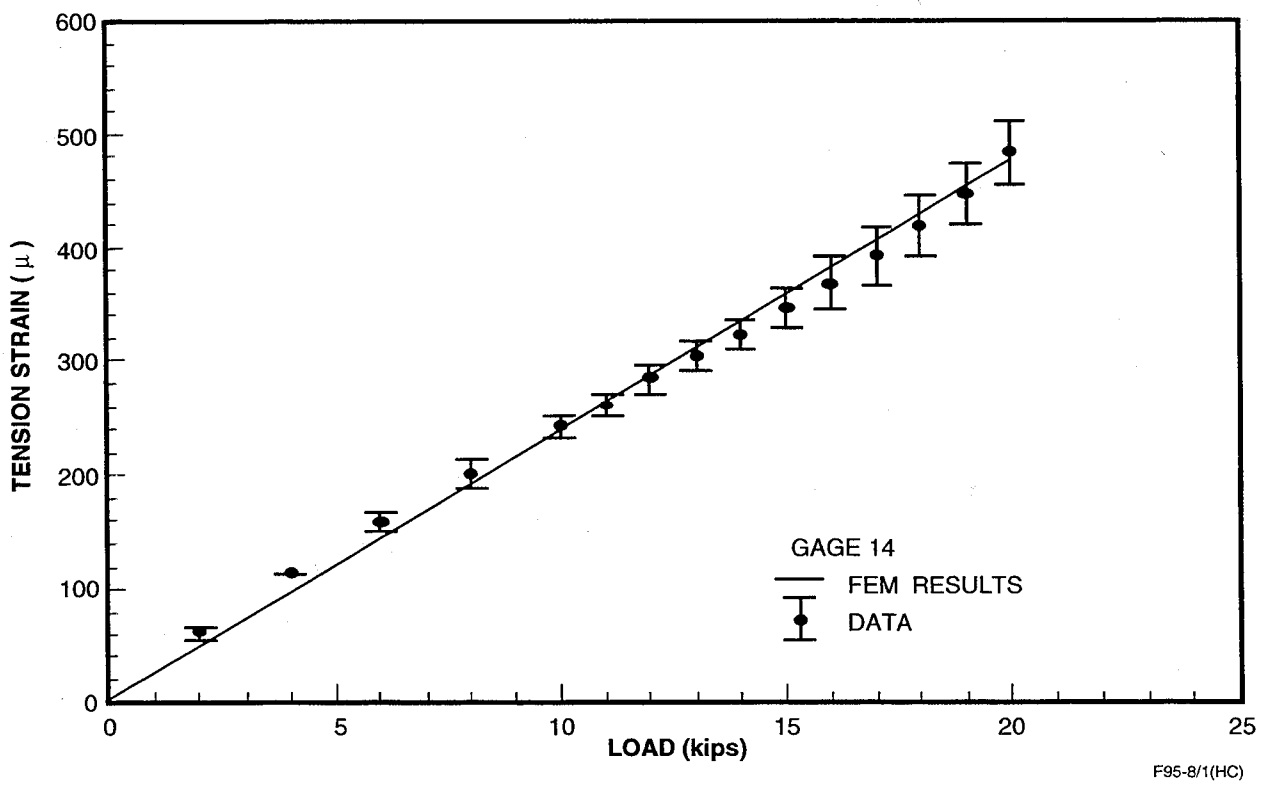

FIGURE 31. COMPARISON OF MEASURED AND PREDICTED STRAINS FOR STRAIN GAGE GROUP G OF THE TENSION SPECIMENS.

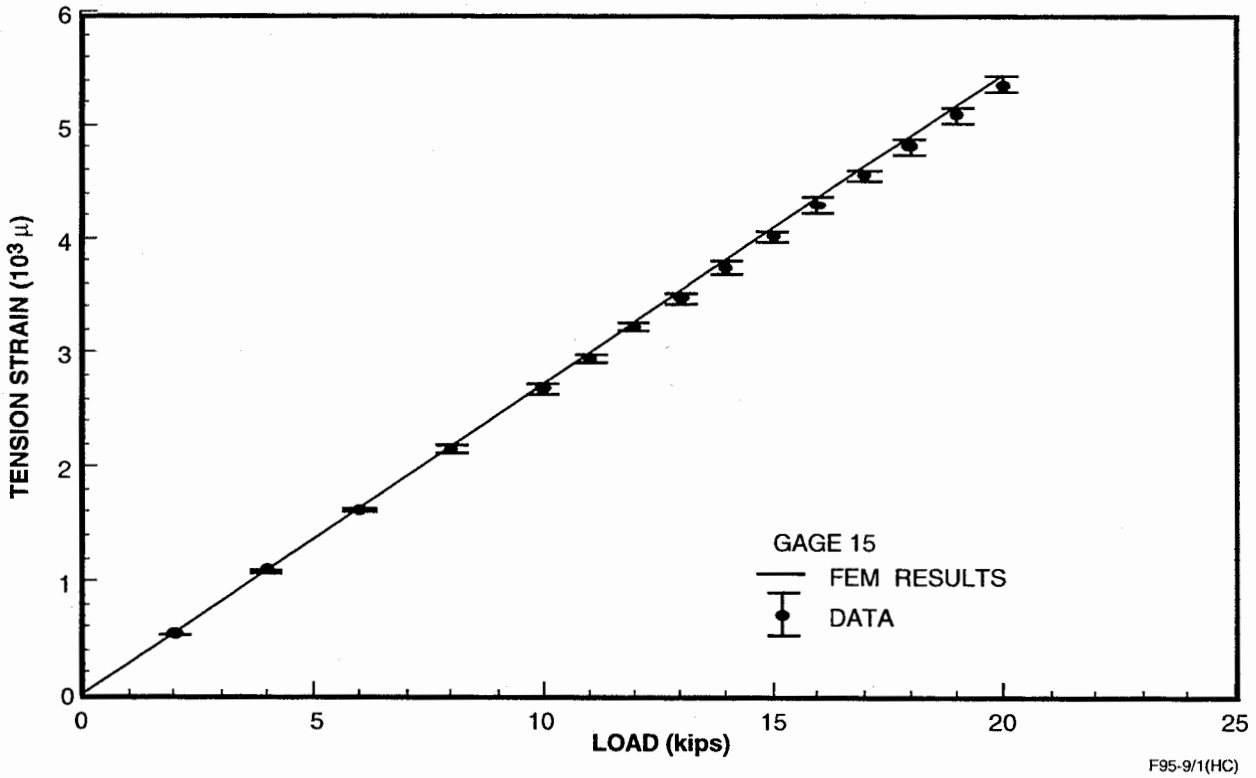

FIGURE 32. COMPARISON OF MEASURED AND PREDICTED STRAINS FOR STRAIN GAGE GROUP H OF THE TENSION SPECIMENS.

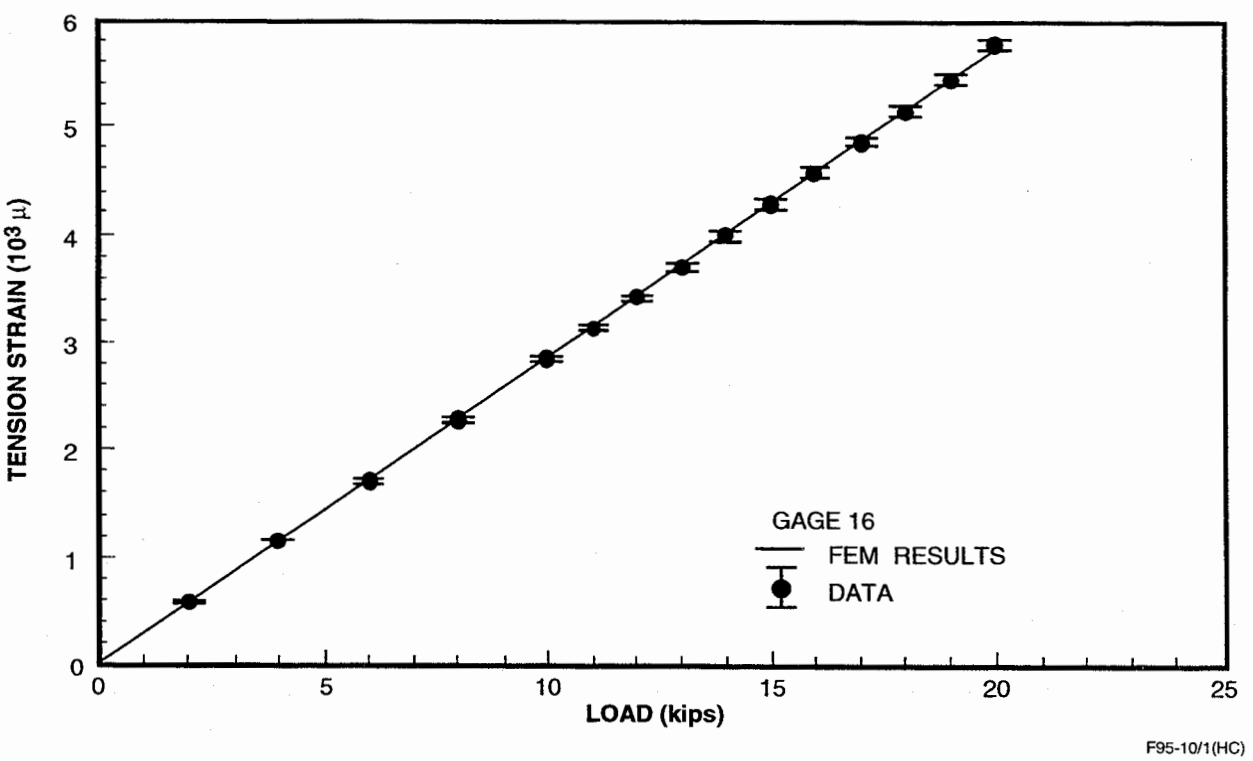

FIGURE 33. COMPARISON OF MEASURED AND PREDICTED STRAINS FOR STRAIN GAGE GROUP I OF THE TENSION SPECIMENS.

The ratio between the strain predicted by the finite element analysis and the experimentally measured strain shown in Table 5 is the overall ratio. The average strains from the six static tension specimens over the load range up to 20 kips are compared to the FEM results. As shown in the table, excellent correlation between the test data and FEM results were achieved, except for Group D. The predicted strains fall within ± 8 percent of the test data.

Strain gages 9 and 14 (Groups D and G) are located along the stiffener cap centerline with Gage 9 3 inches from the termination and Gage 14 1.5 inches from the termination. Both the analytical results and the test data show very little load is carried in this portion of the specimen. In fact, due to the bending effects, the stiffener cap is under compression when the specimen is subjected to tensile loading. A small compressive strain along the stiffener cap centerline is shown in both test data and FEM results. Due to the magnitude of the strain, accurate measurements during tests were a problem. This is believed to be the cause of the large difference between the predicted and measured strains in Gage 9. However, the correlation appears good for Gage 14.

Overall, the strain data show a linear relationship between strain and applied tension up to 20 kips. This indicates that a linear finite element analysis is appropriate to simulate the specimen response up to the initial failure. However, such an analysis does not have failure prediction capability, since the FEM model provides the global stress/strain response to the applied load but lacks the capability to describe the local behavior which causes the initial failure. The local behavior is three-dimensional in nature, and an accurate analysis is difficult. A more detailed local analysis for failure prediction will be discussed in a subsequent section of this report.

Further examination of the measured and predicted strains provides a better understanding of the mechanics of the specimen. By comparing the average strains of Groups A and B, a slight bending effect is seen. The skin strain on the stiffener face is slightly lower than the skin strain on the flat face of the specimen. This is consistent with both the test data and the FEM results. The FEM results show approximately 16 percent higher strain on the flat face, whereas the test data only show an average of 6 percent. This trend of bending affects the local three-dimensional stress pattern at the stiffener termination. With the higher stress/strain on the flat or unstiffened face of the skin, the stiffener will tend to be compressed toward the skin at the termination, which reduces the driving force for stiffener separation. This behavior is a result of the test specimen set up and the location of the applied load. In the actual structure, such behavior would depend on the stiffener arrangement and the stiffener termination configuration.

Thus, it is important to conduct a good stress analysis to design a structure with stiffener terminations.

The effects of bending can also be observed by comparing the strains in Groups E and F. These groups of strain gages are located closer to the stiffener termination (1.5 in.). The results, both measured and predicted, show a reduction in bending but still exhibit the same trend; the flat face skin strains are higher than those of the stiffened face. As in Groups A and B, the analytic results show more pronounced bending effects, with the flat face skin strain 13 percent higher than that of the stiffened face. The average test data only show a 2 percent difference.

The variation of skin strain in relation to the stiffener termination location can be examined by comparing strain Groups A and E, B and F, as well as H and I. Strain gage groups A, B, and I are located 3 inches from the termination, and the strains are considered to be far field strains. Strain gage groups E, F and H are located 1.5 inches from the termination ends, and the strains are considered as near termination end strains. Strains in Group E are slightly higher than those in Group A, both analytically and experimentally, but the difference is less than 4 percent. The differences between the strains in Group B and F, and those of Group H and I are even smaller. This indicates that the strain distribution within the range from 1.5 to 3 inches from the termination are quite uniform. In other words, the global stress is not significantly disturbed by the stiffener termination in this region of the specimen. This also confirms that failure initiation of the specimen takes place in a very small, local region and that strain gage measurements and global stress analysis are not sufficient to determine the local failure initiation.

The uniformity of the skin strains in a particular cross section of the specimen can be observed by comparing strains in gage Groups B and I, and F and H. Both FEM results and test data show that these strains differ only slightly. This indicates that the skin strains are uniformly distributed across the sections that are 3 and 1.5 inches away from the stiffener termination.

The effects of the termination angle on the compression strength were investigated by testing specimens with 45° and 75° termination angles. Specimens with 75° termination angles were used as a baseline in the present program; 9 specimens were tested with this configuration. Three specimens with 45° termination angles were tested for comparison purposes. A FEM analysis was conducted for these two specimen configurations and the resulting strains were compared with the corresponding test data. As discussed in Section 3, some of the compression specimens had constraint pins to prevent local buckling. However, for compression loads below the local buckling load, the constraint pins have little effect on the strains at various strain gage

locations. Therefore, the test data for specimens with and without constraint pins are combined in the following correlation.

The strain gage locations for the compression specimens are identical to those of tension specimens. Therefore, strain data are grouped in the same manner as shown in Table 5. For the baseline specimens with a 75° termination angle, the measured and the predicted strains are compared in figures 34 through 42. Figure 34 shows the far field strain on the stiffener face of the specimen (Group A). The figure shows that the predicted strains agree very well with the average measured strains. The FEM predicted strains are approximately 3.5 percent above the measured strains up to an applied compression load of 18 kips. The comparisons are conducted only to 18 kips of compression load because local buckling took place for the specimens without constraint pins at or below this load level.

The comparison of far field skin strains on the flat face (Group B) of the specimens are shown in figure 35. This figure again shows excellent correlation of the measured and FEM predicted strains. Up to a compression load of 18 kips, the average measured strain differs from the predicted strain by 3.5 percent.

Comparing the stiffened face and flat face strains provides an indication of the bending produced by the applied compression loading. From the results of Figures 34 and 35, both the experimental and analytical results show that the flat face strains are slightly higher than that of the stiffened face. Both the FEM results and the average test data show that the flat face strain is 5.5 percent higher than that of the stiffened face. These results suggest that the test set up used in the present program caused a small amount of bending that tended to "open" the specimen at the termination site under compression loading. The effects of this bending will reduce the strength for stiffener separation, however, will not affect scatter of the results.

Figure 36 shows the comparison of measured and predicted strains for strain gage Group C. This group of gages measured strains on the stiffener flange near the termination site. Figure 36 shows that the predicted strains are approximately 25 percent higher than the measured strains. This deficiency may be due to diminished load transfer from the skin to the stiffener. However, because these gages are located in the proximity of a skin thickness discontinuity, direct comparison of strain data is more difficult.

Figure 37 shows the comparison of predicted and measured strains for strain gage Group D. As in the case of tension loading, the correlation is poor at this location. The reason for the poor correlation is the very small amount of load carried by this portion of the specimen, as discussed previously for the tension specimens. Similar correlation is obtained for strains at strain gage

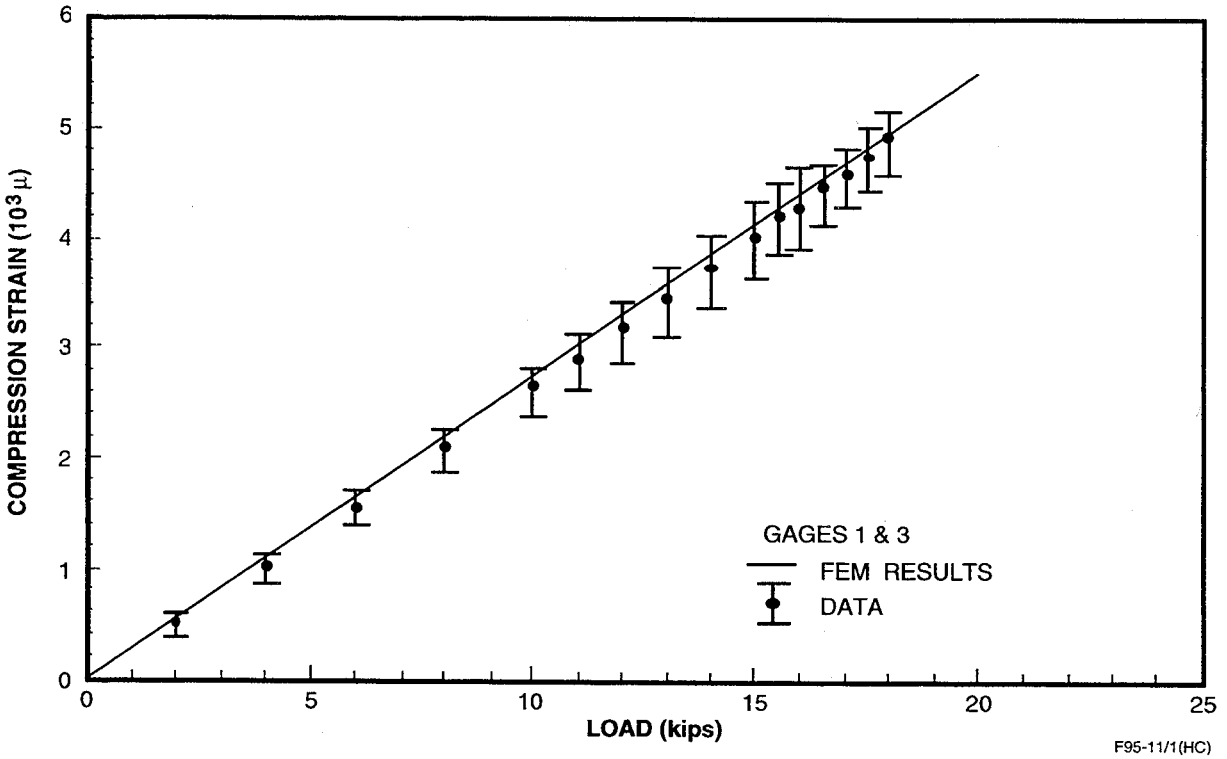

FIGURE 34. COMPARISON OF MEASURED AND PREDICTED STRAINS FOR STRAIN GAGE GROUP A OF THE COMPRESSION SPECIMENS WITH 75° TERMINATION ANGLE.

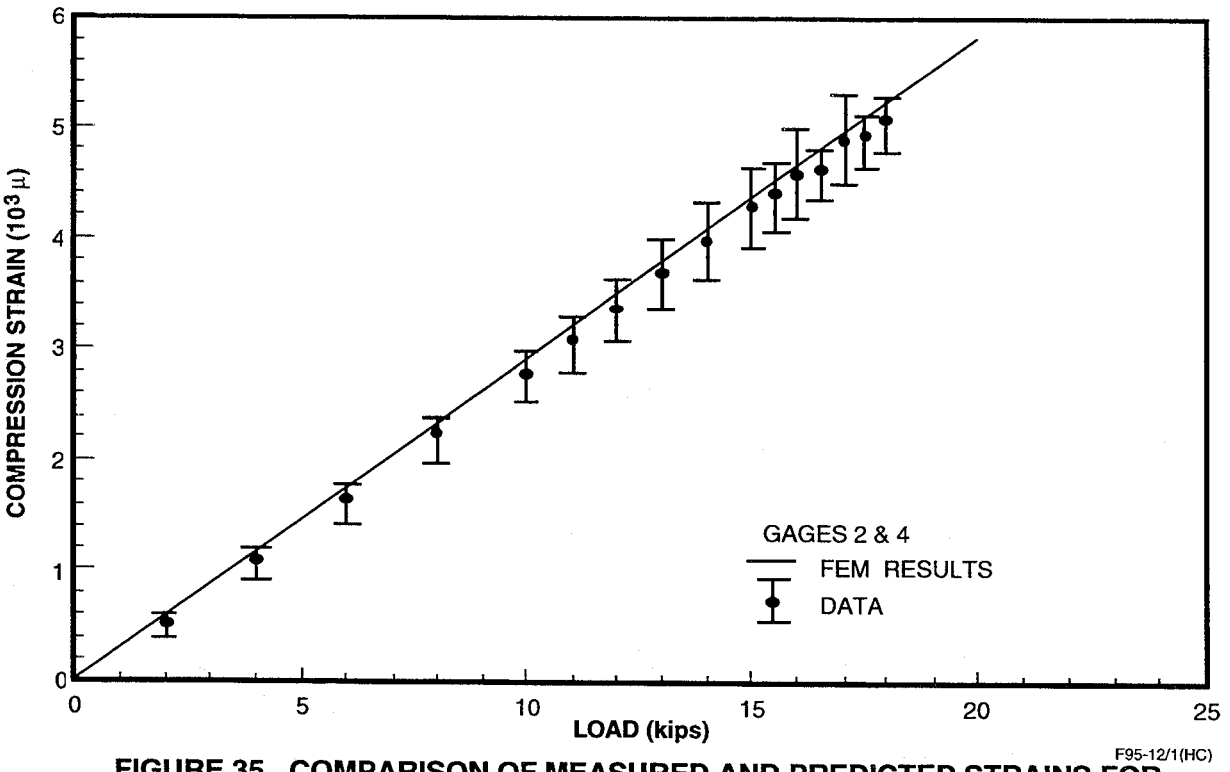

FIGURE 35. COMPARISON OF MEASURED AND PREDICTED STRAINS FOR STRAIN GAGE GROUP B OF THE COMPRESSION SPECIMENS WITH 75° TERMINATION ANGLE.

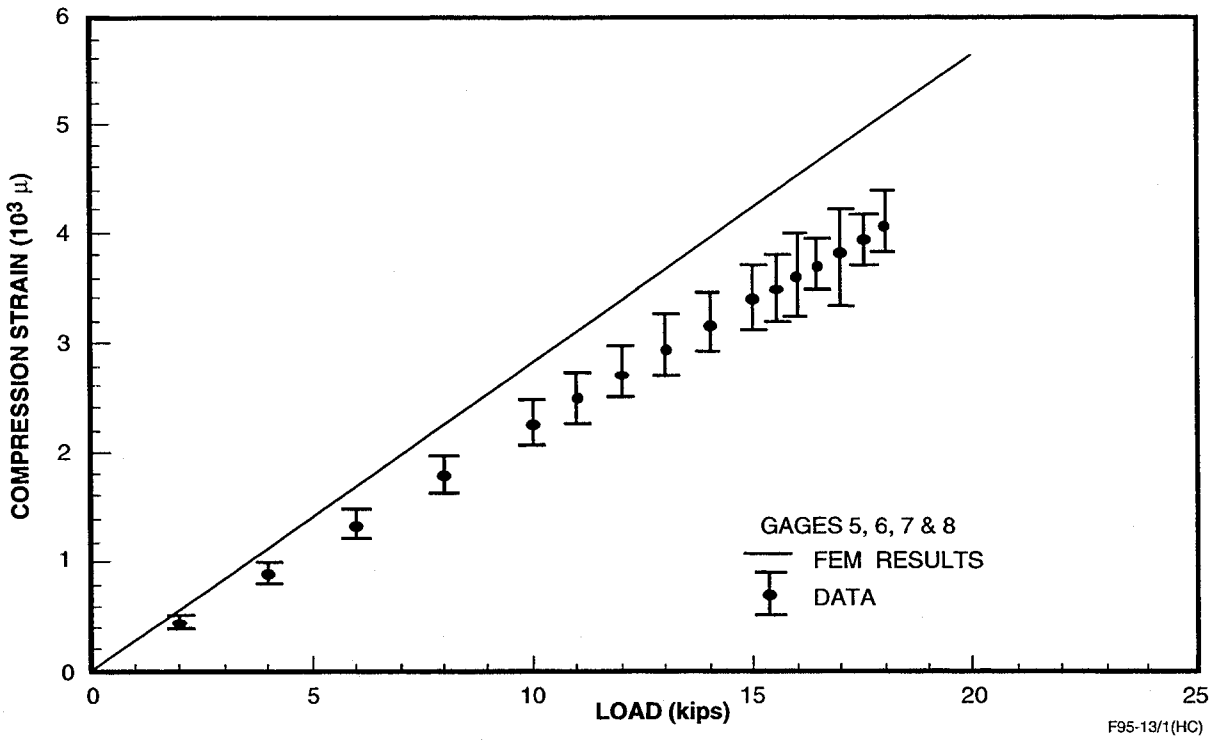

FIGURE 36. COMPARISON OF MEASURED AND PREDICTED STRAINS FOR STRAIN GAGE GROUP C OF THE COMPRESSION SPECIMENS WITH 75° TERMINATION ANGLE.

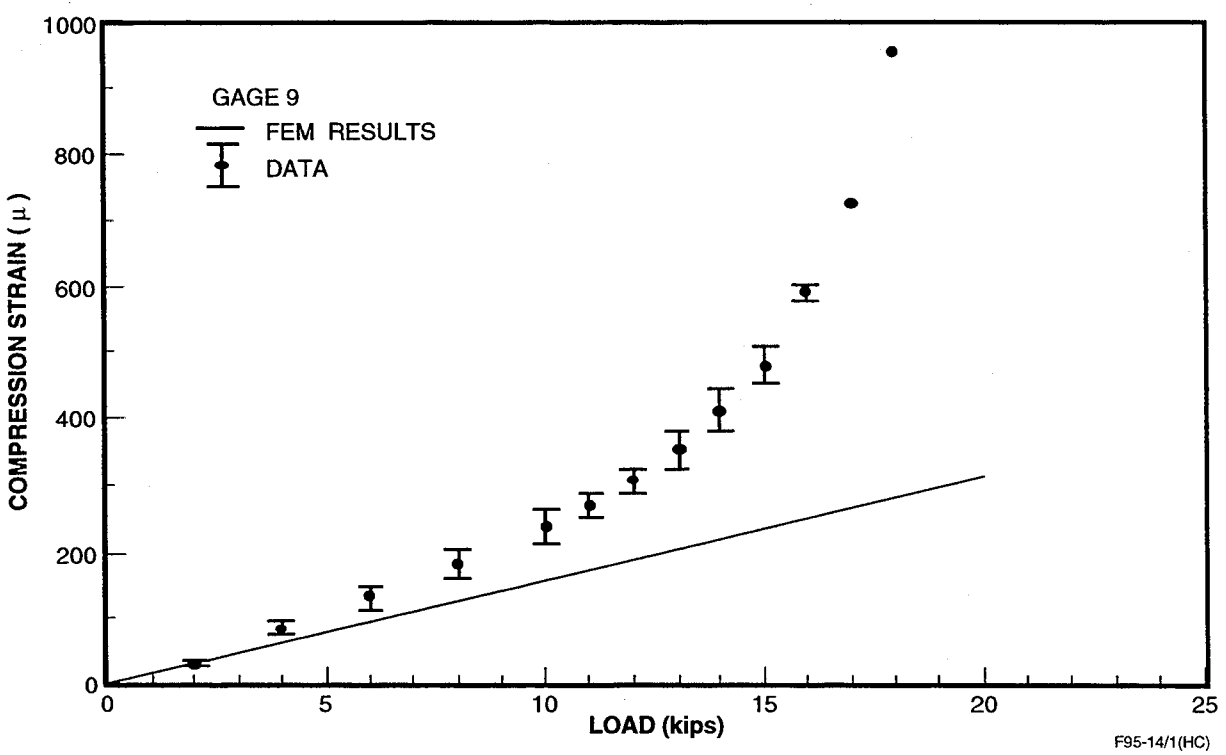

FIGURE 37. COMPARISON OF MEASURED AND PREDICTED STRAINS FOR STRAIN GAGE GROUP D OF THE COMPRESSION SPECIMENS WITH 75° TERMINATION ANGLE.

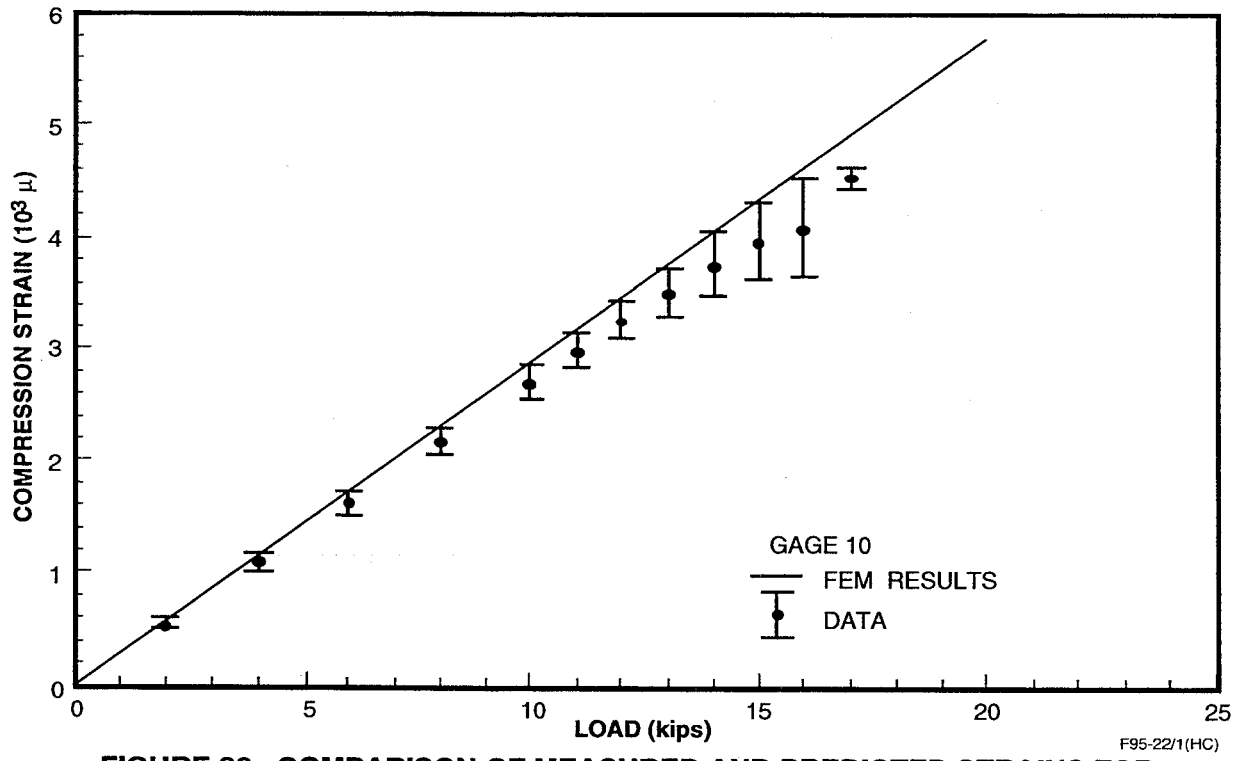

FIGURE 38. COMPARISON OF MEASURED AND PREDICTED STRAINS FOR STRAIN GAGE GROUP E OF THE COMPRESSION SPECIMENS WITH 75° TERMINATION ANGLE.

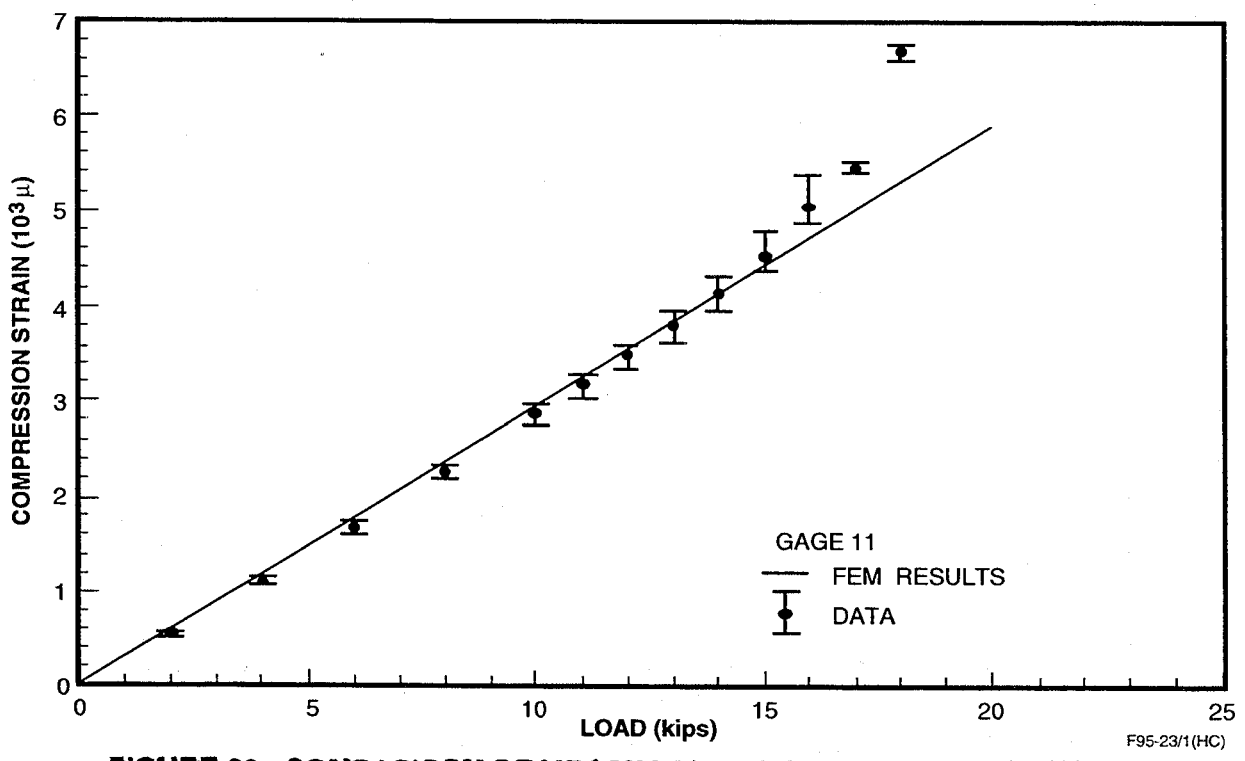

FIGURE 39. COMPARISON OF MEASURED AND PREDICTED STRAINS FOR STRAIN GAGE GROUP F OF THE COMPRESSION SPECIMENS WITH 75° TERMINATION ANGLE.

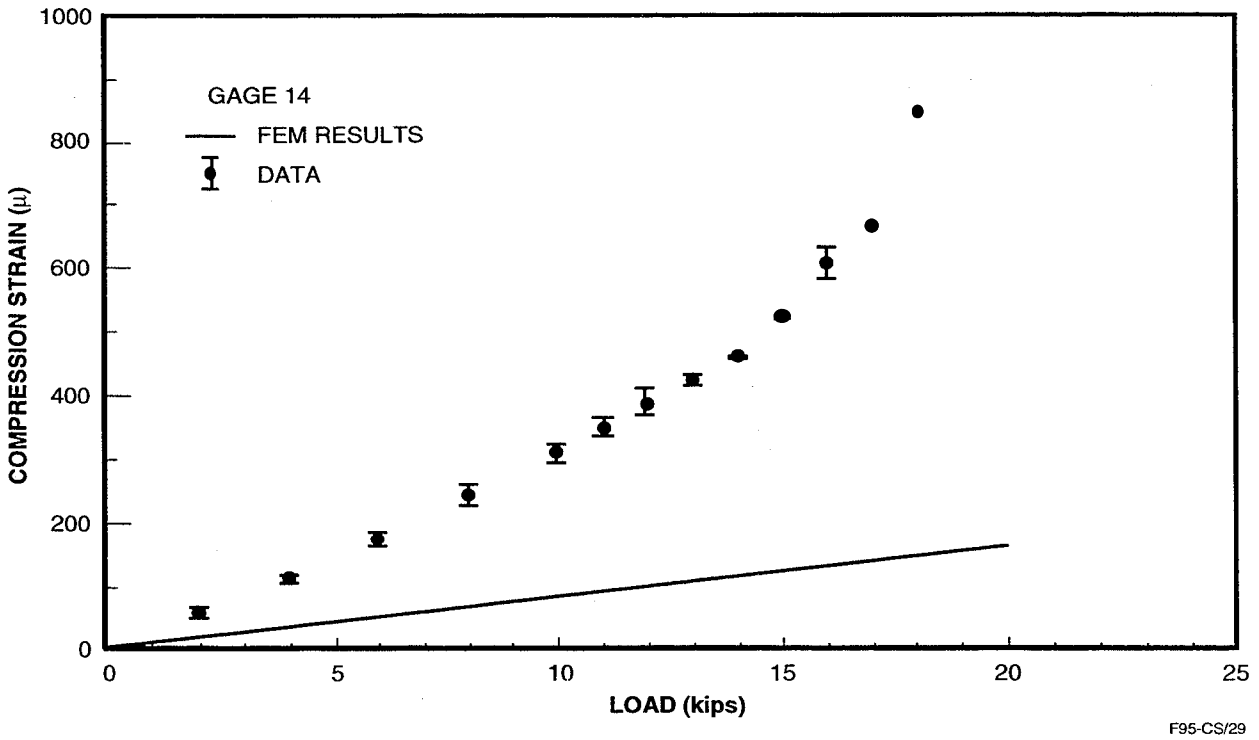

FIGURE 40. COMPARISON OF MEASURED AND PREDICTED STRAINS FOR STRAIN GAGE GROUP G OF THE COMPRESSION SPECIMENS WITH 75° TERMINATION ANGLE.

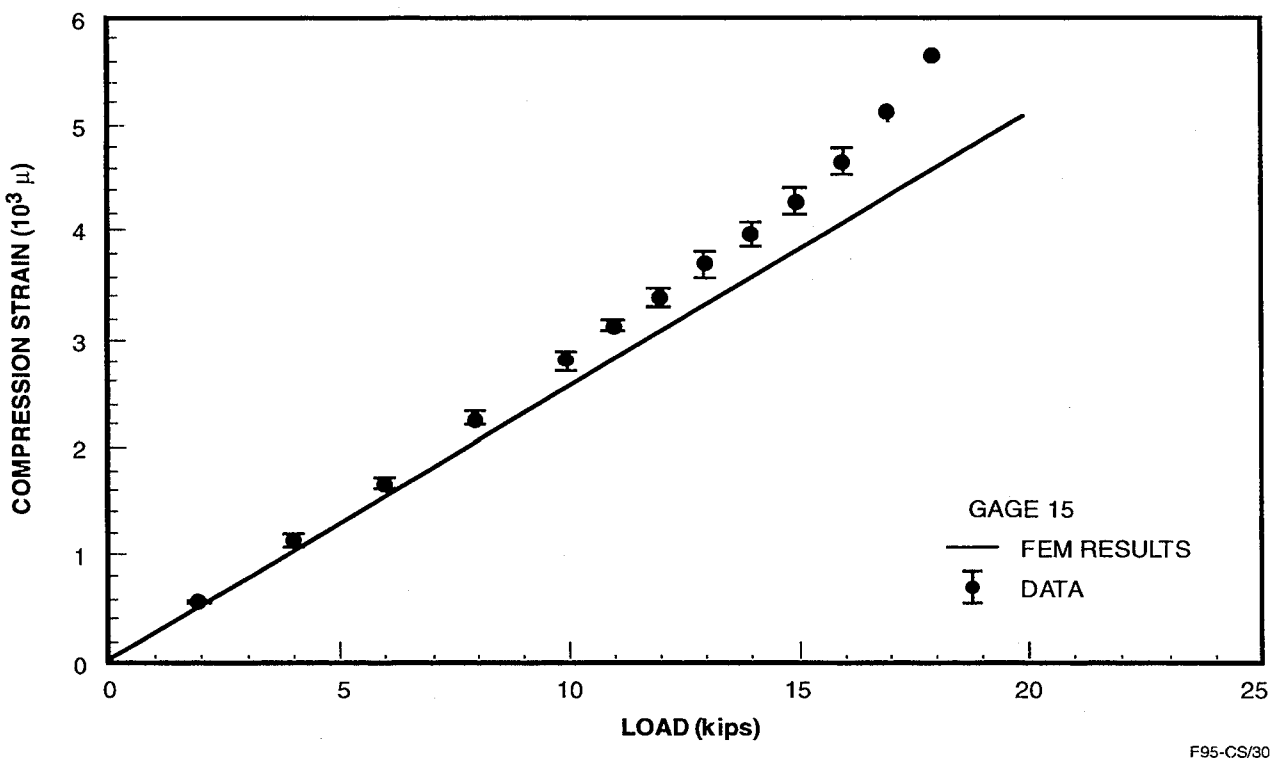

FIGURE 41. COMPARISON OF MEASURED AND PREDICTED STRAINS FOR STRAIN GAGE GROUP H OF THE COMPRESSION SPECIMENS WITH 75° TERMINATION ANGLE.

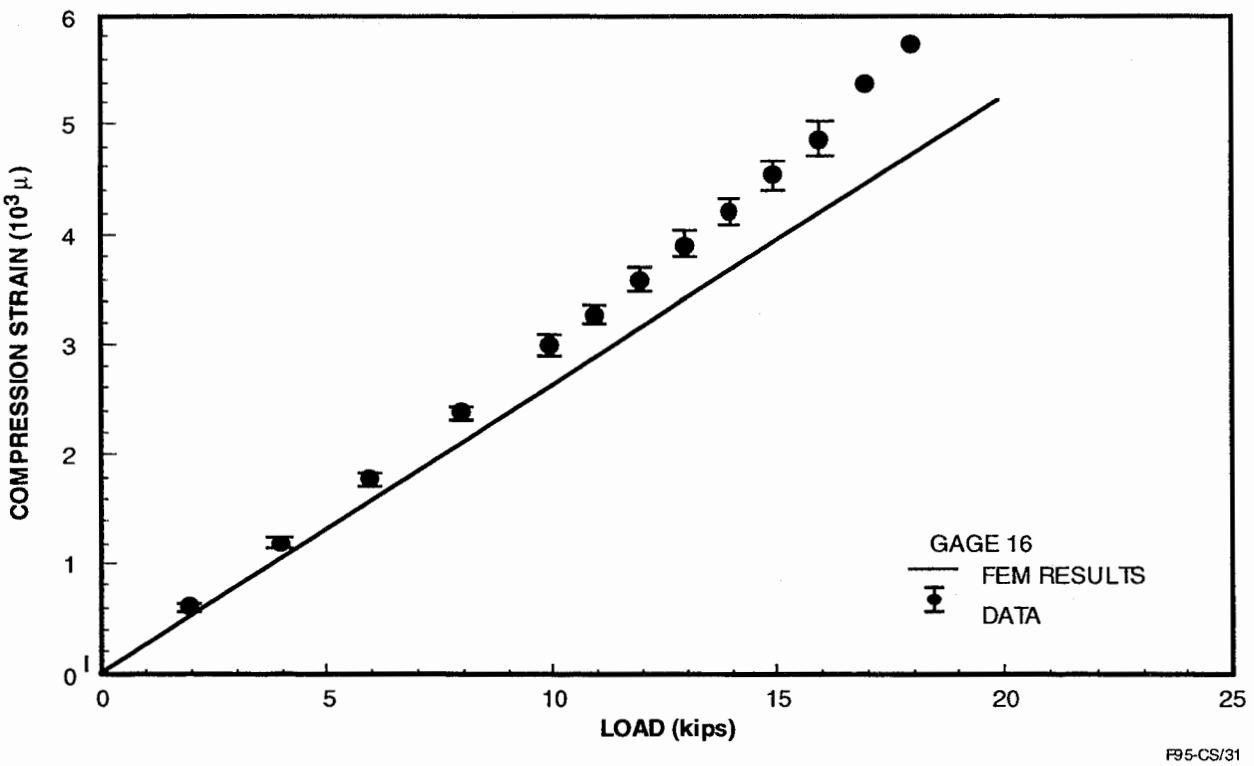

FIGURE 42. COMPARISON OF MEASURED AND PREDICTED STRAINS FOR STRAIN GAGE GROUP I OF THE COMPRESSION SPECIMENS WITH 75° TERMINATION ANGLE.

Group G (Figure 40). In comparing test data at Groups D and G, Figures 37 and 40 show the strains at Group G is initially higher until the strain-load relationship becomes significantly nonlinear, at approximately 16 kips of applied compression. Overall, the strains for Group G are an average of 18.6 percent higher than those for Group D. This difference is not consistent with the FEM results, where Group D strain is higher.

The comparisons of the predicted and measured strains for strain gage Groups E and F are shown in Figures 38 and 39 respectively. These strains are representative of near termination end strains with Group E on the stiffener face and Group F on the flat face. Figure 38 shows the predicted stiffener face strain exceeds the measured strain by 7.8 percent whereas Figure 39 shows the prediction is 1.1 percent below the measured strains on the flat face. Test data show Group F strains are higher than that of Group E, indicating the bending effects near the termination. This trend of bending is consistent with that observed for the far field strain (Groups A and B). The results also show that there is no significant change in strain from far field (Groups A and B) to near termination (Groups E and F). This indicates that the local response has no significant effect at locations 1.5 inches from the termination.

The comparisons of the far field (Group I) and near termination (Group H) strains along specimen centerline on the flat face are shown in Figures 41 and 42. These figures show the FEM results are between 11 percent to 12.5 percent lower than the measured strains. The results show slightly higher strain towards the stiffener termination. Further examination of the results also found that strains along the specimen centerline are slightly higher (Group B vs. Group I).

Three specimens with 45° termination angle were tested, two with constraint pins and one without constraint pins. The strain data for these specimens were combined for analytical results comparisons. These specimens were instrumented with eight strain gages (gage Group A, B and C in Table 5). Figures 43, 44, and 45 show the comparisons of measured and predicted strains. Figure 43 shows that the FEM results agree reasonably well with the measured strain for strain gage Group A. The predicted compression strains are approximately 6 percent lower than the average measured strain. Similar results are shown in Figure 44 for strain gage Group B. This figure shows the predicted strains are approximately 3 percent lower than the average measured strain.

As in the case of the specimens with 75° termination angle, strain results for specimens with 45° termination angle also show slight bending effects. This effect can be seen by comparing strains in Figures 43 and 44. The average test data show that the strains in the flat face are 2.7 percent higher than the strains in the stiffened face. The FEM results predict a higher bending effect, with the flat face strains 5.5 percent higher than the stiffened face strains.

Figure 45 shows the strain comparison for Group C. This figure shows that the analysis overpredicts the strains at the stiffener flange location by an average of 15 percent. This trend is consistent with the results for the compression specimens with 75° termination angle.

Because the termination angle only affects the local behavior of the specimen near the stiffener termination location, the stress and strain at the strain gage locations should not be significantly changed by the termination angle. This is confirmed by the test data as well as the analytical results. The average test data shown in Figures 34 and 43 indicate that the strains for those two specimen configurations differ by less than 2 percent. This same trend appears at strain gage Groups B (Figures 35 and 44) and C (Figures 36 and 45). The independence of global strains on the termination angle is a further indication that the failure of structures with stiffener termination is controlled by the stress-strain response of a small local region near the stiffener termination site.

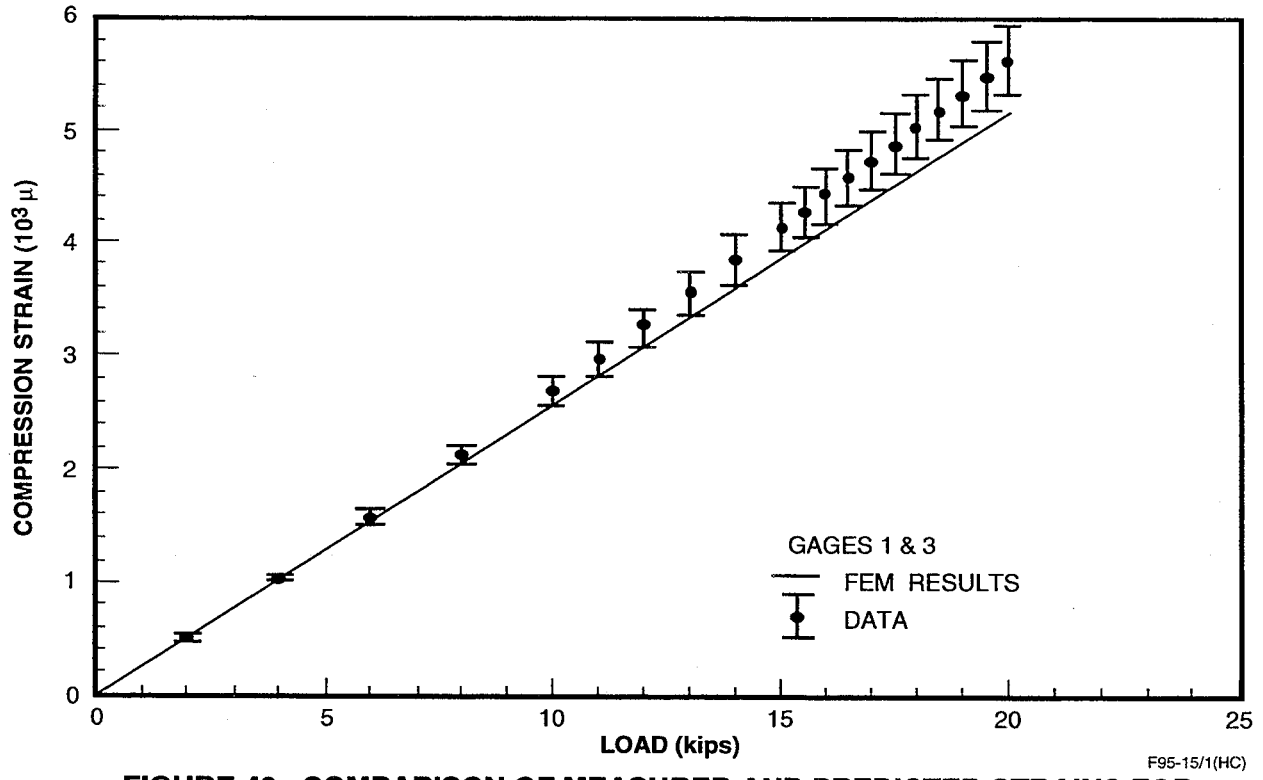

FIGURE 43. COMPARISON OF MEASURED AND PREDICTED STRAINS FOR STRAIN GAGE GROUP A OF THE COMPRESSION SPECIMENS WITH 45° TERMINATION ANGLE.

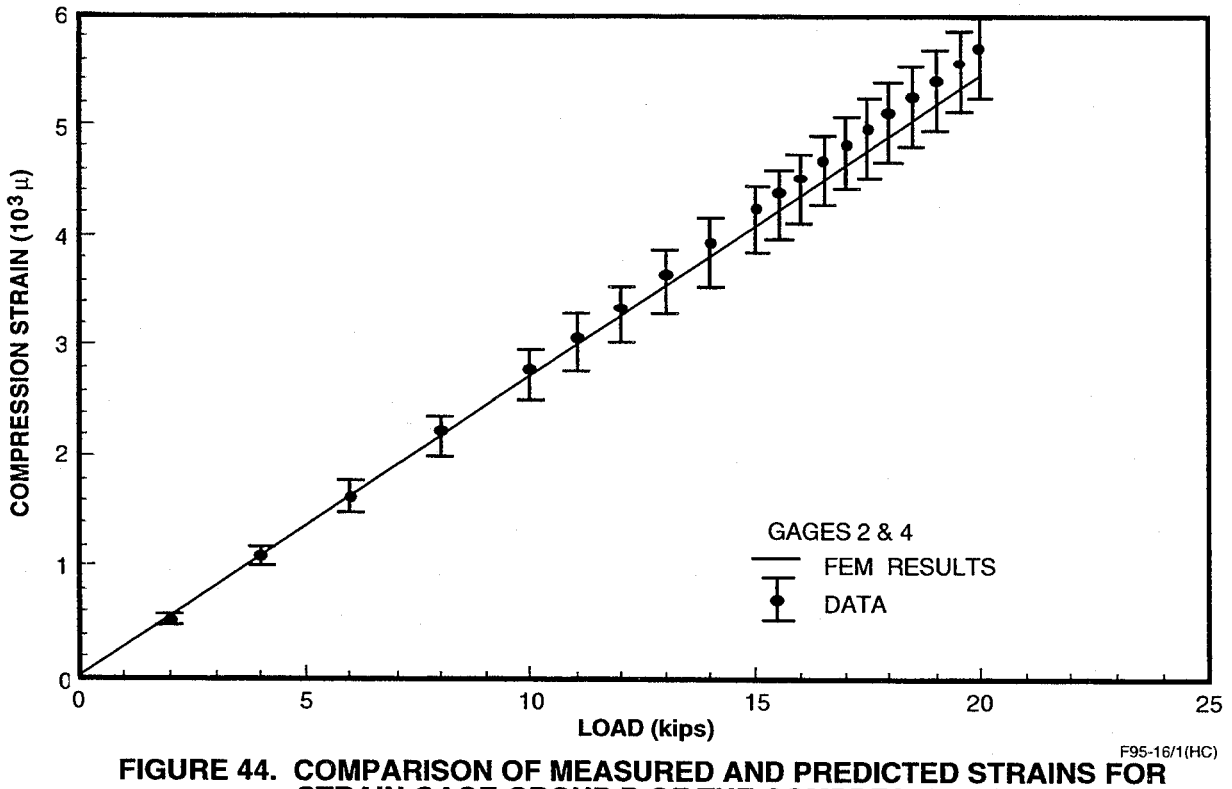

FIGURE 44. COMPARISON OF MEASURED AND PREDICTED STRAINS FOR STRAIN GAGE GROUP B OF THE COMPRESSION SPECIMENS WITH 45° TERMINATION ANGLE.

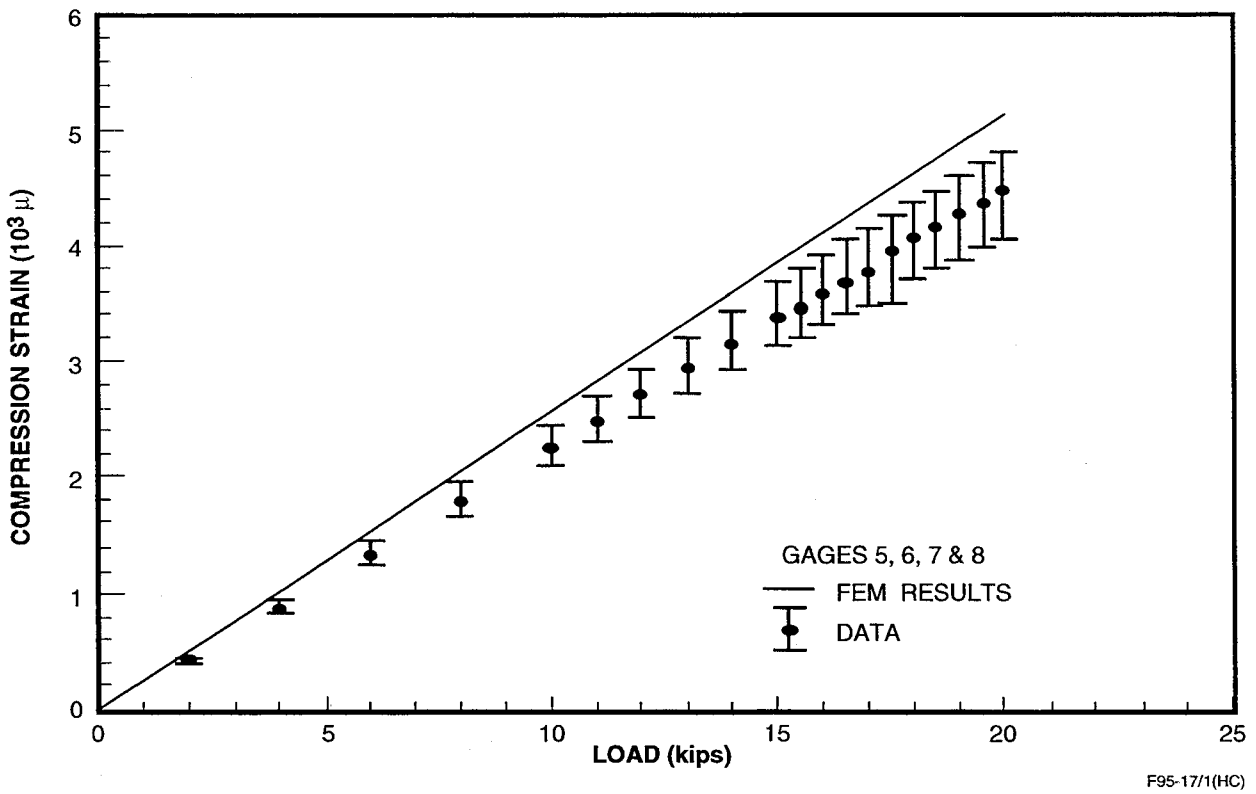

FIGURE 45. COMPARISON OF MEASURED AND PREDICTED STRAINS FOR STRAIN GAGE GROUP C OF THE COMPRESSION SPECIMENS WITH 45° TERMINATION ANGLE.

5.2 LOCAL FAILURE ANALYSIS.

The finite element analysis of the specimen discussed in the previous subsection indicated that even though the analytical results agreed well with the test data, the FEM is not capable of predicting failure of the specimen. In order to predict the initial failure of the specimen, a local elasticity model is employed. The stress analysis code WEBSTER, developed in Reference 1, was used to predict the stiffener/skin separation at the stiffener termination. The WEBSTER code is based on linear elasticity theory with a complex stress function formulation.

The stiffener termination specimen is idealized by two layers of orthotropic plates with one plate terminated. The representative structure and the idealized analytical model were shown in Figure 3. Failure by stiffener/skin separation is predicted by using a quadratic stress criterion together with an average stress scheme. Details of the analytical development for this model can be found in Reference 1.

The quadratic stress criterion is defined as:

$$\sqrt{\left(\sigma_z/\sigma_{z_{ALLOW}}\right)^2 + \left(\tau_{xz}/\tau_{xz_{ALLOW}}\right)^2} = 1.0 \text{ at failure}$$

In the present program, a longitudinal cut, Section A-A in Figure 3, was considered. The applied loads to the WEBSTER model included an axial skin load and a bending moment. These loads were obtained from the results of the finite element analysis discussed in Section 5.1. Because both the FEM and the WEBSTER analyses are based on linear theory of elasticity, the actual loads applied to the WEBSTER model were normalized to an equivalent specimen load of 10,000 lbs.

The quadratic stress failure criterion used in the WEBSTER model requires the interfacial normal and shear strength as material property inputs. Because the stiffener is cocured to the skin in the present program, those properties can be represented by the flatwise tensile strength and the interlaminar shear strength of the composite material system. For the AS4/3501-6 graphite/epoxy system used in the present program, the flatwise tensile strength is 3300 psi and the interlaminar shear strength is 18500 psi. The strengths used in the analysis are supplier (Hercules) provided typical proprietary values. In addition to the strength values, the model also requires a characteristic length for the average stress scheme. A characteristic length of 0.1 inch is used in the analysis.

The applied load input and the analytical results for initial failure prediction are summarized in Table 6, and the predicted and measured initial failure loads for the three specimen configurations are compared in Figure 46. As can be seen in the figure, the analysis underpredicted the initial failure load for the tension specimens and the compression specimens with constraint pins, and overpredicted the initial failure load for compression specimens without constraint pins. The overprediction for the unconstrained specimens is expected because these specimens failed in local buckling before the stiffeners were separated from the skins. Failures of the tension specimens and the compression specimens with constraint pins were all induced by stiffener/skin separation. The analysis underpredicted the initial failure by 20 and 22 percent respectively for the tension and compression specimens. This underprediction can be attributed to two sources. First, the test setup was not instrumented to measure the initial failure and the strain gage data were not sufficient to indicate initial failure due to the localized nature of the event. The initial failure load reported was obtained mainly from the load deflection plot, which may not be accurate. Second, the interfacial strengths used in the analysis may have been too low. These out-of-plane strength values are difficult to obtain and large scatter is expected.

5.3 STATISTICAL DATA ANALYSIS.

Both the static strength and fatigue life data were statistically analyzed to determine the data scatter. A two parameter Weibull model was used for the statistical analysis. Because the number of specimens in each specimen type and loading condition are relatively small, individual Weibull analyses are not suitable; joint Weibull analyses were conducted for the strength and fatigue life data. The static strength data included only the final failure strengths because of the difficulty experienced in accurately measuring the initial failure load, as discussed in Section 5.2.

Four groups of static strength data were selected for the joint Weibull analysis. They are (1) tension strengths, (2) compression strength for specimens without constraint pins, (3) compression strengths for specimens with constraint pins, and (4) compression strength for specimens with constraint pins and flange fasteners. Only the specimens with 75° termination angle were included in the analysis. Of the three specimens with 45° termination angle, two were with constraint pins and one without constraint pins. Thus, the small number of specimens in each type excluded itself from statistical analysis. Individual Weibull analysis was conducted for each data set only for the purposes of scatter comparison. The results of the individual Weibull analysis indicated that the Weibull shape parameter (α's) were not significantly different among the four groups of data This screening process resulted in a joint Weibull data set with four groups of data and a total of 18 data points.

The results of the joint Weibull analysis for the static strength data give a Weibull shape parameter (α) of 22.65 with an equivalent coefficient of variation of 0.055. The probability distribution of the combined data is shown in Figure 47. In this figure, the static strength is normalized with respect to the Weibull scale parameter (β). Figure 47 shows that the normalized strength correlates very well, based on the results of a chi-square goodness-of-fit test, with the Weibull distribution. Furthermore, the data from different test groups dispersed randomly in the normalized strength distribution, indicating that the joint Weibull model is suitable for the data analysis. The use of joint Weibull analysis for a complete statistical assessment of the test data would be questionable in this case, as different failure modes were combined into one data set. However, this method provides a reasonable result when scatter is the only parameter of interest as in the present study.

It should be pointed out that the Weibull shape parameter (α) obtained from the static strength data generated under the present program agrees with the scatter of the static strength data of commonly used composite laminates (Reference 29). An extensive survey of the static

TABLE 6. SUMMARY OF STIFFENER/SKIN SEPARATION ANALYSIS.

	TENSION SPECIMEN	COMPRESSION SPECIMEN	
		WITHOUT PINS	WITH PINS
APPLIED AXIAL LOAD (lbs)	2505	-2790	-2612
APPLIED MOMENT (in-lb)	-6.06	8.51	8.25
FAILURE INDEX	0.5855	0.6129	0.5730
PREDICTED FAILURE LOAD (lbs)	17,080	-16,316	-17,452

F95-18/1(HC)

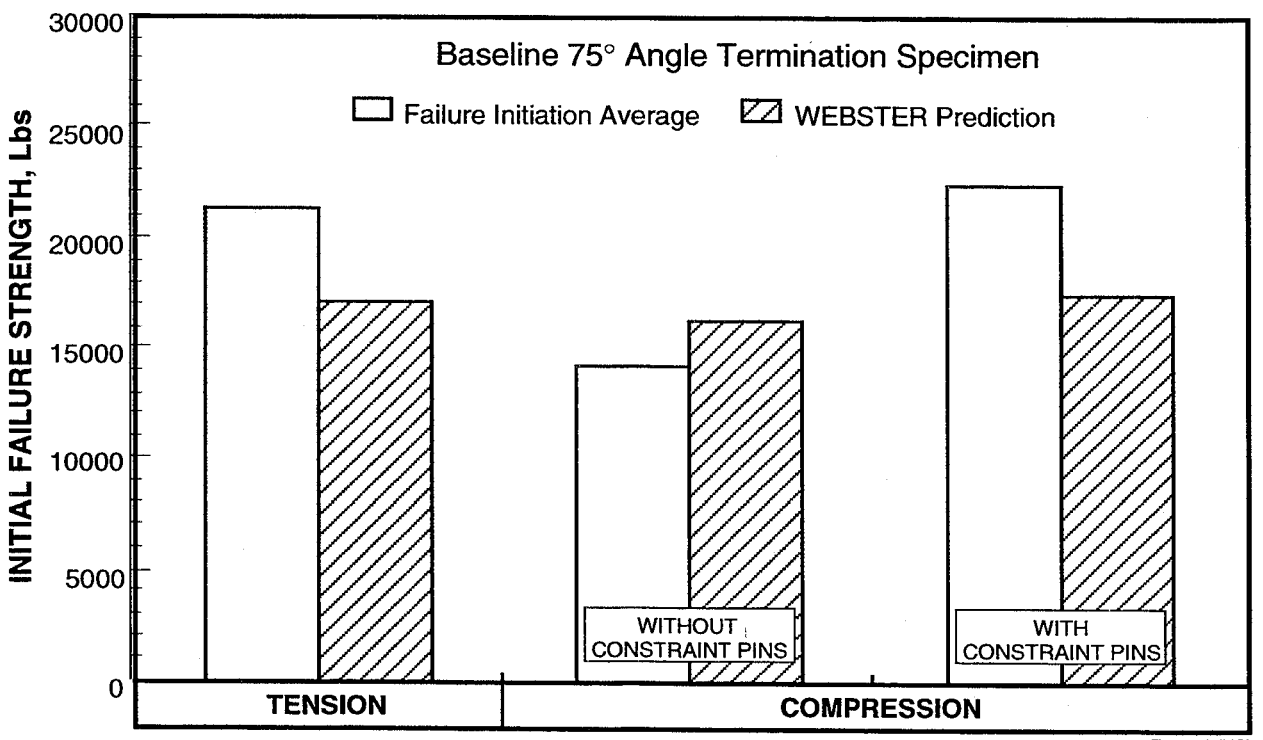

F95-21/1(HC)

FIGURE 46. COMPARISON OF MEASURED AND PREDICTED INITIAL FAILURE LOAD FOR THE THREE SPECIMEN CONFIGURATIONS.

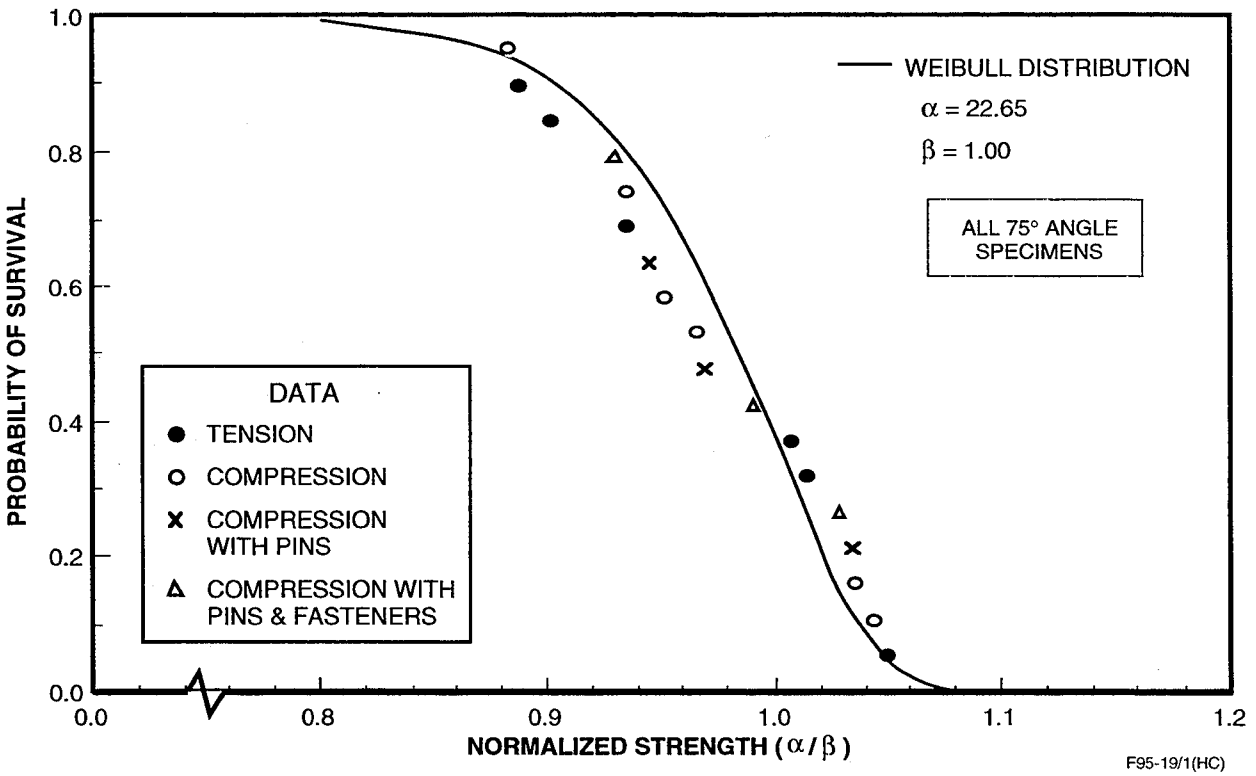

FIGURE 47. PROBABILITY DISTRIBUTION FOR THE NORMALIZED STATIC STRENGTH DATA.

strength data conducted in Reference 29 has shown that for commonly used composite laminates, the mean Weibull shape parameter is 23.2 with a modal value of 20. Thus, from the strength certification point of view, the static allowable knockdown for structures with stiffener terminations is similar to that of laminate static strength.

Since the stiffener is cocured to the skin in the specimens used in the present program, and the initial failure mode is stiffener/skin separation, the scatter for the initial failure is expected to be similar to that of bonded structure. Reference 30 conducted an extensive survey of the static strength scatter of bonded joints. The results of this survey show that the bonded joint static strength has a mean Weibull shape parameter of 12.2 with a modal value of 9.0. That is, bonded joint static strength scatter is significantly higher than that of composite laminates and bolted joints. The scatter of the initial failure strength for the stiffener termination was not assessed because of the limited amount of data and the difficulty in correctly measuring the initial failure. However, from the limited amount of data available, the preliminary indication is that the scatter for initial failure is higher than the final strength, but lower than that of bonded joints. The reason for the lower scatter for initial failures of stiffener termination relative to bonded joints may be due to the adhesive layer in bonded joints. The adhesive/adherends interface usually tend to have more scatter than the cocured interface between composites.

However, further research is needed to fully quantify the scatter of the initial failure of the stiffener terminations.

Fatigue life data were analyzed in the same manner as static strength data. By the same screening process discussed previously, the database has five groups of data with 21 data points. The five data groups include the baseline specimens loaded in compression at load levels of 19,000, 18,500, 17,000, 15,000 lbs and the specimens with 45° termination angle loaded at 18,500 lbs. For specimens loaded at 15,000 lbs, the runout (10^6 cycles) specimens were included in the analysis and treated as censored data points.

The results of fatigue data analysis (Reference 29, vol. I) show a Weibull shape parameter α of 1.45 with an equivalent coefficient of variation of 0.70. The probability distribution of the normalized life is shown in Figure 48. The fatigue life shown in the figure is normalized with respect to the Weibull scale parameter for the respective data Group. Figure 48 shows that the probability distribution deviates from the data where the censored data points are encountered. This is expected because the theoretical distribution is a projected life distribution accounting for the effects of the runout. Overall, the Weibull model reasonably describes the distribution of the data.

The high scatter in fatigue life data is as expected. In fact, the Weibull statistics for the fatigue data variation generated here agree with life distribution for composite laminates, bolted joints, and bonded joints, as summarized in References 29 and 30. In Reference 31, the mean fatigue life Weibull shape parameter, α, for composites and bolted joints was found to be 2.17 with a modal value of 1.25. These parameters are 1.76 and 1.25, respectively, for bonded joints. Therefore, it may be concluded that the fatigue life scatter for stiffener termination specimens is similar to commonly used composites and composite joints.

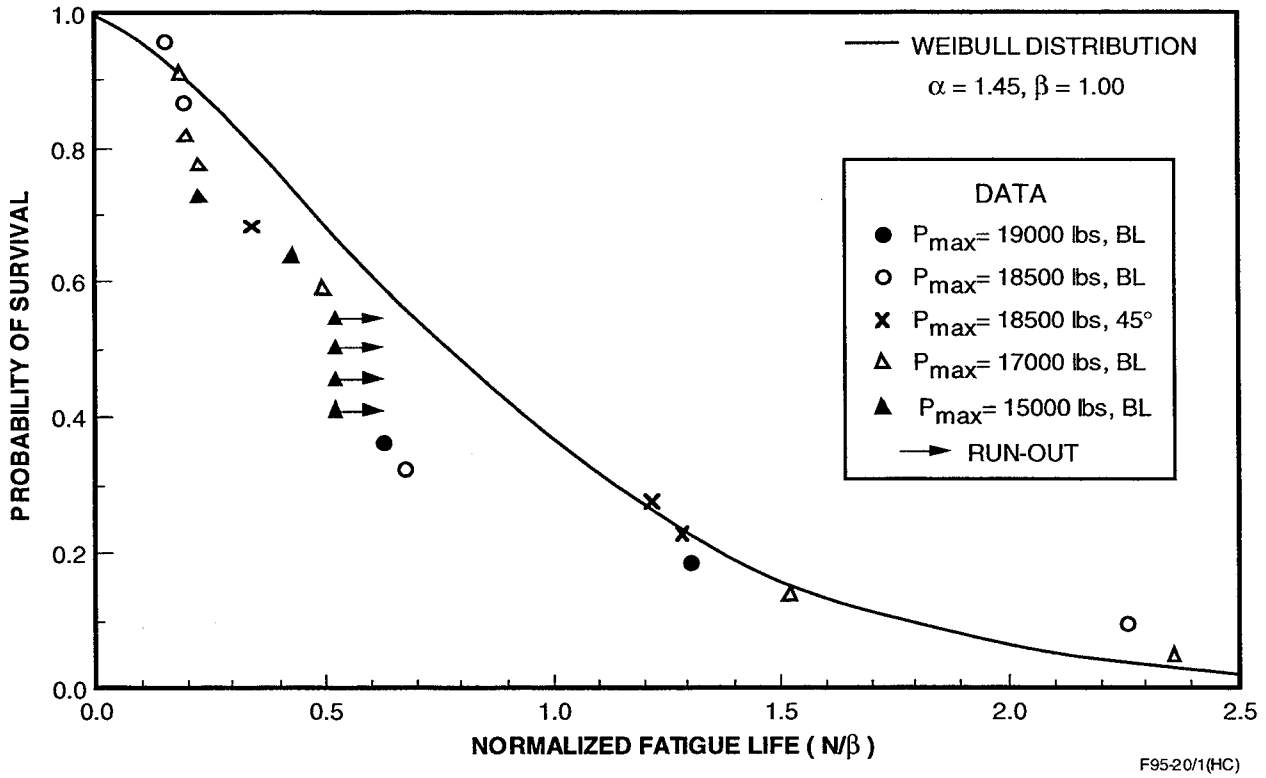

FIGURE 48. PROBABILITY DISTRIBUTION FOR THE NORMALIZED FATIGUE LIFE.

6. CERTIFICATION APPROACH.

The results of the present study were used to formulate an approach to certify composite aircraft structures with stiffener termination details. This approach was then integrated into the overall composite aircraft structural certification methodology developed in References 29 through 32. The overall certification methodology is summarized in Figure 49. The overall certification procedures for composite structures include three key elements (1) static strength, (2) durability, and (3) damage tolerance. The static strength and durability certification procedures are discussed in detail in Reference 29, and the impact damage tolerance certification method is presented in Reference 30. The procedures for assembly-induced damage tolerance are detailed in Reference 31. Reference 32 outlines a certification approach for structures with large area disbonds. In the following paragraphs, an approach to certifying composite structures with stiffener termination details is recommended. Because the stiffener termination is a specific structural detail, the proposed certification approach is part of the building-block approach under static strength and durability, as shown in Figure 49. Damage tolerance aspects of certification related to stiffener termination details are not discussed.

6.1 STATIC STRENGTH CERTIFICATION.

A building-block approach was adopted in Reference 29 for both static and durability certification of composite structures. The testing requirements in this approach include design allowable, design development and full-scale testing. The details of the building-block approach can be found in Reference 33. As an element in the building-block approach, certification of stiffener termination details requires design allowables as well as structural element testing.

The purpose of the design allowable tests is to evaluate the material scatter and to establish strength parameters for structural design. MIL-HDBK-17D, Reference 34, contains adequate guidelines for planning of design allowable testing and these guidelines should be closely followed. In addition to the strength allowables commonly generated for composite materials, two out-of-plane strengths are required for the design and analysis of stiffener termination details. These are the interlaminar tension and shear strengths, which are important

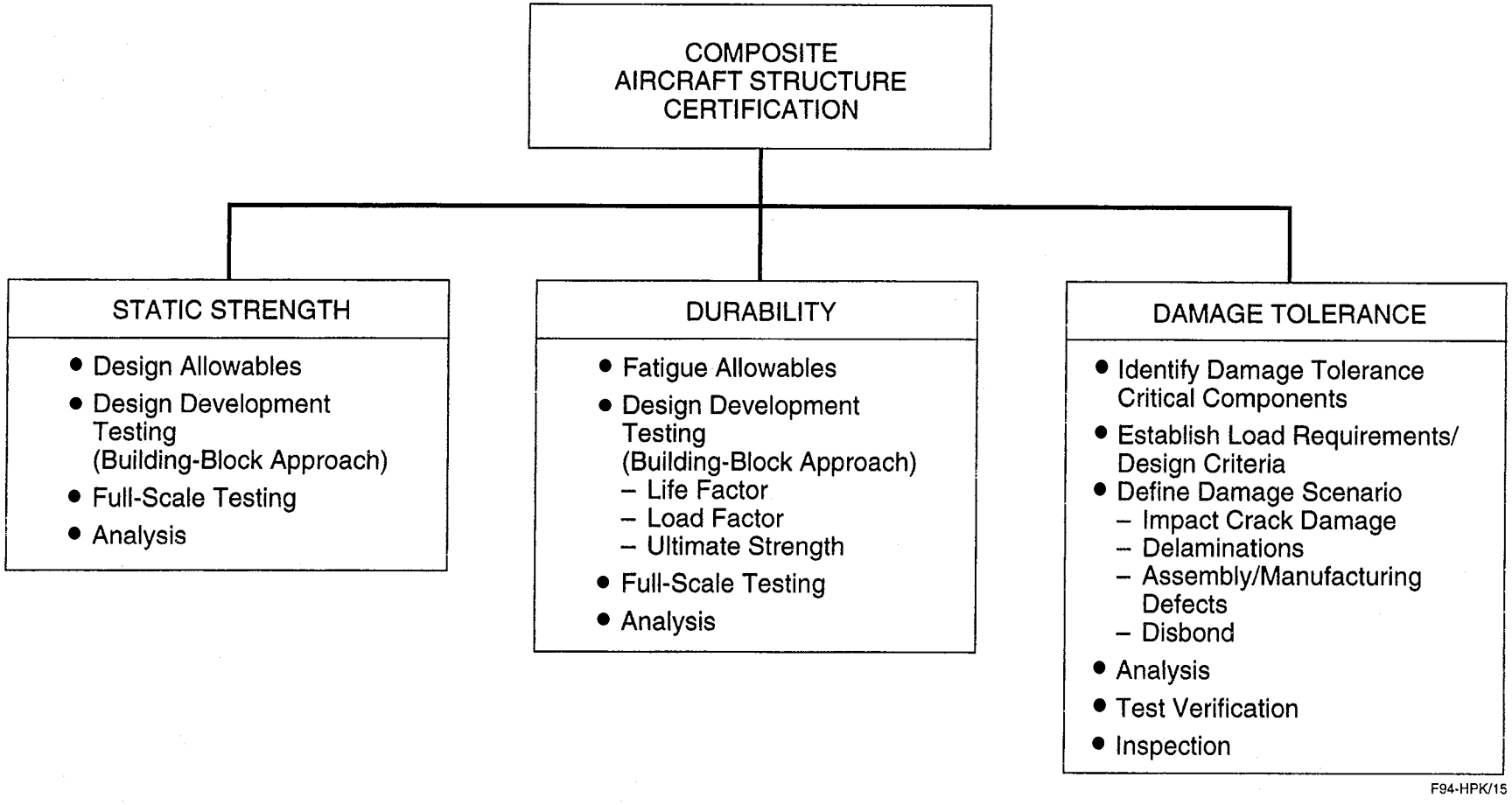

FIGURE 49. KEY ELEMENTS OF THE OVERALL COMPOSITE STRUCTURAL CERTIFICATION METHODOLOGY.

because they control the initial failure in the stiffener/skin separation mode. Therefore, tests to determine interlaminar strengths should be included in the design allowable development when stiffener termination details are anticipated in the composite structure. The "short beam shear test" and the "angle tension test" are suggested. The "short beam shear test" determines the apparent interlaminar shear strength by 3-point loading a "short" beam (length = 1.00 inch, width = 0.25 inch, thickness ≥ 0.125 inch). The "angle tension test" determines the interlaminar tension (ILT) strength by "opening" the corner of a 90 degree angle (2.00 inch by 2.00 inch by 1.50 inch wide). Flatwise tension tests also provide ILT strengths.

A combined test and analysis approach is recommended for the certification of structural elements with stiffener terminations. In this approach, the basic requirements are no initial failure at design limit load and no catastrophic failure at design ultimate load with a commonly used factor of safety of 1.5. Analysis should be conducted to verify that initial failure will not occur below design limit load. The finite element method can be used to simulate the overall structural response. Detailed local analysis, such as the elasticity model WEBSTER (Reference 1), should be conducted to predict initial failure. The analytical results discussed in Section 5 indicate that initial failure predictions tend to be conservative. Further development or refinement of the analytical model is also recommended.

Based on the experimental data generated under the present program, these requirements provide reasonable level of conservatism for the structure. This is because the test data indicate that the ratio between final failure and the initial failure is sufficiently below 1.5. Therefore, a requirement that no final failure at design ultimate load assures that initial failure will not take place below limit load. This approach also addresses the difficulty of detecting initial failure during static test. Thus, emphasis can be placed on the measurement of final failure during static tests.

The scatter assessment conducted under the present program suggested that the scatter for static strength (final failure) for stiffener termination specimens is comparable to that of commonly used composites and composite bolted joints. Thus pooling of static strength data to establish B-basis strength is possible and a large number of structural element tests is not necessary for this type of structural detail. With a sample size of five, the B-basis strength is approximately 0.9 of the average strength.

6.2 DURABILITY CERTIFICATION.

The building-block approach is also recommended for durability certification of composite structures in Reference 29. The fatigue allowables may be determined by the life factor approach, the load factor approach, or the ultimate strength approach. The details of these approaches are contained in Reference 29. As discussed in the reference, the use of a simple life factor approach requires long test durations because of the high fatigue life scatter observed in composite structures. The load enhancement factor approach or the ultimate strength approach is recommended in planning fatigue design development testing. A sufficient number of replicates should be used to verify the failure modes and to reasonably estimate the required fatigue reliability.

Based on the test data generated in the present program, a B-basis fatigue life requirement is recommended. Compliance with this requirement can be demonstrated by the life factor approach, the load factor approach, or the combined use of life and load factors. For a sample size of five specimens, the life factor derived from the test data for B-basis reliability is 6.5, and the load factor is 1.131. For a combination of life and load factor, the load enhancement factor (F) can be expressed as a function of the planned test duration (N lifetimes). For fatigue tests with five replicates, the relationship between load and life factors based on the data generated are shown below:

TEST DURATION N	LOAD FACTOR F
1	1.131
2	1.081
3	1.052
4	1.032
5	1.017

7. CONCLUSIONS AND RECOMMENDATIONS.

7.1 SUMMARY.

The steps conducted in the research program are summarized below:

1. A technology assessment was conducted to determine stiffener termination design practices in industry, collect available test data, and review available analysis methods.
2. A test program, including 21 static and 24 fatigue tests, was conducted to investigate the failure mode, static strength, and fatigue life of typical commercial aircraft composite structures containing stiffener terminations.
3. Analyses were conducted to verify the global load distribution and the local failure mechanism of the test specimens. Results of the analysis were compared with the test data.
4. Statistical analyses were performed to assess the static strength and fatigue life scatter.
5. Structural certification procedures for composite structures with stiffener termination details were recommended.

7.2 CONCLUDING REMARKS.

The following observations may be drawn from the investigation undertaken in this program.

1. For composite structures with cocured or bonded stiffeners, out-of-plane failure in the form of stiffener/skin separation at the stiffener termination site can occur prior to the overall failure of the structural element.
2. The finite element method can be used to simulate the overall structural performance. Measured static load distributions correlated very well with results of the finite element analysis.

3. Stiffener/skin separation takes place in a local region near the stiffener termination. A local out-of-plane stress analysis is required to predict the initial failure.
4. Initial failure is difficult to detect during static and fatigue tests.
5. Static strength and fatigue life scatter for stiffener termination specimens are comparable to that of commonly used composites and composite bolted joints.
6. Existing certification approaches for static strength and fatigue life for composite structures are applicable to stiffener terminations.

7.3 RECOMMENDATIONS.

Certification procedures for composite structures with stiffener terminations were recommended in Section 6 and are summarized below.

1. Static strength certification is based on the requirements that no initial failure is allowed below limit load and no element failure below ultimate load with a conventional safety factor of 1.5.
2. Compliance to the static strength requirements is demonstrated by a combined experimental and analytical approach.
3. Fatigue life certification is based on the B-basis reliability requirement.
4. A combined life and load enhancement factor approach is recommended for demonstration of compliance of life requirement.
5. Further development or refinement of the local stress analysis method for initial failure prediction is also recommended.

REFERENCES

1. Paul, P. C., Saff, C. R, Sanger, K. B., Mahler, M. A., Kan, H. P. and Deo, R. B., "Out-of-Plane Analysis for Composite Structures," Vol I DOT/FAA Report No. DOT/FAA/CT-91/22-1, September 1994.

2. Starnes, J. H. Jr., et al., "Postbuckling Behavior of Selected Flat Stiffened Graphite-Epoxy Panels Loaded in Compression," Presented at the 23rd AIAA/ASME/ASCE/AHS SDM, New Orleans, LA, May 10-12, 1982, Proceedings-Part I, pp 464-478.

3. Aniversario, R. B., et al., "Design, Ancillary Testing, Analysis, and Fabrication Data for the Advanced Composite Stabilizer for Boeing 737 Aircraft, Volume II, Final Report," Boeing Commercial Airplane Company, Seattle, WA., NASA CR-166011, December 1982.

4. Horton, R. E., Whitehead, R. S., et al., "Damage Tolerance of Composites, Volume II, Investigation of Thermoplastics AS4/PEEK (APC-2), Configuration Effects, and Battle Damage Tolerance, Final Report," Boeing Military Airplanes, Seattle, WA, AFWAL-TR-87-3030, July 1982.

5. Shuart, M. J., et al., "Technology Integration Box Beam Failure Study: Status Report," Lockheed Aeronautical System Company, Second NASA ACT Technology Conference, Lake Tahoe, Nevada, November 4-7, 1991, NASA CP 3154, pp 99-111.

6. Jackson, A. C., et al., "Advanced Manufacturing Development of a Composite Empennage Component for L-1011 Aircraft, Phase III Final Report, Design and Analysis," Lockheed-California Company, Burbank, CA, NASA CR-165634, April 1981.

7. Shah, C. H., Bhatia, N. M., "Stiffener Termination Assessment of Cocured Composite Stiffened Panels," Northrop Corp. Aircraft Division, NOR 88-57, January 1989.

8. Circle, R. L., O'Brien, R. D., "Manufacturing Technology for Large Composite Fuselage Structure," Lockheed-Georgia Company, Marietta, GA, ACEE Composite Structures Conf. August 13-17, 1984, pp 53-66.

9. Carrier, W. L., "Damage Tolerance and Repair of Composite Fuselage Structure," McDonnell Aircraft Company, St. Louis , MO., Proceedings of the Seventh Conference on Fibrous Composites in Structural Design, AFWAL-TR-85-3094, June 1985.

10. Madan, R. C., "Composite Transport Wing Technology Development," Douglas Aircraft Company, Long Beach, CA, NASA CR-178409, February 1988.

11. Price, M. A., Beeler, D. R., "Manufacturing Technology for Large Aircraft Composite Wing Structures," Rockwell International Corp., North American Aircraft Operations, Los Angeles, CA, NASA CP-2322, ACEE Composite Structures Technology Conference, August 13-16, 1984, Seattle, WA 1984, pp 21-66.

12. Starnes, J. H. Jr., Knight, N. F. and Rouse, M. "Postbuckling Behavior of Selected Flat Rectangular Graphite-Epoxy Laminated Plates," AIAA Paper 81-0543, 1981.

13. Knight, N. F., and Starnes, J. H. Jr., "Postbuckling Behavior of Selected Curved Stiffened Graphite-Epoxy Panels Loaded in Axial Compression," AIAA Paper #85-768 presented at the 26th AIAA/ASME/ASCE/AHS SDM Conference.

14. Deo, R. B., Kan, H. P. and Bhatia, N. M., "Design Development and Durability Validation of Postbuckled Composite and Metal Panels, Volume III - Analysis and Test Results," WRDC-TR-89-3030, Final Report, Contract F33615-84-C-3220, November 1989.

15. Deo, R. B. and Madenci, E., "Design Development and Durability Validation of Postbuckled Composite and Metal Panels," AFWAL-TR-85-3077, Final Report, Technology Assessment, Contract F33615-84-C-3220, May 1985.

16. Ogonowski, J. M. and Sanger, K. B., "Postbuckling of Curved and Stiffened Composite Panels Under Combined Loads," NADC Report No. NADC-81097-60, prepared under Navy Contract No. N62269-81-C-0384, December 1984.

17. Renieri, M. P. and Garrett, R. A., "Stiffener/Skin Interface Design Improvements for Postbuckled Composite Shear Panels," Report No. NADC-80134-60, under Navy Contract No. N6226981-C-0333, February 1982.

18. Garrett, R. A. and Renieri, M. P., "Postbuckling Fatigue Behavior of Flat Stiffened Graphite/Epoxy Panels Under Shear Loading," Report No. NADC-78137-60 June 1980.

19. Frostig, Y., Siton, G., Segal, A., Sheinman, I. and Weller, T., "Post-Buckling Behavior of Laminated Composite Stiffeners and Stiffened Panels Under Cyclic Loading," presented and the 16th ICAS Congress, Jerusalem, Israel, Aug. 28-Sept. 2, 1988.

20. Fan, S., Kroplin, B. and Geier, B., "Buckling, Postbuckling and Failure Behavior of Composite-Stiffened Panels Under Axial Compression," presented at the 33rd AIAA/ASME/ASCE/AHS SDM Conference, Dallas, Texas, April 13-15, 1992.

21. Arnold, R. R. and Meyers, J., "Buckling, Postbuckling, and Crippling of Materially Nonlinear Laminated Composite Plates," International Journal of Solids and Structures, Vol. 20, Nos. 9 and 10, pp 863-880, 1984.

22. Hyer, M. W. and Cohen, D., "Calculation of Stresses and Forces Between the Skin and Stiffener in Composite Panels," AIAA-CP-0731, presented at the 28th AIAA/ASME/ASCE/AHS SDM Conference, Monterey, CA, April 6-8, 1987.

23. Kan, H. P., Mahler, M. A., and Deo, R. B., "Prediction of Stiffener-Skin Separation in Composite Panels," presented at the First NASA ACT Conference, November 1990, Seattle, Washington.

24. Arnold, R. R., "Disbond Criterion for Postbuckled Composite Panels," AIAA-CP-87-0732, presented at the 28th AIAA/ASME/ASCE/AHS SDM Conference, Monterey, CA, April 6-8, 1987.

25. Tsai, H.C., "Solution Method for Stiffener-Skin Separation in Composite Tension Field Panel," Report No. NADC-82171-60, October 1982.

26. Tsai, H. C., "Approximate Solution for Skin/Stiffener Separation Including Effect of Interfacial Shear Stiffness in Composite Tension Field Panel," Report No. NADC-83131-60, November 1983.

27. Wang, J. T .S. and Biggers, S. B., "Skin/Stiffener Interface Stresses in Composite Stiffened Panels," NASA Contract Report No. 17261, January 1984.

28. Kassapoglou, C. and DiNicola, A. J., "Efficient Stress Solutions at Skin Stiffener Interfaces of Composite Stiffened Panels," AIAA Journal, Vol. 30, No. 7, pp 1833-1839, July 1992.

29. Whitehead, R. S., Kan, H. P., Cordero, R. and Saether, E. E., "Certification Testing Methodology for Composite Structures," Report No. NADC-87042-60, October 1986.

30 Kan, H. P., Cordero, R. and Whitehead, R. S., "Advanced Certification Methodology for Composite Structures," Final Report, Control No. N62269-87-C-0259, Naval Air Development Center, September 1989.

31. Kan, H. P., "Delamination Methodology for Composite Structures," Report No. NAWCADWAR-94097-60, DOT/FAA Report No. DOT/FAA/CT-93/64, February 1994.

32. Kan, H. P. and Mahler M. A., "Effect of Stiffener/Rib Separation On Damage Growth and Residual Strength," Task 11 Final Report, Contract No. NAS1-19347, January 1995.

33. Whitehead, R. S., Deo, R.B., Richie, G.L., Guadagnino, C.L. and Kinslow, R.W., "Composite Wing/Fuselage Program," AFWAL-TR-88-3098, Volumes I-IV, February, October 1987.

34. MIL-HDBK-17D, Polymer Matrix Composites, Volume I – Guidelines.

APPENDIX

STIFFENER TERMINATION CADAM DRAWING

PLY CHART		
PLY NO.	ORIENTATION	MATERIAL
P1	+45	
P2	-45	
P3	90	
P4	+45	
P5	-45	
P7	0	
P8	+45	
P9	-45	
P11	90	
P12	+45	
P13	-45	
P14	0	
P15	0	
P16	-45	
P17	+45	
P18	90	
P20	-45	
P21	+45	
P22	0	
P24	-45	
P25	+45	
P26	90	
P27	-45	
P28	+45	

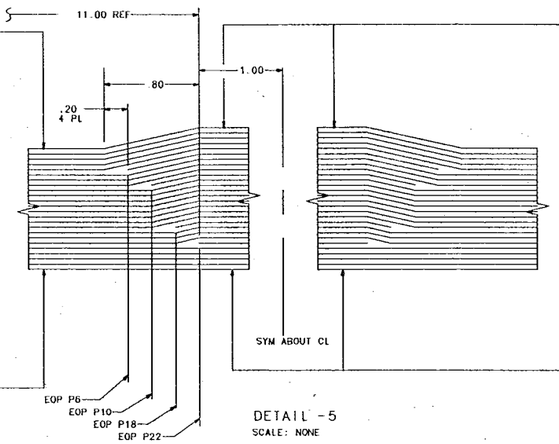

DETAIL -5
SCALE: NONE

PLY CHART B		
PLY NO.	ORIENTATION	MATERIAL
P1	+45	5
P2	-45	
P3	90	
P4	+45	
P5	-45	
P6	90	
P7	0	
P8	+45	
P9	-45	
P10	90	
P11	90	
P12	+45	
P13	-45	
P14	0	
P15	0	
P16	-45	
P17	+45	
P18	90	
P19	90	
P20	-45	
P21	+45	
P22	0	
P23	90	
P24	-45	
P25	+45	
P26	90	
P27	-45	
P28	+45	

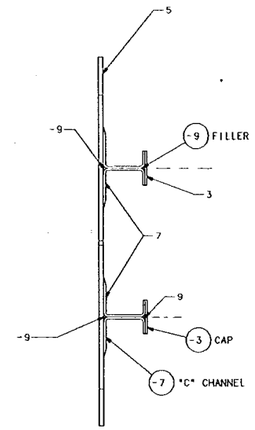

SECT A-A
SCALE: 1/1

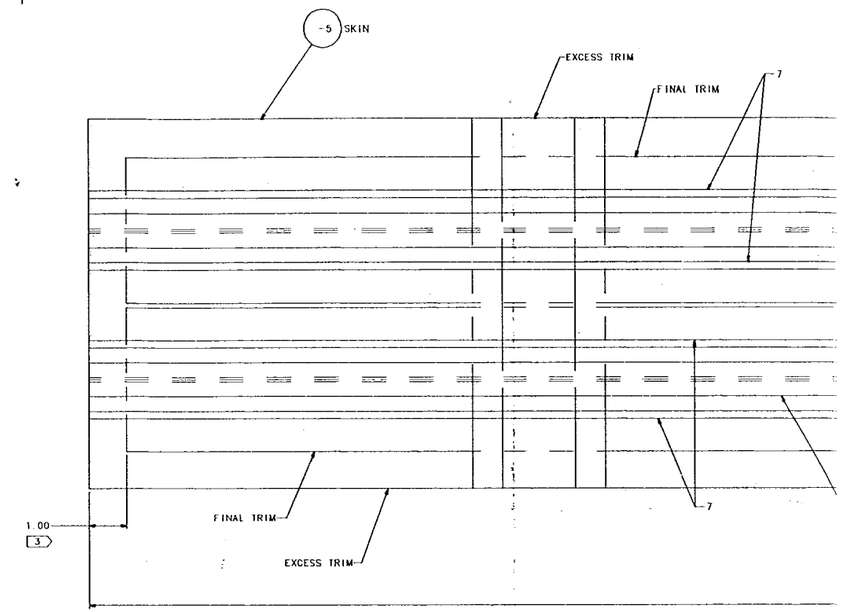

SCALE: 1/1

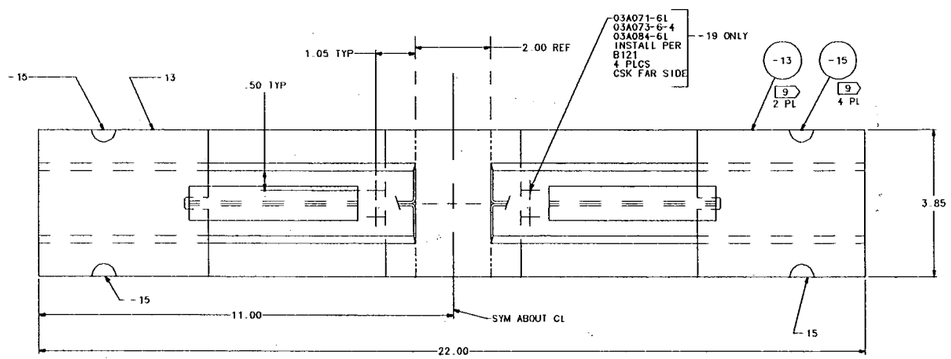

SCALE: 1/1

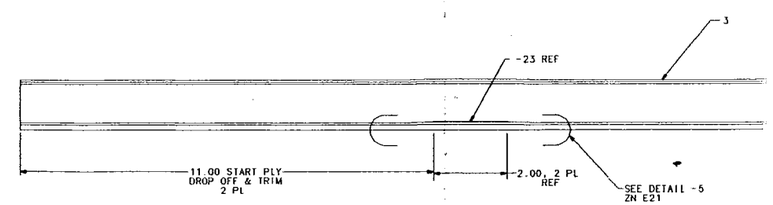

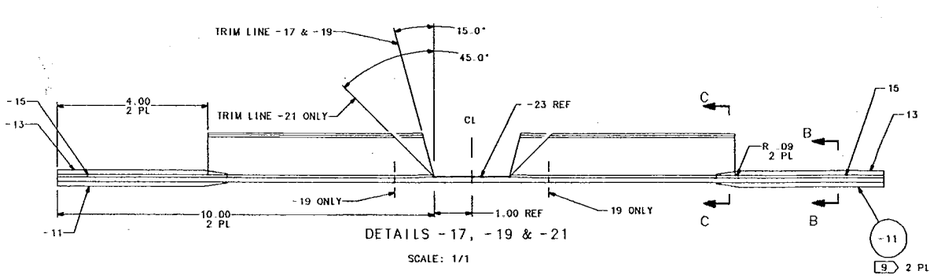

DETAILS -17, -19 & -21
SCALE: 1/1

PLY CHART A		
PLY NO.	ORIENTATION	MATERIAL
P1	+45	6
P2	0	
P3	0	
P4	0	5
P5	0	
P6	0	
P7	0	
P8	+45	6

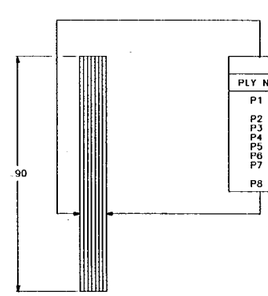

DETAIL -3
SCALE: NONE

DWG NO. SC048000 SH 1 REV

MICROFILM OVERLAP AREA

Unclassified

TRIM

-15-

REVISION NOTES	RLY NOTE	ZONE	REV
1 REFER TO APPLICATION USAGE LIST FOR EFF			

REVISIONS		
DESCRIPTION	DATE	APPROVED
RELEASED BY EO ASCXXX	3/23/93	MWR
REDEFINE -17, -19, & -21	8/31/93	CHS

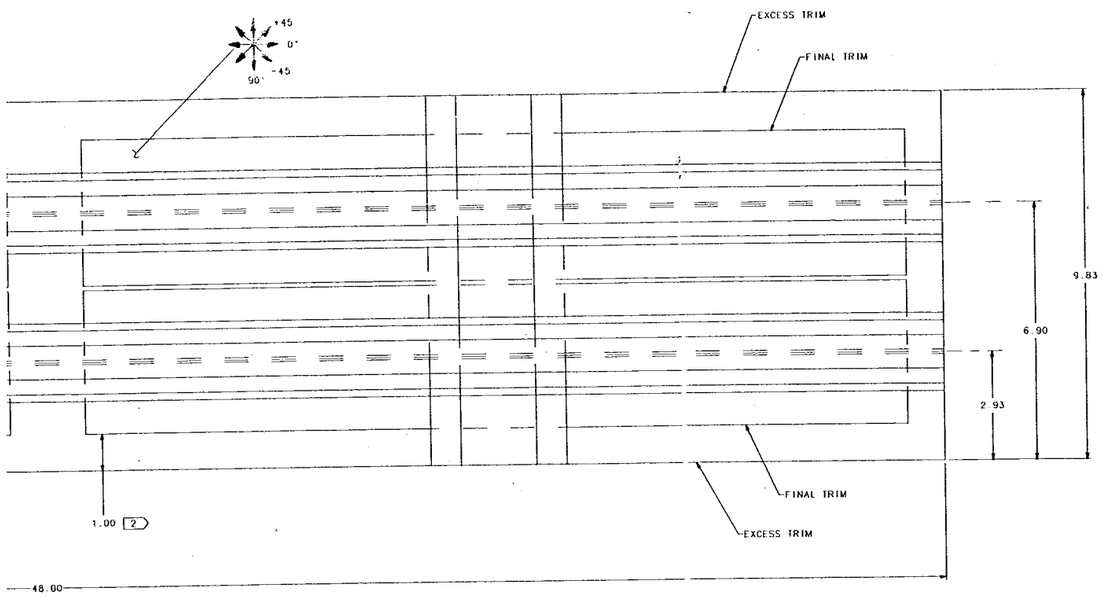

MANUFACTURE A TOTAL OF 48 SPECIMENS OF 3.85 X 22 AS FOLLOWS:

DASH #	QNTY	DESCRIPTION
-17	34	75° SCARFED ANGLE AT TERMINATION ENDS WITHOUT FASTENERS
-19	7	75° SCARFED ANGLE AT TERMINATION ENDS WITH 3/16 DIA FASTENERS
-21	7	45° SCARFED ANGLE AT TERMINATION ENDS WITHOUT FASTENERS
TOTAL	48	

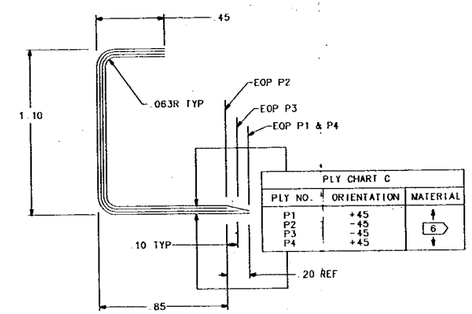

PLY CHART C

PLY NO.	ORIENTATION	MATERIAL
P1	+45	6
P2	-45	
P3	-45	
P4	+45	

DETAIL -7
SCALE: NONE

GENERAL NOTES

1 LAST VIEW/SECTION LETTER USED IS B
2 TRIM LINE FOR COUPON
3 ALLOWANCE FOR SAW CUT
4 NOTE -1 TEST PANEL ASSY IS CUT TO MAKE 3 TEST COUPONS
5 AS4/3501-6 TAPE, CARBON FIBER SPEC NAI-1460
6 AS4/3501-6 WOVEN, CARBON FIBER SPEC NAI-1462
7 ROLLED INTO .10 DIA AND TWISTED @ 3"
8 MS 519 S/GLASS/R6376 CURED PER R201 PLY ORIENT: $(0/90)_3$
9 BOND PAD TO ASSY USING FM 73 ADHESIVE PER NORTHROP SPEC MA-108
10 DIM FOR SLOT -13 ONLY
11 INSPECT AND EVALUATE INDICATIONS PER PS IT-89 CLASS A

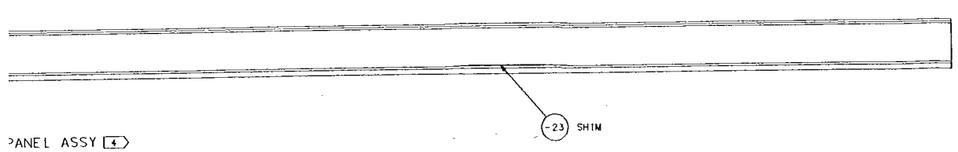

PANEL ASSY 4
SCALE: 1/1

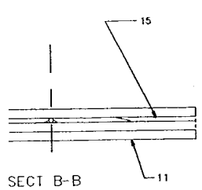

SECT B-B
SCALE: 2/1

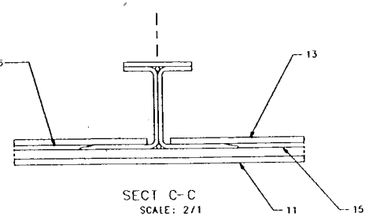

SECT C-C
SCALE: 2/1

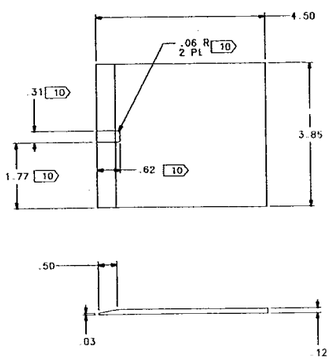

PAD -11 & -13
SCALE: 1/1

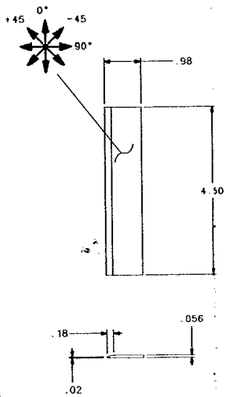

PAD - 15
SCALE: 1/1

QTY REQD -21	-19	-17	-1	PART OR IDENTIFYING NO.	SEE NOTES	NOMENCLATURE OR DESCRIPTION	MATERIAL OR CODE IDENT NO.	SIZE OR PROCUREMENT DATA	SPECIFICATION	ZONE	ITEM
			2	-23		SHIM	ALUMINUM	2.0 X 9.83 X .016			
		4		03A084-6L		WASHER	NAS STD			D21	14
		4		03A073-6-4		PIN	NAS STD			D21	13
		4		03A071-6L		COLLAR	NAS STD			D21	12
				-21		TEST COUPON	MAKE FROM -1			A21	11
				-19		TEST COUPON	MAKE FROM -1			A21	10
				-17		TEST COUPON	MAKE FROM -1			A20	9
4	4	4		-15		PAD	8			D20	8
2	2	2		-13		PAD	SCOTCH PLY 1002			D20	7
2	2	2		-11		PAD	SCOTCH PLY 1002			A19	6
			6	-9		FILLER	5 7			E12	5
			6	-7		CHANNEL	SEE PLY TABLE C ZN B17			S7	4
			1	-5		SKIN	SEE PLY TABLE B ZN G19			G10	3
			3	-3		STRAP	SEE PLY TABLE A ZN H16			S7	2
1	1	1		-1		TEST PANEL ASSY			PS14240 & PS14290	A9	1

PARTS LIST

UNLESS OTHERWISE NOTED	CONTRACT NO.	
LINEAR .X ±0.1; .XX ±0.04; .XXX ±.010	DRAWN	W CVITANICH
LINEAR DIM. ARE IN INCHES	DESIGN	
ANGULAR DIM EXCEPT SHEET METAL FLANGE ± 0°30'	CHECKED	
MFG ACCEPTANCE TOL PER	PROGRAM	
FINISH PER	NORTHROP APPROVAL	
CDU DASH NO. SHOWN EVEN DASH NO. OPPOSITE	OTHER APPROVAL	
FOR USAGE DATA SEE APPLICATION LIST		

STIFFENER TERMINATION

SIZE J | CAGE CODE 74828 | DWG NO. SC048000 | REV

SCALE - NOTED | SHEET 1 OF 1

CADAM DWG 1

DWG NO. SC048000 REV

MICROFILM OVERLAP AREA

A-1